



This is to certify that the

dissertation entitled

Synthetic Approaches to Porphyrin-Fe $_4$ S $_4$ Assemblies, FAB-MS Characterization of the of the Fe $_4$ S $_4$ Clusters and Ligand Binding of Ni-oxoporphyrins

Wen-Lian Lee

has been accepted towards fulfillment of the requirements for

Ph.D. degree in Chemistry

Chik Clay
Major professor

Date 2-7-92

MSU is an Affirmative Action/Equal Opportunity Institution

0-12771

LIBRARY Michigan State University

PLACE IN RETURN BOX to remove this checkout from your record.

TO AVOID FINES return on or before date due.

DATE DUE	DATE DUE	DATE DUE

MSU Is An Affirmative Action/Equal Opportunity Institution

SYNTHETIC APPROACHES TO PORPHYRIN-Fe₄S₄ ASSEMBLIES, FAB-MS CHARACTERIZATION OF Fe₄S₄ CLUSTERS AND LIGAND BINDING OF Ni-OXOPORPHYRINS

By

Wen-Lian Lee

A DISSERTATION

Submitted to
Michigan State University
in partial fulfillment of the requirements
for the degree of

DOCTOR OF PHILOSOPHY

Department of Chemistry

1992

ABSTRACT

SYNTHETIC APPROACHES TO PORPHYRIN-Fe₄S₄ ASSEMBLIES, FAB-MS CHARACTERIZATION OF Fe₄S₄ CLUSTERS AND LIGAND BINDING OF Ni-OXOPORPHYRINS

By

Wen-Lian Lee

The newly-discovered naturally occurring isobacteriochlorins, siroheme and heme d₁, have generated much interest because both are involved in ecologically significant nitrite reduction processes. In the first part of this research, nickel porphyrindione and related porphyrinoids have been examined for their axial ligand affinity. In general, electron-withdrawing or positively charged Ni(II) porphyrinoids favor the formation of hexacoordinate complexes. ligand binding equilibrium constant is a function of the basicity and reduction potential of free base porphyrinoids. X-ray crystallographic studies revealed that the tetracoordinate Ni(AcOOEP-trione) complex has a characteristic saddle-shaped conformation. However, the hexacoordinate Ni(AcOOEP-trione)(py)2 and Ni(OEP-dione)(py)2 possess much less ruffled porphyrin conformations, in accordance with the Ni(II) spin state change upon axial ligation.

In pursuit of an active site model of the siroheme-dependent nitrite reductase, we attempted the use of appropriately-tailored porphyrin-thiol

ligands to achieve porphyrinyl-Fe₄S₄ assemblies. A series of nickel-porphyrin thiol ligands, equipped with tetra-, di-, and mono- thiol function groups has been successfully synthesized. Three types of nickel porphyrinyl-Fe₄S₄ assemblies have been obtained. The preparation of the mixed ligand complex [Fe₄S₄(SPh)₂(NiPS₂)]²⁻ appeared to be the closest example of a porphyrin-Fe₄S₄ assembly.

Fast atom bombardment mass spectrometry (FAB-MS) has been used to analyze a series of iron-sulfur clusters, (A)₂Fe₄S₄X₄, where A= R₄N or Ph₄P, and X=Cl, Br, SEt, SPh. Clusters with mixed Cl, SPh ligands have also been studied. The best FAB-MS results for these clusters were obtained with 3-nitrobenzyl alcohol (NBA) and 2-nitrophenyl octyl ether (NPOE) as matrices. The most unique feature of the negative-ion FAB mass spectra is the identification of the intact ionic core, [Fe₄S₄X₄]-, preformed anions [(A)Fe₄S₄X₄]-, and a series of cluster fragment ions. A mechanism is proposed to explain the formation of small [Fe_mS_n] clusters through unimolecular reduction processes that involve only +2 and +3 oxidation states for the Fe atoms. This work demonstrates that FAB-MS can be employed as a valid method for rapid molecular weight determination as well as structural elucidation of [Fe₄S₄] cluster-containing complexes.

To my Family

ACKNOWLEDGEMENTS

I would like to express my sincere gratitude to Professor Chi K. Chang for his encouragement and support throughout the course of this research work. I would also like to thank Professor Mercouri Kanatzidis who taught me the syntheses of iron-sulfur clusters. Special thanks are extended to Professor John Allison, Dr Douglas Gage, and Dr. Zhi-Heng Huang who taught me how to apply FAB mass spectrometry to the field of bioinorganic chemistry. I would also like to thank Professor Shih-Ming Peng at the Department of Chemistry, National Taiwan University, who carry out the X-ray structural determination of Ni porphyrinoids.

Financial support from Michigan State University in the form of teaching assistantships, and National Institute of Health in the form of research assistantships are gratefully acknowledged.

My deepest appreciation is due to my wife, Dr. I-Chia Chen, and my family for their love, patience and encouragement.

TABLE OF CONTENTS

	I	Page
LIST OF TAB	LES	x
LIST OF FIG	URES	. xii
LIST OF ABI	BREVIATIONS	. xvi
GENERAL IN	NTRODUCTION	1
CHAPTER I	AXIAL LIGATION OF NICKEL	
	PORPHYRINDIONE AND RELATED	
	PORPHYRINOIDS	6
INTRO	DUCTION	7
RESUI	TS AND DISCUSSION	10
1.	Ultraviolet-visible Absorption Spectra	10
2.	Equilibrium Constants of Nickel Porphyrinoids and	
	Basicity of Free Base Porphyrinoids	15
3.	Redox Potentials of free Base and Nickel Porphyrinoids	20

4.	Description of the Structure of Ni(AcOOEP-trione)(I),	
	Ni(AcOOEP-trione) (py)2 (II), and Ni(AcOOEP-	
	dione)(py) ₂ (III)	24
CONCI	LUSION	39
EXPER	IMENTAL SECTION	39
1.	Materials	39
2.	Physical Measurements	40
3.	Cyclic Voltammtry	40
4.	Preparation of Ni(II) Porphyrinoids	40
5.	Preparation of Ni(II) (OEP-trione) and Ni(II) (AcOOEP- $\mbox{.}$	••••
	trione)	41
6.	Preparation of Ni+(PhOEP)ClO ₄	··· 4 3
7.	The Basicity of Porphyrinoids	43
8.	Spectrometric Titration	44
9.	Crystallography	44
CHAPTER II	SYNTHETIC MODELS FOR ASSIMILATORY	
	NITRITE REDUCTASE	46
INTRO	DUCTION	47
RESUI	TS AND DISCUSSION	51
1.	Ligand Design	51

2. Synthesis of Appended Nickel Porphyrin Thiol Ligand53
3. Synthesis of Mono-substituted Porphyrin Thiol Ligand58
4. Synthesis of Iron-sulfur Cluster65
5. Preparation of Ni-porphyrinyl-Fe ₄ S ₄ Assemblies65
6. Characterization of Ni-porphyrinyl-Fe ₄ S ₄ Assiblies67
SUMMARY72
EXPERIMENTAL SECTION74
1. Physical Measurements74
2. Materials
3. Synthesis of Appended Porphyrins75
4. Synthesis of Mono-substituted Porphyrin Thiol Ligand81
5. Preparation of Iron-sulfur Cluster87
6. Preparation of Ni-porphyrin-Fe4S4 Assemblies88
CHAPTER III CHARACTERIZATION OF IRON-SULFUR
CLUSTERS BY FAB MASS SPECTROMETRY90
INTRODUCTION91
EXPERIMENTAL SECTION93
RESULTS AND DISCUSSION94
1. Mass Spectral Characterization of Iron-sulfur
Clusters94
A. Positive- and Negative-ion FAB Mass Spectra of
Halogenated Clusters, (A) ₂ Fe ₄ S ₄ Br ₄ and

	$(A)_{2}Fe_{4}S_{4}Cl_{4}95$
В.	Negative-ion FAB Mass Spectra of Thiolated
	Iron-sulfur Cubane Clusters, (A) ₂ Fe ₄ S ₄ (SR) ₄ 104
C.	The FAB-MS Analysis of Mixed Ligand Cubane
	Cluster
2. Pr	roposed Fragmentation Mechanisms: Correlations
be	etweenNegative Ion FAB-MS Data and Known
Ir	on-sulfur Cluster Chemistry in Condensed Phases 115
CONCLU	SIONS126
REFERENCES A	AND NOTES

LIST OF TABLES

-	۰.
~~	•

1.	Wavelength of Absorption Maxima (in nm) of the Nickel	
	Porphyrinoids in Various Coordinating and Noncoordinating	
	Solvents	11
2.	Experimental Ligand Binding Equilibrium Constants for Ni	
	Porphyrinoids and the Basicity of Related Free Base	
	Porphyrinoids	16
3.	Redox Potentials (Volts) of Free Base and Nickel	
	Porphyrinoids	21
4.	Crystallographic Data for Ni(AcOOEP-trione)(I),	
	Ni(OEP-dione)(Py) ₂ (II), and Ni(AcOOEP-trione)(Py) ₂ (III)	27
5.	Comparsion of Selected Bond Distances (Å) and Angles	
	(deg) in Ni(AcOOEP-trione)(I), Ni(AcOOEP-trione)(py)2(II),	
	and Ni(OEP-dione)(py) ₂ (III)	28
6 .	Summary of stereochemical parameters of reduced porphyrin	
	species	31
7 .	The Various Oxidation States of E. Coli Sulfite/Nitrite	
	Reductase	49

8.	¹ H NMR (δ) Assignments for Free Base Porphyrins (6a-6c)
	and Nickel Porphyrins (7a-7c)(300MHz, CDCl ₃)57
9.	¹ H NMR (δ) Assignments of NiPSAc(13), NiPS ₂ (19), (NiPS) ₂ (20)
	and NiPSH(21a), NiPSH(21b) (300MHz, CDCl ₃)64
10.	Selected ¹ H NMR (δ) Assignments for Complexes I-III (300MHz,
	CDCl ₃)70
11.	Cations in the FAB Mass Spectra of Complexes, (A) ₂ Fe ₄ S ₄ X ₄
	(designated as M), X = Br and Cl, using the matrix NBA100
12.	Relative Intensities of Anions in the Negative Ion FAB Mass
	Spectra of Complexes, $(A)_2$ Fe ₄ S ₄ X ₄ , $X = Br$ and Cl, using
	the matrix NPOE101
13.	Relative Intensities of Peaks in the Negative Ion FAB Mass
	Spectra of Complexes, (A) ₂ Fe ₄ S ₄ (SR) ₄ , R=Et and Ph, using
	the matrix NPOE
14.	Relative Intensities of Peaks in the Negative FAB Mass
	Spectrum of (Ph ₄ P) ₂ Fe ₄ S ₄ (SEt) ₄ , (designed as M), using
	the matrix NBA111
15.	Relative Intensities of Peaks in the Negative Ion FAB Mass
	Spectrum of the complex, (Ph ₄ P) ₂ Fe ₄ S ₄ (SPh) ₂ Cl ₂ , in DMF/NPOE 114

LIST OF FIGURES

	1	page
1.	Examples of metalloporphyrinoids and their parent ring π -	
	conjugation	2
2.	UV-visible spectra of Ni(OEP-trione)and Ni(AcOEP-trione)	
	in toluene solution	12
3.	Spectrophotometric titration of $5x10^{-5}$ M NiT(F ₅)PP	
	in toluene solution with pyrrolidine. The concentrations	
	of pyrrolidine are as follows: 0, 0.6, 1.2, 2.4, 3.6, 4.8, 6.0, 7.2,	
	10.2, 30 mM. Inset: plot of log $[(A_i-A_o)/(A_c-A_i)]$ vs. log [B].	
	B = pyrrolidine	13
4.	Spectrophotometric titration of 1x10 ⁻⁴ M Ni(AcOOEP-trione) in	
	toluene with pyridine. The concentration of pyridine are as	
	follows: 0, 1.24, 2.48, 3.72, 4.96, 6.20, 30 mM. Inset: plot of	
	$\log [(A_i-A_o)/(A_c-A_i)]$ vs. $\log [Py]$. $Py = pyridine$	14
5.	Correlation between log K_{eq} of nickel porphyrinoids and	
	pK ₃ of free base porphyrinoids (open points: pyrrolidine	
	binding and solid points: pyridine binding)	18
6.	Cyclic voltammograms of +2/+1, +1/0, and 0/-1 processes	
	of Ni(OEP-trione)(A) and Ni(AcOOEP-trione)(B) recorded at	
	100mVs ⁻¹ in CH ₂ Cl ₂ , 0.1M Bu ₄ NClO ₄ supporting electrolyte	23

		page
13.	Edge-on view of the skelton of Ni(OEP-dione)(py)2 (III).	
	The deviations of the macrocycle from a plane defined	
	by four nitrogens	36
14.	(a) Schematic description of the bridging cofactors,	
	Fe ₄ S ₄ cluster and siroheme of nitrite/sulfite reductases.	
	(b) The structure of siroheme	48
15 .	¹ H NMR spectrum (300 MHz, CDCl ₃) of NiP(SAc) ₂ (7b).	
	Me ₄ Si peak is not shown	59
16.	¹ H NMR spectrum (300 MHz, CDCl ₃) of (a) NiPSAc (13).	
	and NiPSH (21a)	63
17.	Far-infrared spectra of (a) (Ph ₄ P) ₂ [Fe ₄ S ₄ (SPh) ₂ (NiP(S ₂))]	
	and (b) $(Ph_4P)_2[Fe_4S_4(SPh)_2Cl_2]$. The vibration mode at	
	529 cm ⁻¹ corresponds to the aromatic C-H bending of Ph ₄ P+	69
18.	¹ H NMR spectrum (300 MHz, DMSO-d ₆) of	
	$[\mathrm{Fe_4S_4(SPh)_2(NiP(S_2))}]^{2\text{-}}(\mathbf{III})$	71
19.	¹ H NMR spectrum (300 MHz, DMSO-d ₆) of	
	$[Fe_4S_4(SPh)_2Cl_2]^{2-}(25)$	73
20 .	A portion of the Positive-ion FAB mass spectrum of	
	[(Et ₄ N) ₂ Fe ₄ S ₄ Br ₄] (M), using the matrix NBA	97
21.	Negative-ion FAB mass spectrum of [(Et ₄ N) ₂ Fe ₄ S ₄ Br ₄] using	
	the matrix NPOE. Matrix ions are designated by an (*)	98

22 .	Comparison of isotope abundance for an experimentally
	observed (scribed bar) and theoretically calculated (blank bar)
	clusters (a) [(Et ₄ N) ₃ Fe ₄ S ₄ Br ₄]+ and (b) [Fe ₄ S ₄ Br ₄]- $\cdots 102$
23 .	Negative-ion FAB mass spectrum of (Ph ₄ P)2Fe ₄ S ₄ (SPh) ₄ ,
	using the matrix NPOE. Matrix ions are designated by an (*) 105
24 .	Negative-ion FAB mass spectrum of (Ph ₄ P)2Fe ₄ S ₄ (SEt) ₄ ,
	using the matrix NPOE. Matrix ions are designated by an (*).
	Assignment of cluster peaks: 1. $[Fe_2S_2(SEt)_2]$ -, 2. $[Fe_4S_4]$ -, 3.
	$[Fe_4S_4(O)]^-$, 4. $[Fe_4S_5]^-$, 5. $[Fe_4S_4(SEt)]^-$, 6. $[Fe_4S_5(SEt)]^-$, 7.
	$[Fe_4S_4(SEt)_2]^-, 8. [Fe_4S_5(SEt)_2]^-, 9. [Fe_4S_4(SEt)_3]^-, 10. [Fe_4S_5(SEt)_3]^-, 10. [Fe_4S_5(SEt)_4]^-, 10. [Fe_4S_5(SEt)_4]^-$
	11. [Fe ₄ S ₄ (SEt) ₄]-, 12. (Ph ₄ P)[Fe ₄ S ₄ (SEt) ₄]
25 .	Negative-Ion FAB mass spectrum of (Ph ₄ P) ₂ Fe ₄ S ₄ (SEt) ₄ ,
	using the matrix NBA. Matrix ions are designated by an (*) 110

acac

00sk

DFDP

DMF

DVISC

ЭC

MeOE

θEP

0EP-0

0EP-d

Ĵ⋛₽.ti

LIST OF ABBREVIATIONS

acac acetylacetonate

AcOOEP-trione 5-acetoxy-2,2,7,7,12,12,17,18-octaethyl-3,8,13-

porphintrione dianion

DFDPTMP 4.8-diformyl-2,6-di-n-pentyl-1,3,5,7-tetramethylporphyrin

dianion

DMF N,N-dimethylformamide

DMSO dimethyl sulfoxide

iBC isobacteriochlorin

MeOEC 2-hydro-2-methyl-3,3,7,8,12,13,17,18-octaethylporphyrin

dianion

OEP 2,3,7,8,12,13,17,18-octaethylporphyrin dianion

OEP-one 3,3,7,8,12,13,17,18-octaethyl-2-porphinone

dianion

OEP-dione 3,3,8,8,12,13,17,18-octaethyl-2,7-porphindione

dianion

OEP-trione 2,2,7,7,12,12,17,18-octaethyl-3,8,13-

porphintrione dianion

PhO

py

TBA

TΤξ

THE

7\9

TPC

Pil

TPP

PhOEP 2,2,7,7,12,12,17,18-octaethyl-2-phenyl-3,8,13-

porphyrin dianion

py pyridine

TBAP tetra-n-butylammonium perchlorate

T(F₅)PP 5,10,15,20- tetrakis(pentafluorophenyl)porphyrin

dianion

THF tetrahydrofuran

TMPyP tetrakis(1-methyl-4-pyridyl)porphine dianion

TPC 2,3-dihydro-5,10,15,20-tetraphenylporphyrin

dianion

TPiBC 2,3,7,8-tetrahydro-5,10,15,20-tetraphenylporphyrin

dianion

TPP 5,10,15,20-tetraphenylporphyrin dianion

div ran

in

po (m

В

m tu

n

(

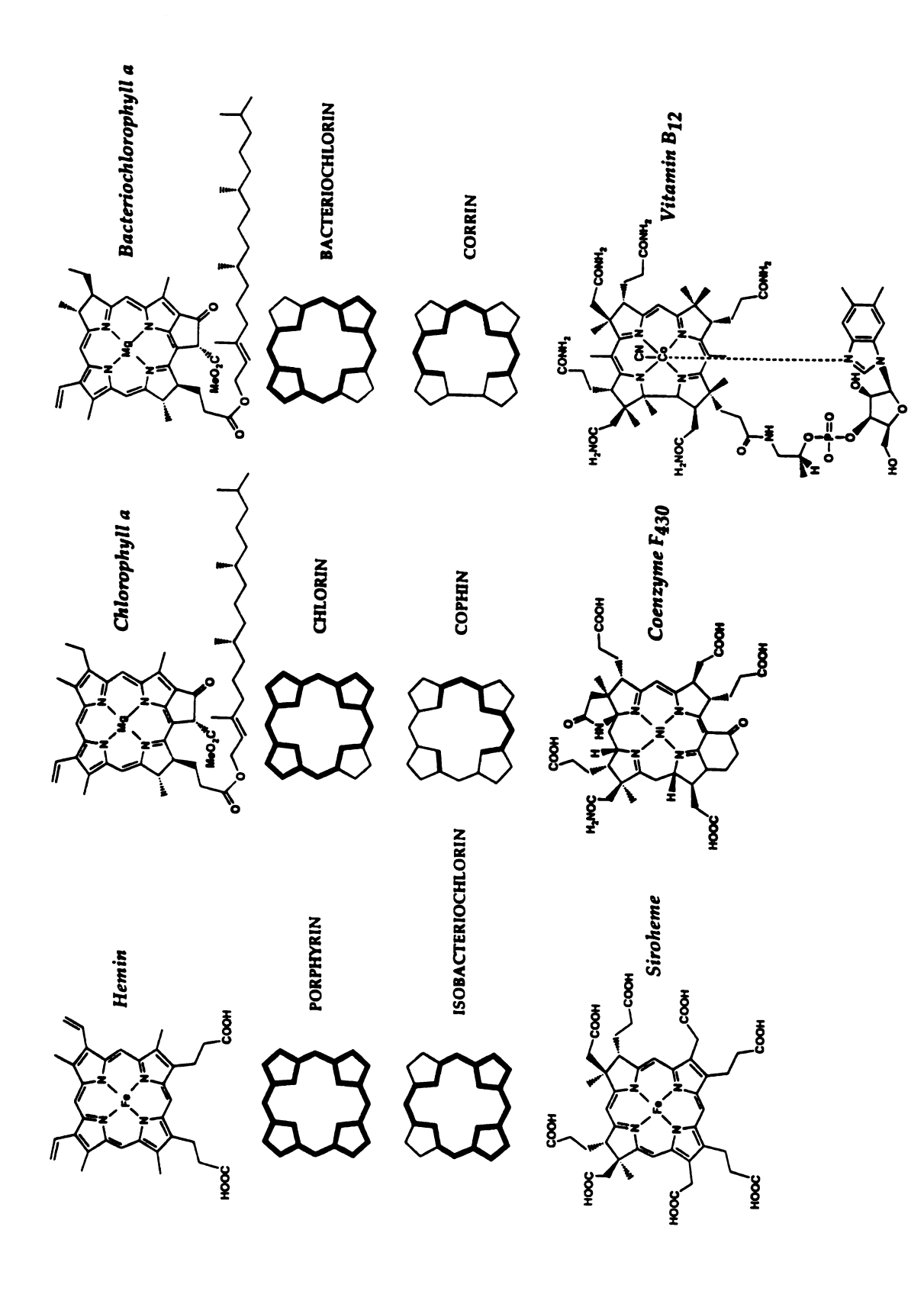
GENERAL INTRODUCTION

Nature has selected a rich variety of porphyrinoids to take part in a diversity of fundamental biological functions in all kinds of organisms ranging from bacteria to plant, and from insect to man¹. Examples shown in Figure 1 are the better known porphyrin family compounds; hemin (iron porphyrin)², chlorophyll a (magnesium chlorin)³, bacteriochlorophyll a (magnesium bacteriochlorin)³, siroheme (iron isobacteriochlorin)³, vitamin B₁₂ (cobalt corrin)⁴ and coenzyme F₄₃₀ (nickel corphin)⁵. These metalloporphyrinoids represent the exceptional examples of nature's finetuning of the macrocyclic ligand sphere as well as the central coordinated metal to optimize a particular biological function¹.

This thesis research deals with the isobacteriochlorin class of compounds. The two naturally occurring iron complexes of isobacteriochlorin (iBC) whose structures were determined during the last decade are siroheme³ and heme $d_1^{6,7}$; both are involved in ecologically significant nitrite reduction processes.

As outlined in the Scheme I, nitrite reduction in the biological world involves many metalloenzymes. Nitrate is first reduced to nitrite by molybdenum-containing nitrate reductase^{8,9}. Studies have shown that assimilatory nitrite reductases which are present in plants have Fe₄S₄ cluster and siroheme cofactors¹⁰⁻¹². Siroheme is the active site carrying out the remarkable 6-electron reduction of NO₂- to NH₃¹³⁻¹⁴, a process whose mechanism is essentially unknown.

Figure 1. Examples of metalloporphyrinoids and their parent ring π -conjugation.



01

Th be

0 V

the

col

str

Scheme I

In the parallel denitrification route, NO₂- is reduced to N₂O and N₂. Our knowledge on the dissimilatory nitrite reduction is equally inadequate. The delineation of the general pathway only occured recently. It is now believed that a common nitrite reductase, cytochrome cd₁ present overwhelmingly in denitrifing bacteria^{15,16}, reduce nitrite to N₂O which is then converted to nitrogen through a separate nitrous oxide reductase (a copper enzyme)^{17,18}.

Cytochrome cd₁ contains an unusual green heme called heme d₁, its structure and properties have recently been studied extensively by Chang and coworkers^{6,7,19-21}.

Part of our research is to continue the ongoing effort to understand the intrinsic properties of dioneheme and related metal complexes. We focus on the study of axial ligation of nickel (II) complexes of porphyrindione and related porphyrinoids. It is particularly interesting that such a study is relevant to the chemistry of nickel-containing F_{430} , in which axial coordination may be the key to its function.

On another front, in order to understand the overall chemical principles involved in biological nitrite reductase, it is desirable to obtain chemical models that mimic the active site of siroheme-dependent nitrite reductase present in plants.

In this regard, the principal objectives of this thesis research included the following:

- (I) Axial ligation of nickel porphyrindione and related porphyrinoids.
- To determinate the affinity constants between a number of bases and nickel
- (II) complexes of porphyrindione and related porphyrinoids.
- (II) Synthetic models for assimilatory nitrite reductase. To build nickel porphyrin equipped with appropriately-positioned thiol ligands for attaching to a Fe₄S₄ unit in order to achieve a porphyrin-linked iron sulfur cluster.
- (III) Characterization of iron sulfur clusters by FAB mass spectrometry.

 To characterize synthetic iron-sulfur clusters and biologically relevant complexes by fast atom bombardment mass spectrometry.

In the following chapters, chapter 1 is devoted to investigating the axial ligation of a series of Ni(II) porphyrinoids to determine the effects of

pyrroline ring saturation and substituents on nickel coordination. Chapter I also describes the crystal and molecular structures of a novel tetracoordinate Ni(II)porphyrinoids, as well as two hexacoordinate Ni(II) complexes, which were characterized by a single crystal x-ray diffraction study. In chapter II, we demonstrate an initial approach to synthesize the models for assimilatory nitrite reductase. Finally, the characterization of Fe_4S_4 clusters by fast atom bombardment mass spectrometry is presented in Chapter III, a mechanism is proposed to explain the formation of small $[Fe_mS_n]$ chusters through unimolecular reduction processes.

CHAPTER I

AXIAL LIGATION OF NICKEL PORPHYRINDIONE AND RELATED PORPHYRINOIDS

v 1 c

> st r: E

> > S. Ci

a r

.

INTRODUCTION

Metallohydroporphyrins have been identified as being essential in a variety of biological systems including nitrite and sulfite reductases 10 - 13,22,23 , and S-methyl coenzyme M reductase 24,25 . Of special interest is cofactor F_{430} , a nickel containing porphyrinoid, found in the latter enzyme of methanogenic bacteria, which catalyzes the final reduction step in methane genesis, where MeSCH₂CH₂SO₃ is reduced to methane as shown in eq. 1.

$$CH_3S-CH_2CH_2SO_3^- + 2H^+ + 2e^- ----> CH_4 + HS-CH_2CH_2SO_3^-$$
 (1)

Althrough X-ray structure data are still lacking, the detailed structure of F_{430} has been determined^{5,26-27}. Systematic chemical and X-ray structural studies on related hydroporphyrinoid carried out by Eschenmoser, Kratky and coworkers have revealed that these low spin nickel (II) complexes share a general structural characteristic: a saddle shaped, ruffled conformation of the macrocycle²⁸⁻³⁰. This saddle conformation has been interpreted "as resulting from the tendency of the Ni (II) to achieve saturation of its electrophilicity by pulling the four nitrogen atoms within the equatorial plane towards the coordination center". Thus, release of ruffling strain energy on going from 4-coordinate Ni(II) to the larger 6-coordinate nickel(II) form is said to be responsible for increasing the residual electrophilicity of nickel in the axial direction, which is why F_{430} exhibits a high axial reactivity.

t. a

N O

re

sŀ

ap ba

als ray

her

Ni

However, counter-examples have been found. Fabrizzi³¹ et. al. described macrocyclic nickel complexes that have planar structure but show high axial reactivity. Recently, Kaplan, Scott and Suslick have measured the equilibrium constants for the binding of six imidazoles with ZnTPP, ZnTPC, and ZnTPiBC as well as two pyrrolidines with NiTPP, NiTPC, and NiTPiBC³². Only very small difference in K_{eq} is obtained as a function of the macrocycles. These authors suggested that even though ring reductions result in distortions from planarity they do not cause an increased ability for axial ligation.

In order to examine the effects of pyrrole ring saturation and substituent groups of the macrocycle on the axial ligation, the purpose of this reseach is to determine the affinity constants between nitrogen bases and a number of nickel porphyrinoids. Particularly, we focus on the study of axial ligation of nickel porphyrindione and related systems including: NiOEP(1), Ni(OEP-one)(2), Ni(OEP-dione)(3), Ni(OEP-trione)(4), Ni(AcO-OEP-trione)(5), Ni(MeOEC)(6), and Ni+(PhOEP)ClO₄-(7), as well as three reference compounds; NiTPP(8), NiT(F₅)PP (9), and Ni(DFDMTMP)(10) as shown in Scheme I.

The results illustrated that the basicity of the tetra-aza porphyrinoids appear to be more important that structural effects; the decrease in the ring basicity would favor the formation of hexa-coordinate Ni(II) complexes. We also reported three molecular structures characterized by single crystal x-ray diffraction: tetracoordinate Ni(AcOOEP-trione)(I), as well as two hexacoordinate Ni(II)porphyrinoids, Ni(AcOOEP-trione)(py)₂(II), and Ni(OEP-dione)(py)₂(III).

Ni(DFDMTMP)(10)

NiT(F)₅PP(9)

Ni(TPP)(8)

]

I

absorpt

pattern

convers

upon tl pyridin

shifts th

T electron

RESULTS AND DISCUSSION

1. Ultraviolet-Visible Absorption Spectra

The UV-visible spectra of Ni-porphyrinoids are strongly dependent on the nature of the peripheral substituents at the ring. For example, the Soret maximum in dichloromethane occurs at 424 nm for Ni(OEP-trione) and at 391 nm for NiOEP (Table 1). The trend indicates a greater red shift for porphyrins with more conjugated keto substituents at the pyrrole periphery (vide infra). Moreover, the electronegative groups not only shift the absorption bands to longer wavelengths but produce large variations in the pattern of the visible bands. Figure 2 shows the intensive red shift of Ni(OEP-trione) and Ni(AcOOEP-trione).

Particularly striking is the red shift for the Soret band upon conversion of four-coordinate species to six-coordinate complexes in the coordinating solvents, pyrrolidine and pyridine. Figure 3 demonstrates that a red shift ca. 20 nm in the Soret region is observed when toluene solution of NiT(F₅)PP is titrated with pyrrolidine. However, the coordination-induced shift of visible spectra is variable. In the case of the Ni(OEP-trione) and Ni(AcOOEP-trione), a dramatic blue shift is observed upon the formation of six-coordinate complexes. As shown in Figure 4, pyridine binding to Ni(AcOOEP-trione) to form six coordinate complex shifts the Q band from 706 nm to 688 nm.

The spectral shift upon ligand binding is indicative of changes in the electron configuration of the Ni(II) complexes, from low spin in a typical

Table 1. Wavelength of Absorption Maxima (in nm) of the Nickel Porphyrinoids in various Coordinating and Noncoordinating Sovents.

	Tollione	Dymoliding	Diriding
	Toldelle	1) i olidilie	1 yildille
NiOEP	391, 515, 551	420, 544, 576	391, 515, 551
Ni(OEP-one)	372, 411, 544, 571, 616	395, 411, 433, 572, 618	394, 411, 433, 572, 618
Ni(OEP-dione)	388, 438, 588, 621	399, 432, 457, 589, 630	396, 436, 451, 584, 624
Ni(OEP-trione)	424, 626, 668, 716	442, 491, 632, 654, 697	442, 490, 651, 694
Ni(AcOOEP-trione)	426, 617, 658, 706	442, 628, 640, 696	442, 628, 642, 688
Ni(MeOEC)	404, 486, 545, 620	423, 541, 570, 620	401, 423, 498, 620
Ni(PhOEP)ClO4	414, 581, 628	423, 579, 611, 624	427, 563, 581, 628
NiTPP	414, 525, 557	413, 433, 520, 564, 603	418, 434, 529
NiT(F ₅)PP	411, 524, 585	430, 563, 603	430, 561, 601
Ni(DFDMTMP)	412, 510, 607	442, 557, 610	442, 575, 627

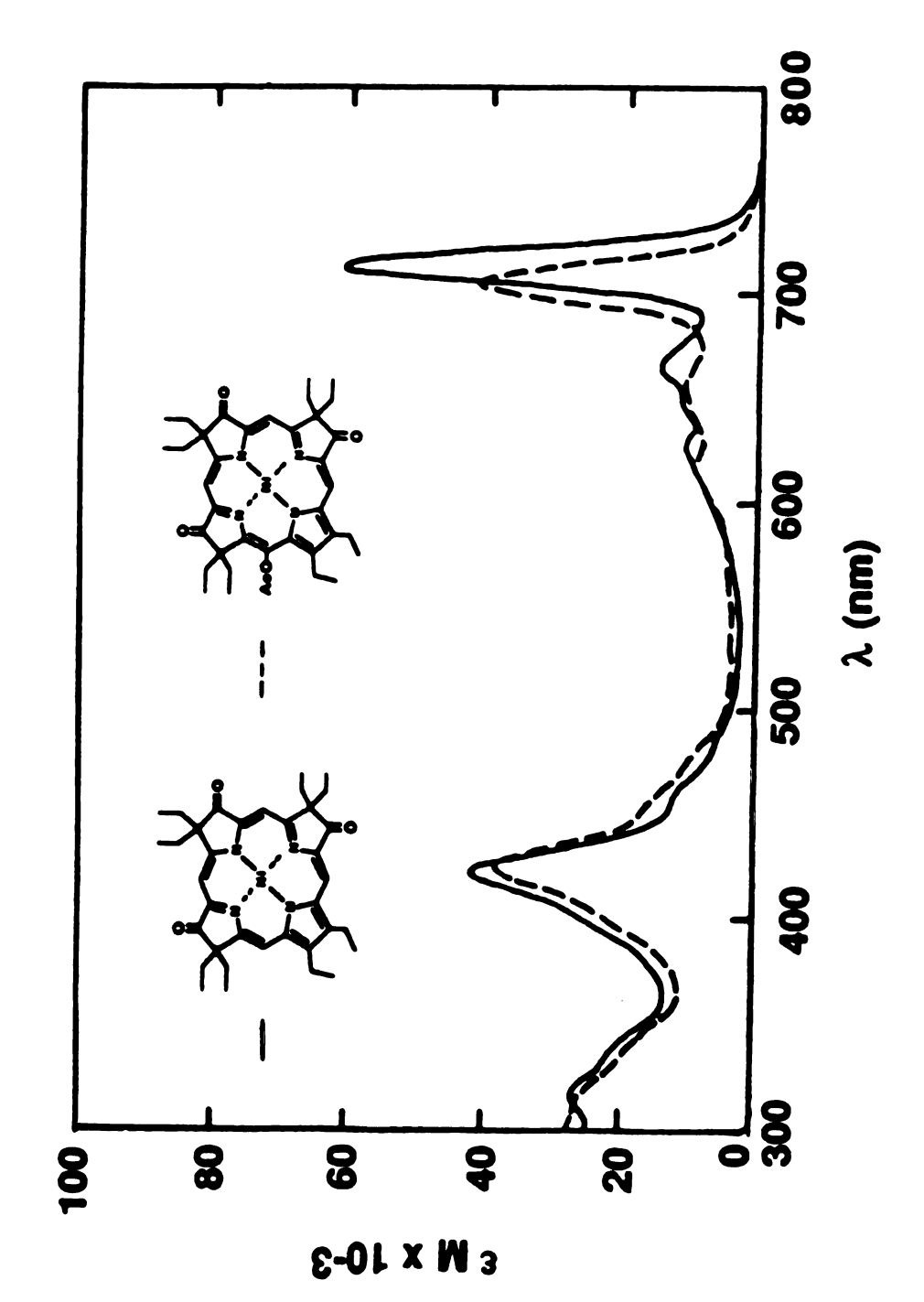


Figure 2. UV-visible spectra of Ni(OEP-trione) and Ni(AcOEP-trione) in toluene solution.

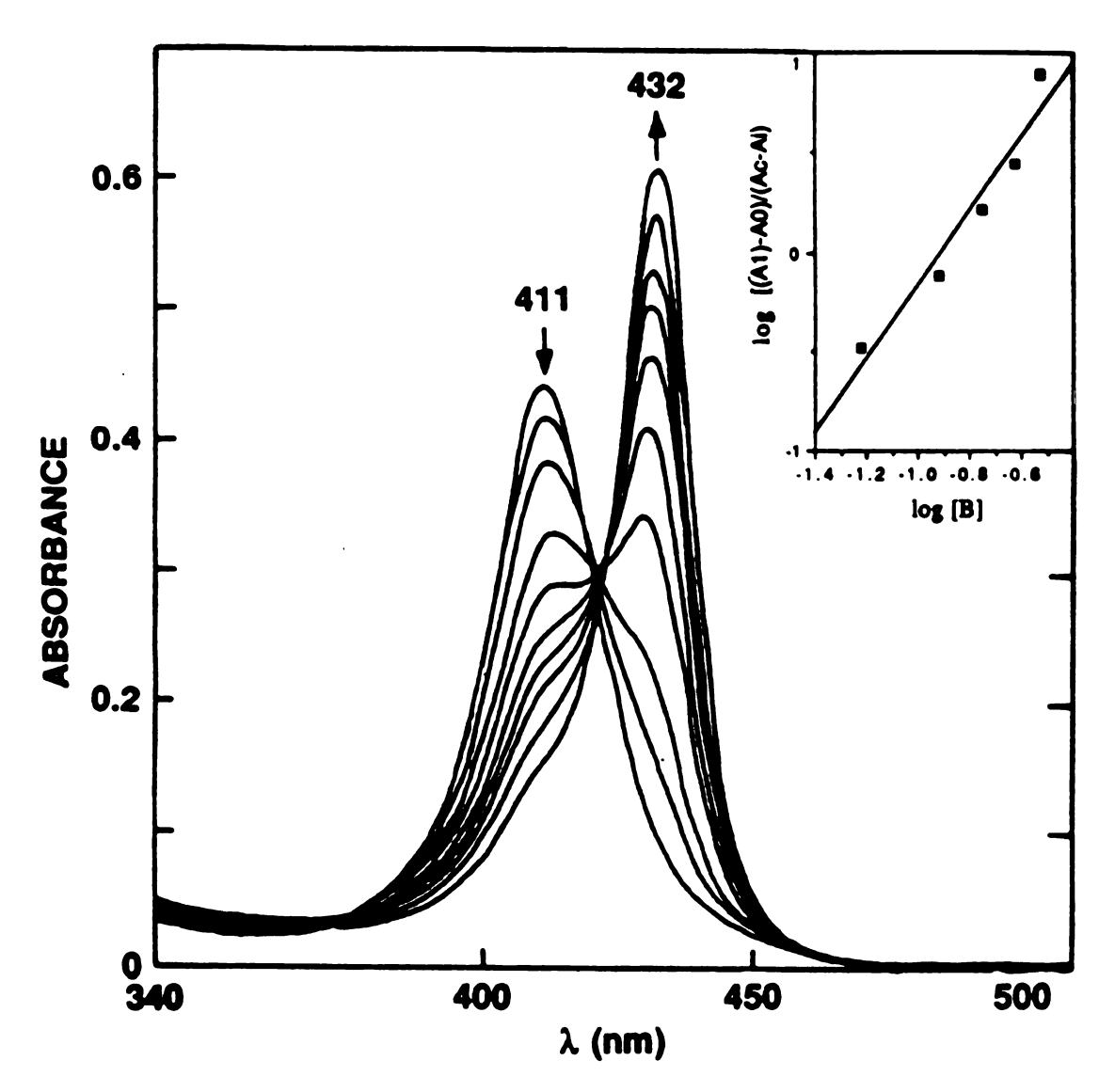


Figure 3. Spectrophotometric titration of $5x10^{-5}$ M NiT(F₅)PP in toluene solution with pyrrolidine. The concentrations of pyrrolidine are as follows: 0, 0.6, 1.2, 2.4, 3.6, 4.8, 6.0, 7.2, 10.2, 30 mM. Inset: plot of log $[(A_i-A_o)/(A_c-A_i)]$ vs. log [B]. B = pyrrolidine.

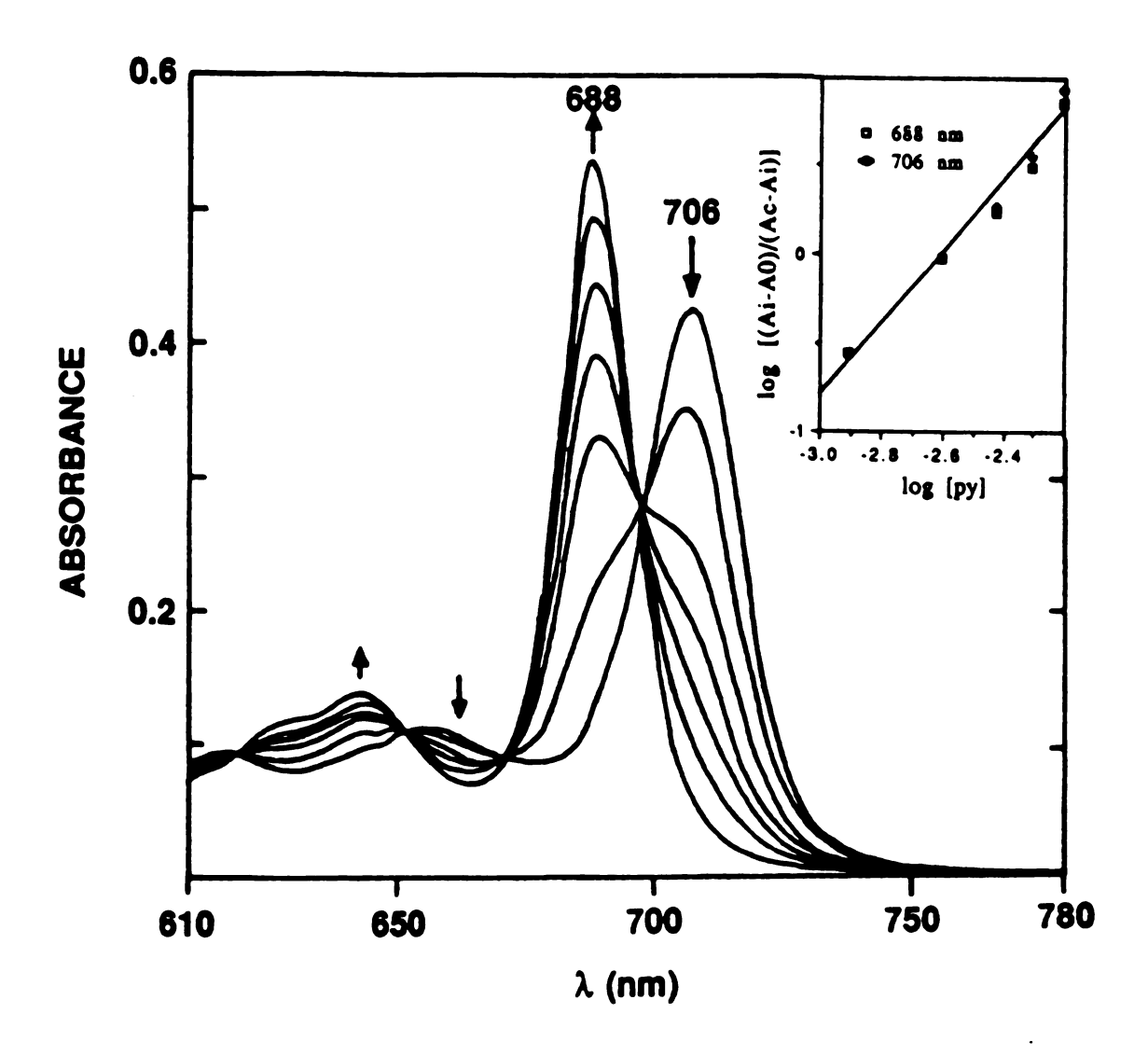


Figure 4. Spectrophotometric titration of 1×10^{-4} M Ni(AcOOEPtrione) in toluene with pyridine. The concentration of pyridine are as follows: 0, 1.24, 2.48, 3.72, 4.96, 6.20, 30 mM. Inset: plot of log [(A_i-A_o)/(A_c-A_i)] vs. log [Py]. Py = pyridine.

metal. I onto the complex substitute formatic

2. Equip Porphys

T

pyrroli

favorab

when the bases, tetracon

 $except \\ log K_{eq}$

Ni(AcO

in our

I

reporte

determi

tetracoordinate to high spin in the hexacoordinate complex. As complexes are formed with additional ligands, electron density builds up in the central metal. If this electron density may be partially dissipated by delocalizing onto the porphyrin ring through $d\pi$ - π * back bonding, the formation of complexes with additional ligands will be more favored. If the peripheral substituent is able to withdraw electron density from the porphyrin, the formation of complexes with additional ligands should be even more favorable.

2. Equilibrium Constants of Nickel Porphyrinoids and Basicity of Free Base Porphyrinoids

The equilibrium constants for the binding of two different bases, pyrrolidine (σ base) and pyridine (π base), were carried out by spectrophotometric titration in toluene. The values are given in Table 2. When tetracoordinate nickel porphyrinoids are treated with coordinating bases, hexacoordinate adducts are formed in toluene. However, tetracoordinate species might be present in the strong coordinating solvent except for those nickel porphyrinoids with high ligand binding affinities (logKeq > 4). Figures 3 and 4 show the titration studies of NiT(F₅)PP and Ni(AcOOEP-trione), respectively.

In general, the average values of equilibrium constant K_{eq} obtained in our studies were determined at four wavelengths in each case, and reported in Table 2. The logarithmic method was used for the determination of K_{eq}^{33} . In the present case, eq 2 could be rewritten as eq. 3,

Table 2. Experimental Ligand Binding Equilibrium Constants for Ni Porphyrinoids and the Bacisity of Related Free base Porphyrinoidsa.

	pK3	logKeq	at 25°C, M-2
Ni(II) complexes		Pyrrolidine	Pyridine
NiOEP	5.8	0.5	•
Ni(OEP-one)	3.3	2.5	0.2
Ni(OEP-dione)	1.8	5.9	3.2
Ni(OEP-trione)	1.0	5.1	4.8
Ni(AcOOEP-trione)		5.8	5.1
Ni(MeOEC)	4.2	1.5	-0.2
Ni(PhOEP)ClO4		2.3	0.1
NiTPP	4.4b	1.20	-0.3
NiT(F ₅)PP	2.5	4.1	1.7
Ni(DFDMTMP)	3.4	2.2	0.2

^a Solvent=toluene. ^b Reference 34. ^c The experimental ligand equilibrium constant is 2.3x10 (log Keq 1.4) (reference 32).

$$K_{eq} = NiP(B)^2/(NiP)(B)^2$$
 (2)

$$K_{eq} = [(A_i - A_0)/(A_c - A_i)][B]^{-2}$$
 (3)

where A_0 = absorbance of a solution of NiP in the absence of Lewis bases, A_c = absorbance of solution of the same concentration of NiP in the presence of a large excess of base, A_i is the absorbance of a solution containing an intermediate concentration of bases and $[B]=[B]_0=[B]_{eq}$. A plot of log $[A_i-A_0/(A_c-A_i)]$ vs. log [B] is expected to give a slope of 2 and an intercept of log $[A_i-A_0/(A_c-A_i)]$ vs. log [B] is expected to give a slope of 2 and an intercept of log $[A_i-A_i]$ and $[A_i-A_i]$ is the values of $[A_i-A_i]$ for the reaction of bases with Ni porphyrinoids. The log-log plots of $[A_i-A_i]$ (Figure 3) and $[A_i-A_i]$ and $[A_i-A_i]$ were linear and all gave slopes close to $[A_i-A_i]$

Our results suggest that the keto substituent on the pyrroline ring is one of the major factor determining the ligand affinity. The tendency of ligand binding of NiOEPs increases with the number of the keto groups. The conjugation interaction of the carbonyl group with the π -system of the porphyrinoid macrocycle reduces the electron density at the macrocycle nitrogen and should, therefore, lead to an decrease in electron density at the metal center.

Combining σ -electron withdrawing effects (inductive effect) and π -interactions (resonance effect) of substituents either in the pyrroline ring or meso position, the basicity of free base of porphyrinoids offers a parallel trend for the axial binding affinity. Examination of Table 2 shows a remarkable correlation between pK₃ and logK_{eq}. Figure 5 depicts the excellent linear relationship obtained between logK_{eq} and pK₃ for the OEPs

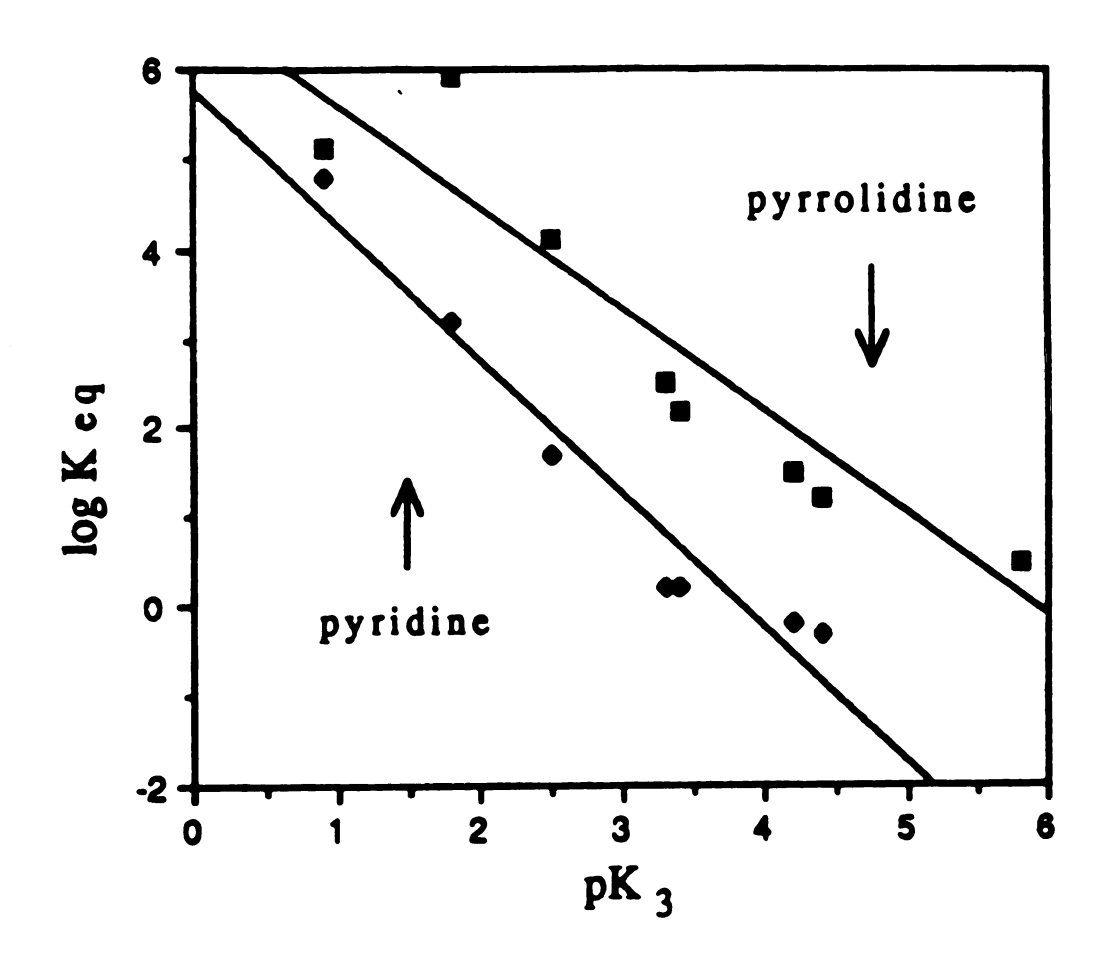


Figure 5. Correlation between $log\ K_{eq}$ of nickel porphyrinoids and pK₃ of free base porphyrinoids (open points: pyrrolidine binding and solid points: pyridine binding).

and the porphyronoids that were chosen for the comparison purpose. The basicity of the ring system can offer a relatively clear prediction of the axial ligand affinity. For example, with almost identical basicity of H_2MeOEC (pK₃ 4.2) and H_2TPP (pK₃ 4.4)³⁴ one finds the similarity in the axial ligand affinity of NiMeOEC (logK_{eq} 1.5) and NiTPP(logK_{eq} 1.2) with pyrrolidine. With different basicity between pyridine (pK_a 5.7) and pyrrolidine (pK_a 2.9) this correlation holds true.

The distinct axial ligand affinity of the nickel ion in enzyme F_{430} may well be related to its biological functions^{24,25}. However, its specific catalytic task remains to be established. In order to explain the high axial reactivity of F₄₃₀, a model complex Ni⁺(PhOEP)-ClO₄-, which contains a monovalent anionic tetraaza ring, similar to the corphin(i. e. hexahydroprphyrin) ring system of F_{430} , has been synthesized for comparison. Complexation of F_{430} with imidazole in dichloromethane shows a large K_{eq} (log K_1 is 2.7 and logK₂ is 2.0)³⁵. However, Ni⁺(PhOEP)-ClO₄- did not have high ligand affinity for imidazole. The ligand binding equilibrium constant ($logK_{eq}$ 2.3) of the bis pyrrolidine adducts of Ni+(PhOEP)(ClO₄) is close to Ni(OEP-one) $(log K_{eq} 2.5)$ and Ni(DFDMTMP) $(log K_{eq} 2.2)$. However, in comparison with NiOEP or NiTPP, the axial ligand binding affinity of Ni+(PhOEP)(ClO₄) is relatively high, since the substituent electronic effect from the phenyl group is not expected to be as large as from peripheral keto or formyl groups. The unusually high axial ligand affinity of Ni⁺(PhOEP)(ClO₄) with pyrrolidine might be due to the positive charge of the Ni metal center accepting axial ligands in order to build up the electron density in the metal center. This might be also the reason why [F₄₃₀M]+ClO₄-exhibits a high axial reactivity.

Regardless of the nature of the substituents or their position on the porphyrinoid periphery, the pK3 values of the macrocycles give a quantitative prediction of the reactivity of Ni porphyrinoids in terms of axial ligation. In general, basic axial ligand and acidic porphyrinoids favor the formation of hexacoordinate complexes. The tendency toward axial ligation in Ni(II) tetrapyrroles does not necessarily correlate with the extent of ring The ligand binding equilibrium constants (Keq) for NiTPP (2.3x10¹), NiTPC (4.0x10¹), and NiTPiBC (1.9x10¹) in pyrrolidine solution demonstrate that the ruffled macrocycles do not increase the propensity to bind axial ligands 32 . Thus, the notion that porphyrin ring saturation as occurred in hydroporphyrinoids in which the macrocycle appears to have greater flexibility for the ligand binding deserves a closer scrutinization. It seems clear that substituent electronic effects can have a greater influence on the affinity for axial ligands, regardless of the saturation level of the ring as postulated for the series of porphyrin, chlorin, isobacteriochlorin, bacteriochlorin, and pyrocorphin²⁷.

3. Redox Potentials of Free Base and Nickel Porphyrinoids

The influence of the keto, formyl, phenyl and fluorophenyl group on porphyrinoid properties can also be examined by redox properties. Redox potentials for Ni porphyrinoids and its free base in 0.1M TBAP/methylene chloride solution are listed in Table 3.

The redox potentials of free base porphyrinoids examined agree well with the published data³⁶⁻³⁸. For example, β -keto porphyrinoids exhibit ring oxidation potentials very similar to those of the parent porphyrin and

Table 3. Redox Potentials (Volts) of Free Base and Nickel Porphyrinoids (vs. SCE) a.

Ni-porphyrinoids	ox. 1	ox. 2	<u>red. 1</u>	red. 2
H ₂ OEP	0.83	1.30	-1.45 ^b	
Ni(OEP)	0.76	1.23	-1.46	
$H_2(OEP-one)$	0.84	1.33	-1.36	
Ni(OEP-one)	0.73	1.13	-1.30	
$H_2(OEP-dione)$	0.82	1.28c	-1.28	
Ni(OEP-dione)	0.71	1.03	-1.13	
H ₂ (OEP-trione)	0.73	1.30d	-1.29	-1.60 ^c
Ni(OEP-trione)	0.63d	0.81	-0.90c	
Ni(AcOOEP-trione)	0.70 ^d	0.84	-0.91	
H_2MeOEC	0.83	1.11 ^c	-1.58	
Ni(MeOEC)	0.48c	1.05°	-1.53 ^b	
Ni(PhOEP)ClO4c	0.44d	0.75	-0.90e	
H_2TPP	0.70 ^b	0.92	-1.20	-1.58
NiTPP	1.20d	1.29^{f}	-1.40	
$H_2T(F_5)PP$	1.18 ^b	1.47 ^e	-0.90	-1.30
NiT(F ₅)PP	1.30		-0.95	-1.52 ^b
$H_2(DFDPTMP)$	1.06	1.48	-0.94	-1.15
Ni(DFDPTMP)	0.98	1.38	-1.06	

^a 0.1 M Tetrabutyl ammonium chloride (TBAP) in methylene chloride with 100 mV/s scan speed. ^b Quasi-reversible. ^c Irreversible. ^d Redox potential for Ni(II)/NI(III). ^e Redox potential for Ni(II)/Ni(I). ^f Ni(III)TPP+.

the ring reduction is made easier by increasing the number of β -keto group as shown in Table 3.

The first and second oxidation process of Ni porphyrinoids are characteristic of diffusion-controlled one-electron process, except that Ni(OEP-trione) and Ni(AcOOEP-trione) show an overlapping but reversible cyclic voltammogram (exemplified in Figure 6). As seen in Table 3, redox potentials for the first oxidation process in methylene chloride solution exhibit a considerably small difference: 0.76 V (NiOEP), 0.73 V (NiOEP-one), 0.71 V (NiOEP-dione), and 0.70 V(NiOEP-trione), and 0.63 V (NiAcOOEPtrione). The first one-electron oxidation of Ni porphyrinoids is tentatively assigned for the cation radical species. The second electron oxidation is possibly removing electron from Ni center to form Ni(III). However, recent evidence³⁹ from EPR data demonstrate that Ni(III)(OEP-trione) could be produced in methylene chloride at liquid nitrogen temperature. The data in Table 3 indicate that within the OEP series, the second oxidation product Ni(III) is stabilized by increasing the number of β-keto groups. With an acetoxy substituent at meso position, Ni(AcOOEP-trione) appears to behave like Ni(OEP-trione).

The β -keto NiOEP derivatives demonstrate that ring reduction becomes easier with increasing number of β -keto groups as shown in Table 3. The most dramatic difference of the reduction potential could be ca. 560 mV between Ni(OEP) (-1.46 V) and Ni(OEP-trione) (-0.90 V). In these one-electron reduction process, typically, the formation of anionic radicals is assumed. However, an irreversible wave was observed for Ni(PhOEP)(ClO₄-) at -0.90V. This could be the reduction of Ni(II) to Ni(I)

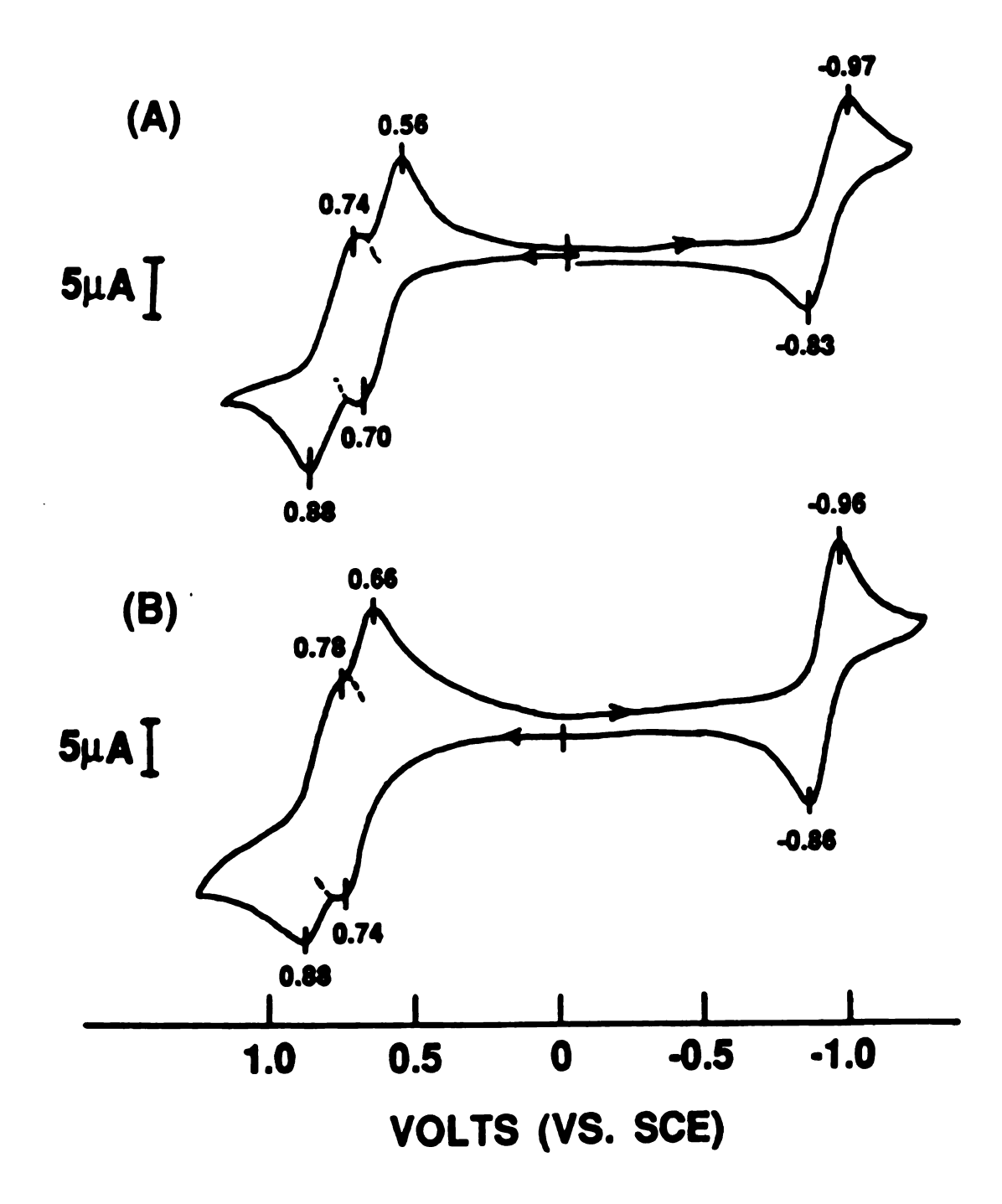


Figure 6. Cyclic voltammograms of +2/+1, +1/0, and 0/-1 processes of Ni(OEP-trione)(A) and Ni(AcOOEP-trione)(B) recorded at 100mVs⁻¹ in CH₂Cl₂, 0.1M Bu₄NClO₄ supporting electrolyte.

analogous to the observation that a model complex of F_{430} has a reduction potential at -0.86 V in CH_2Cl_2 with Bu_4NClO_4 as electrolyte²⁸.

Reduction potentials of free base and nickel keto-substituted OEPs are markedly dependent on their basicity⁴⁰. In most cases the porphyrinoids that are more difficult to reduce also have larger pK₃. A correlation of the reduction potential $E_{1/2}$ values of Ni porphyrinoids and free bases versus their basicity was studied. Figure 7A shows the linear relationship obtained between pK₃ and $E_{1/2}$. This is especially true for H₂OEP and its keto substituted compounds. An excellent linear relationship between the equilibrium constant K_{eq} of NiOEPs and $E_{1/2}$ could also be obtained (Figure 7B).

The studies of reduction potentials of free base porphyrinoids provide a quantitative measurement of porphyrin electron density on the central porphyrin nitrogen atom influenced by peripheral substituents. The trend of reduction potentials (especially for OEP series compounds) reflects the difference between β -ketoOEP and hydroporphyrin.

4. Description of the Structure of Ni(AcOOEP-trione)(I), Ni(AcOOEP-trione)(py)2 (II), and Ni(OEP-dione)(py)2 (III)

A. Ni(AcOOEP-trione) (I).

The crystal structure of Ni(AcOOEP-trione)(I) is shown in Figure 8. The crystallographic data for the compound are given in Table 4. The selected bond distances and angles are listed in Table 5. The molecule

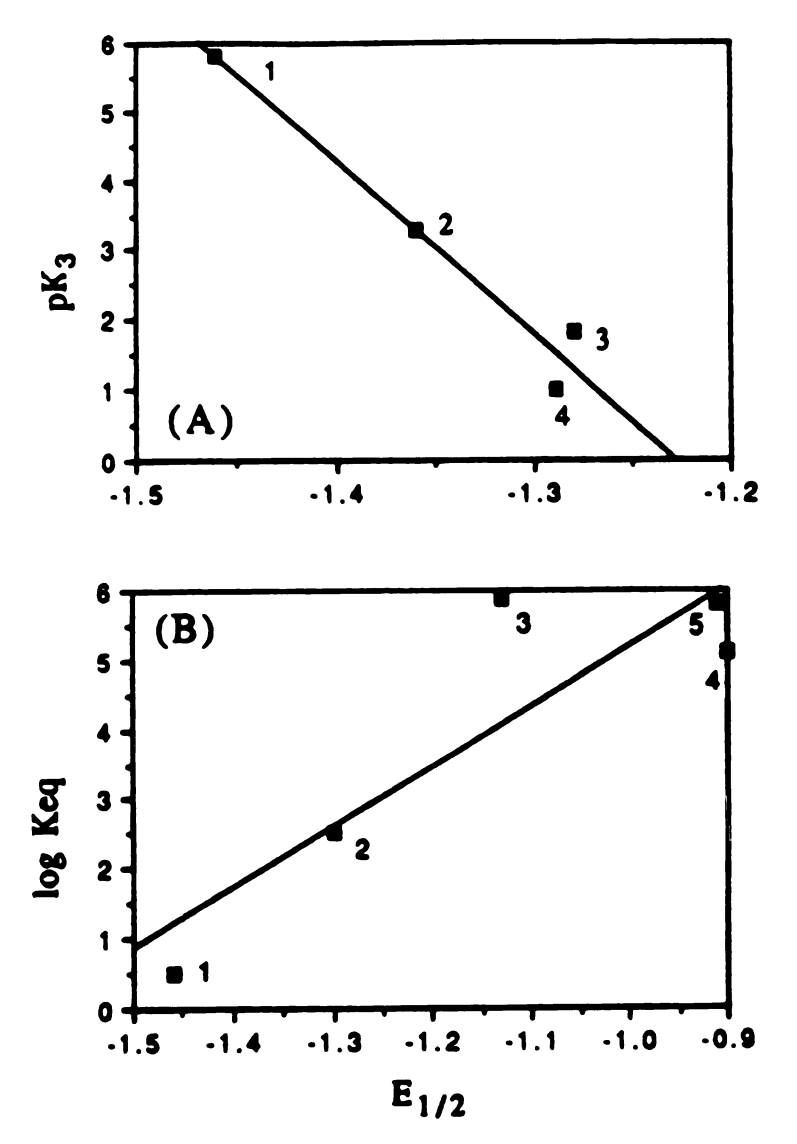
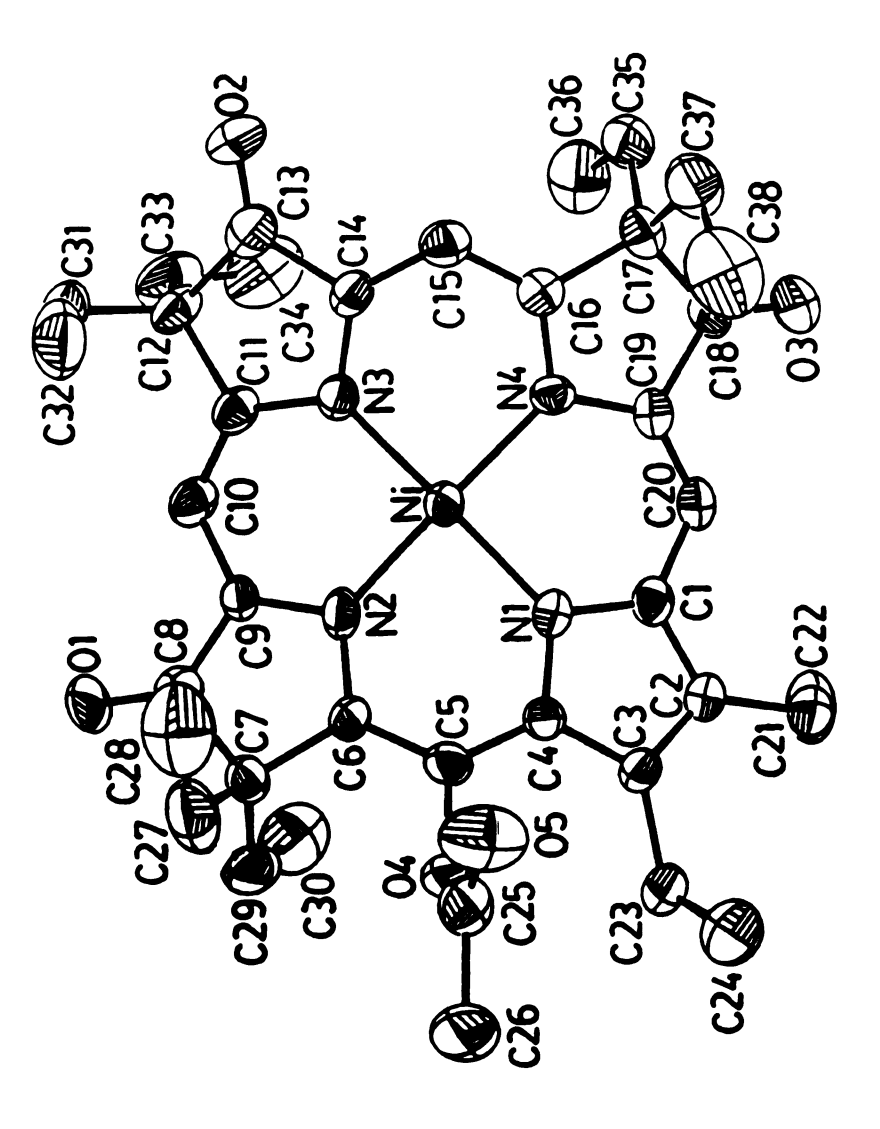


Figure 7. (a) Correlation between pK_3 and $E_{1/2}$ of free base keto-substituted OEP series: 1. H_2 OEP, 2. H_2 (OEP-one), 3. H_2 (OEP-dione), 4. H_2 (OEP-trione). (b) Correlation between K_{eq} and $E_{1/2}$ of nickel keto substituted OEP series: 1. NiOEP, 2. Ni(OEP-one), 3. Ni(OEP-dione), 4. Ni(OEP-trione), 5. Ni(AcOOEP-trione).



Hydrogens are omitted for clarity. Themal ellipsoids are drawn to enclose Figure 8. Molecular structure and atom names of Ni(AcOOEP-trione)(I). 50% probability.

Table 4. Crystallographic Data for Ni(AcOOEP-trione)(I), Ni(AcOOEP-trione)(py)2(II), and Ni(OEPdione)(py)2(III).

Compound	Ι	Π	П
Formula	C44H60N4O5Ni	C ₅₃ H ₆₁ N ₇ O ₅ Ni	C ₅₁ H ₅₉ N ₇ O ₅ Ni
F.W.	769.57	934.82	860.81
а, А	9.998(4)	10.7969(21)	18.432(4)
b, A	10.449(3)	12.653(3)	13.679(6)
c, A	19.902(6)	20.019(3)	18.476(5)
a, deg	00.06	75.124(15)	00.06
b, deg	95.16(3)	86.233(14)	92.10(6)
g, deg	90.00	72.075(19)	00.00
Z. V. A3	2, 2070.7(12)	2, 2514.7(8)	4, 4655(3)
Space group	$\mathbf{P}_{\mathbf{n}}$	P-1	$P2_1/n$
Deale, g/cm ³	1.234	1.235	1.230
m, cm ⁻¹	5.2	4.4	4.6
Crys. size, mm	0.25, 0.33, 0.75	0.30, 0.40, 0.50	0.20, 0.40, 0.40
2qmax., deg	49.8	44.9	44.9
No. of data collected	3635	6580	0809
Data used($F_0^2 > 2s(F_0^2)$)	2870	5140	2863
Min, and max abs.	98.05, 99.94	97.47, 99.93	93.07, 99.15
correction			
No. of variables	486	266	220
No. of atoms per asym	114	127	120
unit (including H)			
Final R/Rw (%)	4.8/4.6	4.2/4.9	6.4/6.0

Table 5. Comparsion of Selected Bond Distances (Å) and Angles (deg) in Ni(AcOOEP-trione)(I), Ni(AcOOEP-trione)(py)₂(III), and Ni(OEP-dione)(py)₂(III).

	I	II	III
Bond distances	(Å)		
Ni-N(1)	1.949(5)	2.0458(25)	2.090(5)
Ni-N(2)	1.918(5)	2.079(3)	2.097(5)
Ni-N(3)	1.923(5)	2.0859(25)	2.030(5)
Ni-N(4)	1.957(4)	2.075(3)	2.052(5)
Ni-N(5)		2.189(3)	2.216(7)
Ni-N(6)		2.190(3)	2.186(6)
Bond Angles(de	g)		
N(1)-Ni-N(2)	88,79(19)	88.42(10)	90.58(18)
N(1)-Ni-N(3)	179.43(21)	176.34(10)	178.01(25)
I(1)-Ni-N(4)	90.24(19)	92.02(10)	90.13(19)
N(1)-Ni-N(5)	91.09(20)	87.43(10)	86.56(22)
(1)-Ni-N(6)	178.94(19)	92.89(10)	91.06(22)
N(2)-Ni-N(3)	89.89(19)	90.79(10)	88.39(18)
I(2)-Ni-N(4)		179.41(10)	178.91(22)
N(2)-Ni-N(5)		90.50(10)	89.41(22)
N(2)-Ni-N(6)		89.76(10)	90.92(22)
N(3)-Ni-N(4)		88.75(10)	90.93(19)
N(3)-Ni-N(5)		89.01(10)	91.72(24)
N(3)-Ni-N(6)		90.68(10)	90.66(24)
N(4)-Ni-N(5)		89.11(10)	91.45(22)
N(4)-Ni-N(6)		90.63(10)	88.25(22)
N(5)-Ni-N(6)		179.59(10)	177.60(20)

structure demonstrates a pronounced saddle-shape ruffled conformation of the macrocyclic ligand system as shown in Figure 9. The molecule is significantly distorted in the conventional fashion; the dihedral mirror planes contain the S_4 axis and opposite pairs of methine carbon atoms. The methine carbons (meso-carbons) have the largest displacements of any macrocycle atom from the mean plane (NiN₄ core is coplanar), alternating 0.66 Å above and below. The average absolute value of the deviation of four meso-carbons (d_m) from the plan is 0.64 Å. However, the Ni(P-dione)⁴¹ exihibits a slight deformation with a d_m parameter of 0.32 as shown in Table 6.

In the structure of Ni(AcOOEP-trione)(I), the average equatorial Ni-N_{red} bond distances are 1.933 Å which agrees well with the Ni-N_{red} bond distance in other nickel porphyrinoids. A summary of selected stereochemical parameters of metallohydroporphyrinoids is given in Table 6^{42} . If comparing the Ni-N_{red} bond distance with two related nickel β -oxoOEP complexes, Ni(oxoOEP) and Ni(P-dione) in Table 6, both Ni-N_{red} and Ni-N_P distance of Ni(AcOOEP-trione) is shorter.

In general, the ring ruffling feature of Ni(AcOOEP-trione) is very similar to Ni (II) hydroporphyrinoids²⁷⁻³⁰ regardless of the keto and acetoxy substituents. As noted in the introduction, the saddle conformation has been interpreted to result from contraction of the coordination core in nickel hydroprophyrinoids. According to the principle that the porphyrin core is enlarged upon pyrrolic ring saturation, the Ni-N bonds would become unfavorably long for Ni(II) ion in Ni(AcOOEP-trione). In order to adjust the Ni-N bond lengths to stablize the tetracoordinate nickel(II) ion, the four

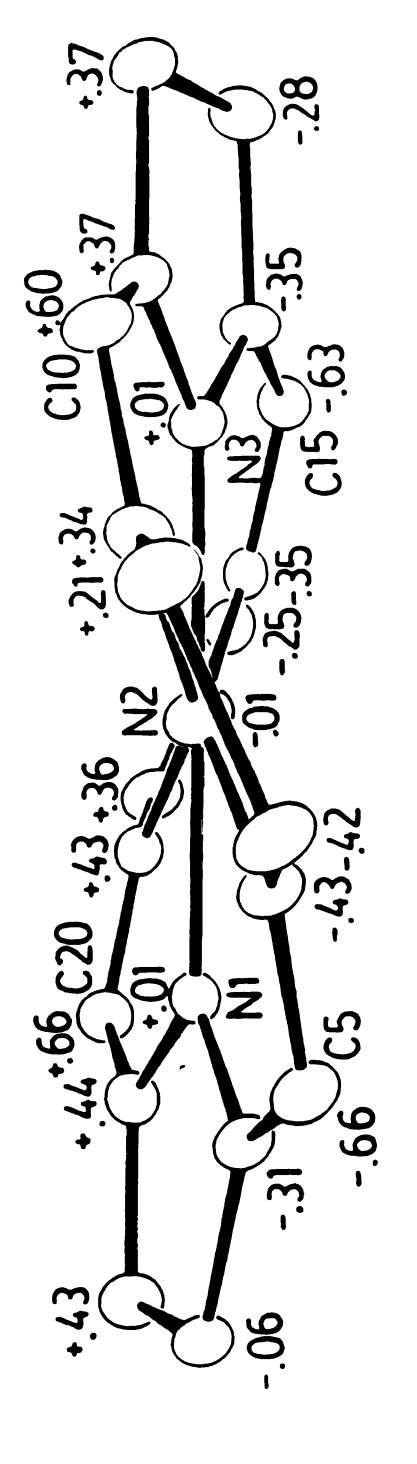


Figure 9. Edge-on view of Ni(AcOOEP-trione) that illustrate the deformation of the macrocyclic skelton. The deviations of the macrocycle from a plane defined by four nitrogens.

Table 6. Summary of stereochemical parameters of reduced porphyrin species^a.

Complex	$Configuration^b$	M-Np	M-N(red)	$ m dm_c$	No.	Ref.
					Red Rings	
Ni(PCOEP)	22222	1.913(8)	1.908(8)	0.74	က	12
Ni(PCOEP)	tetee	1.925(8)	1.931(8)	99.0	က	22
Ni(PCOEP)	tette	1.938(12)	1.927(12)	99.0	က	22
(PCOEP)(Py)]	22202	1.950(7)	1.982(10)	0.51	က	23
Cu(PCOEP)	tctct	1.990(10)	2.045(19)	0.26	က	22
Ni(OEPiBC)	Ħ	1.915(3)	1.920(4)	9.0	87	22
Ni(OEPiBC)	tct	1.94(3)	1.94(4)	0.64	77	27
Ni(OEPBC)	220	1.920(2)	1.922(3)	0.61	87	27
Ni(HHOEP)	tttt	1.91(3)	1.91(3)	0.72	87	27
Ni(HHOEP)	ttct	1.925(7)	1.94(4)	99.0	87	21
Ni(OxoOEP)d		1.967(7)	1.994(18)	0.05	1	42
		1.953(11)	2.030(29)	0.36	1	42
Cu(DioxoOEP)		1.999(10)	2.044(13)	60.0	87	41
Ni(P-dione)		1.969(4)	1.943(4)	0.32	87	83
Ni(AcOOEP-trione)		1.949(5)	1.933(5)	0.64	က	this work
$[Ni(OEP-dione)(Py)_2]$		2.094(5)	2.041(5)	0.04	7	this work
[Ni(AcOOEP-trione)(Py) ₂]	[2]	2.0458(25)	2.080(3)	0.25	က	this work

(a) All values in Å; (b) The configurations describes the relative orientation, in pairs, of the groups on the reduced rings starting with the first substituent on Ring A; (c) dm is the average absolute displacement of the meso-carbon atoms from the mean plane of the four nitrogen atoms. All cores have S4-ruffled geometry; (d) Two independent molecules.

nitrogen atoms are pulled toward the metal center, preserving the square planar of coordination geometry; thus the four meso-carbon atoms are situated alternatively above and below this coordination plane. The resulting distortion of the ligand framework leads to the saddle conformation as shown in Figure 8. However, the deformation also builds up conformation strain.

Finally, it should be noted that the expected increase in the C_{β} - C_{β} and C_{α} - C_{β} bond distances (not shown in Table 5) of the reduced pyrrole ring are observed. It is also expected and generally observed that pyrrole ring is no longer planar²⁷.

B. Ni(AcOOEP-trione)(py)2(II) and Ni(OEP-dione)(py)2(III)

We have succeeded in isolating single crystals of hexa-coordinate Ni(AcOOEP-trione)(py)₂(II) from a saturated pyridine solution of Ni(AcOOEP-trione). Similarly, single crystals of hexacoordinate Ni(OEP-dione)(py)₂(III) were also obtained in the same fashion from a saturated pyridine solution of Ni(OEP-dione)(4). The molecular structure and atom names for Ni(AcOOEP-trione)(py)₂ (II) are presented in Figures 10 and 11. Selected bond distances and angles are listed in Table 5.

Figures 12 and 13 are the edge-on view of the molecules II and III including the deviation from NiN₄ core plane. Both molecules are six coordinate as expected, with the pyridine rings characteristically tilted with respect to the normal of the mean plane. The pyridine plane is oriented to

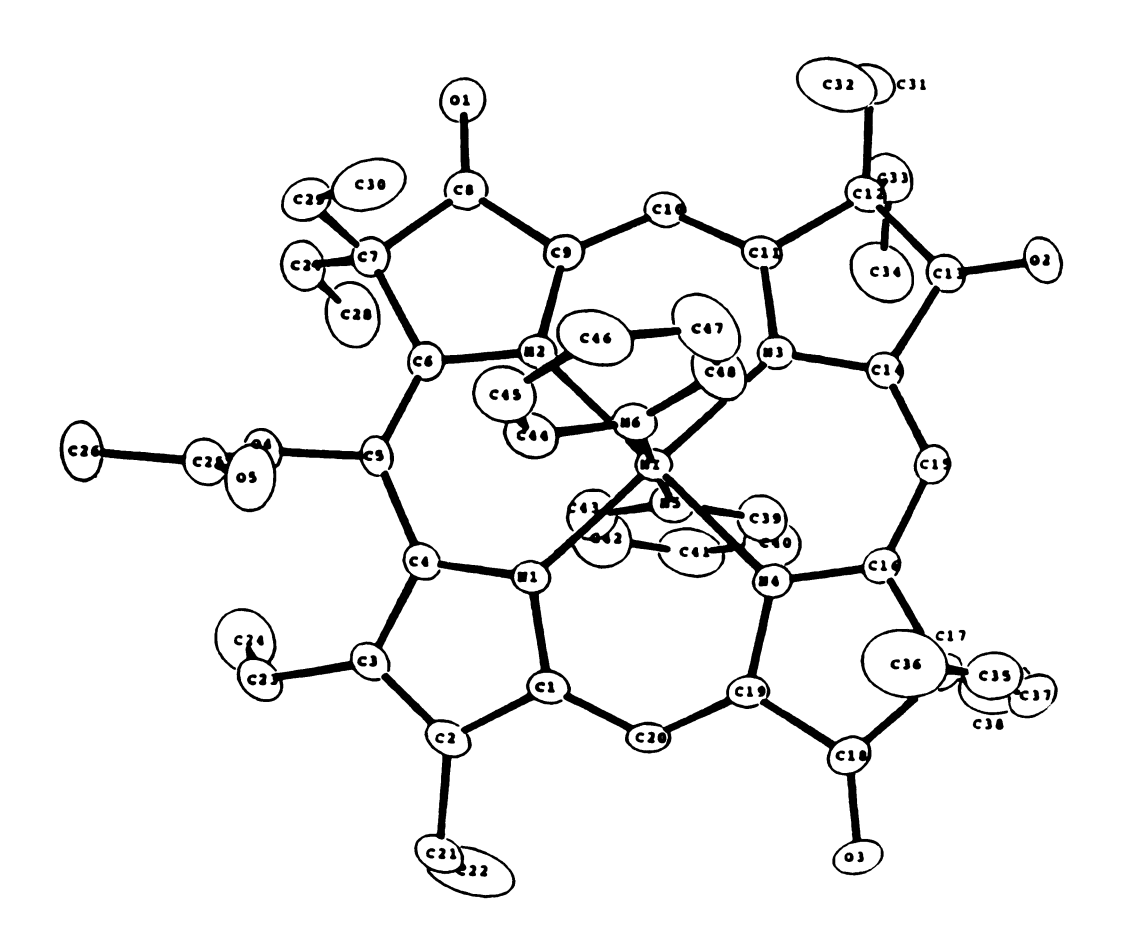


Figure 10. Molecular structure and atom names of Ni(AcOOEP-trione)(py) $_2$ (II). Hydrogens are omitted for clarity. Themal ellipsoids are drawn to enclose 50% probablity.

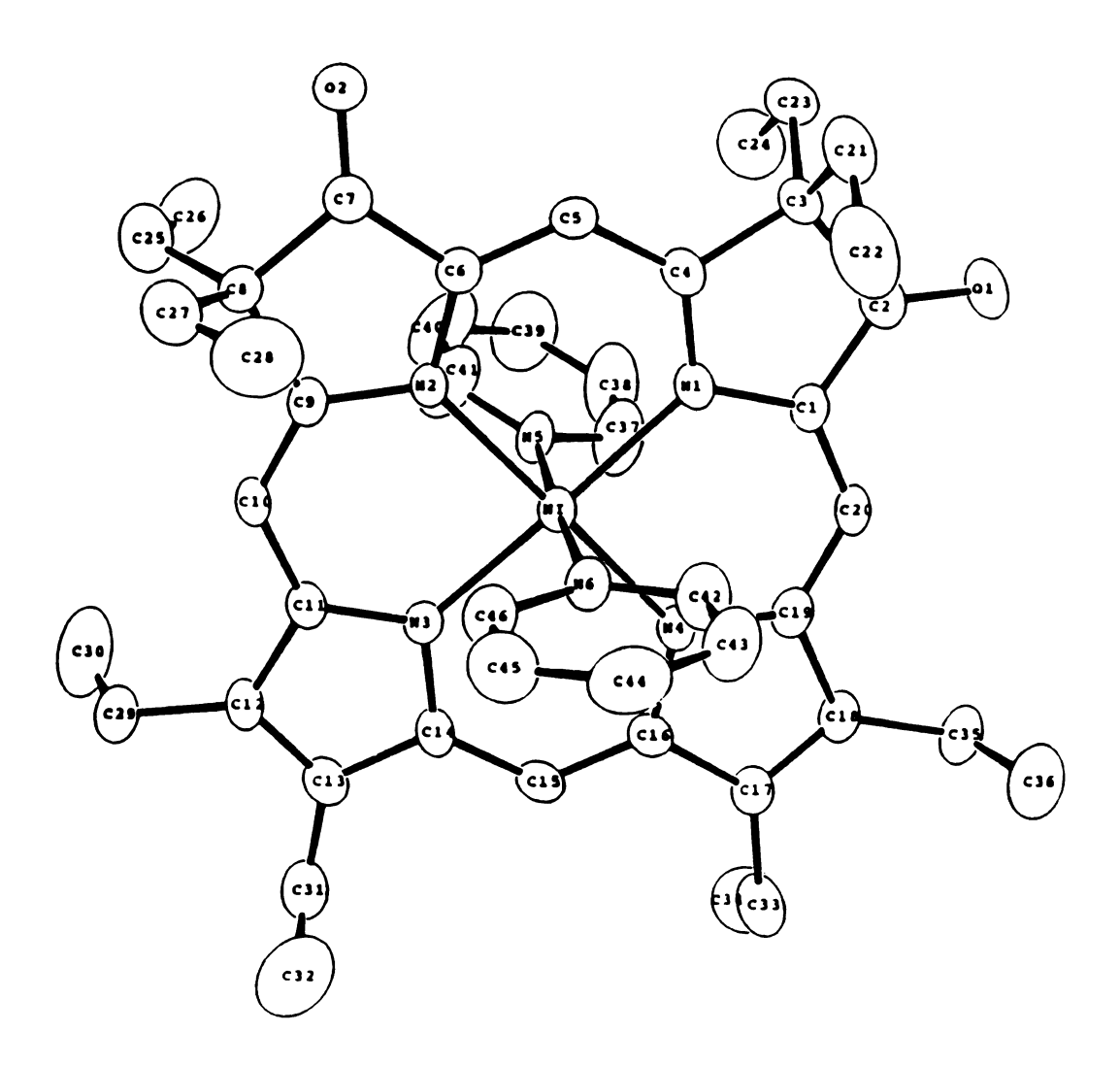


Figure 11. Molecular structure and atom names of Ni(OEP-dione) $(py)_2(III)$. Hydrogens are omitted for clarity. Themal ellipsoids are drawn to enclose 50% probablity.

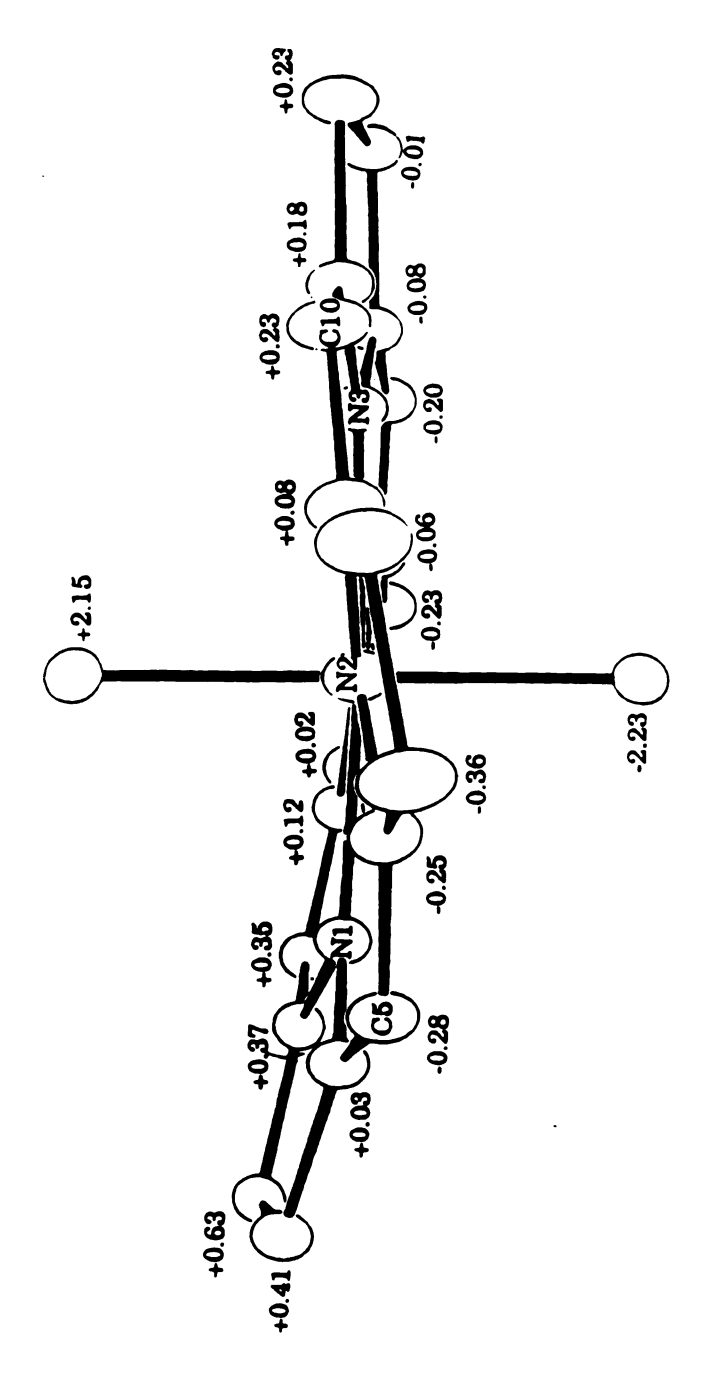


Figure 12. Edge-on view of the skelton of Ni(AcOOEP-trione)(py)2 (II). The deviations of the macrocycle from a plane defined by four nitrogens.

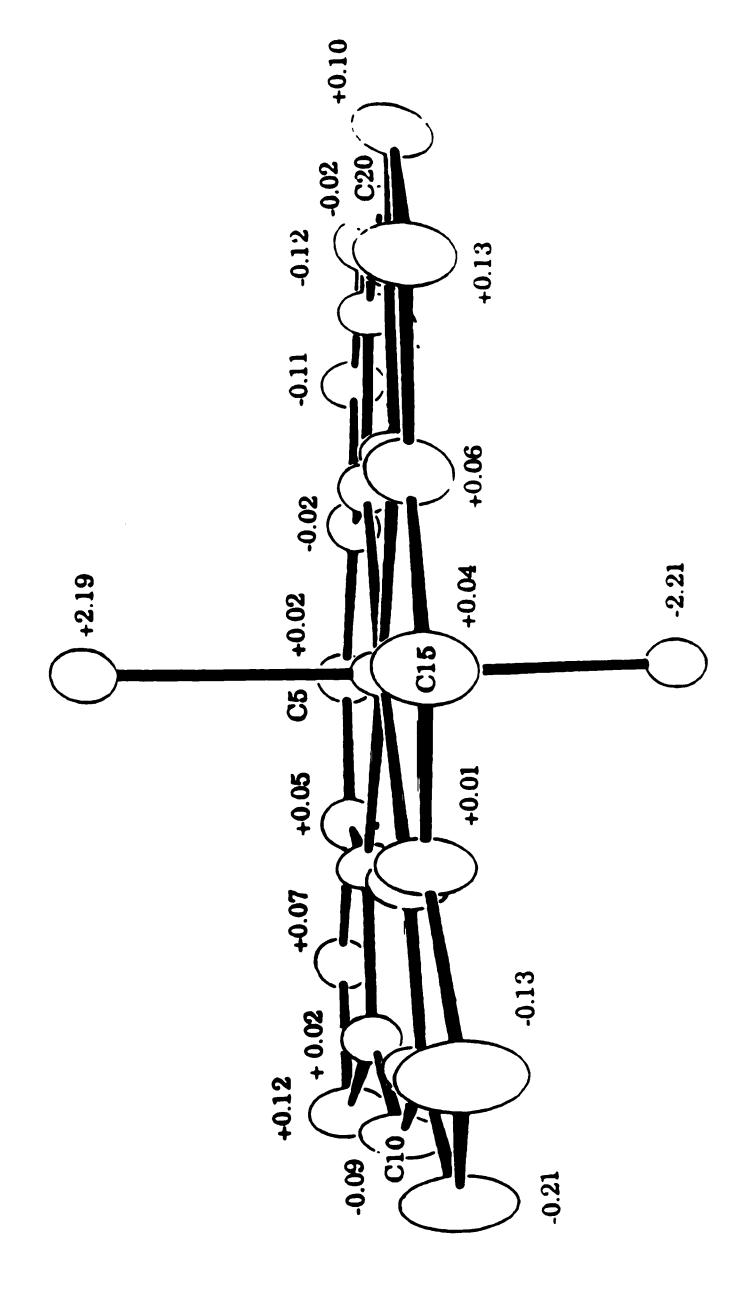


Figure 13. Edge-on view of the skelton of Ni(OEP-dione)(py)2 (III). The deviations of the macrocycle from a plane defined by four nitrogens.

minimize the steric interaction between porphyrin nitrogen atoms and pyridine $hydrogens^{43}$.

The nonplanarity of the macrocycle of II is not as significant as structure I. The meso-carbon atom has displacements from the mean plane, alternating 0.35 Å above and 0.28 Å below as shown in Figure 12. However, the maximum C_{β} atoms of adjacent pyrrole rings are alternatively displaced above and below the macrocycle plane by more than 0.6 Å. The most dramatic difference between complex III and II is that complex III has an almost flat ring gemometry as shown in Figure 13. The average and maximum absolute value of the deviations from the plane are 0.08 Å and 0.21 Å. The methine carbons have small displacements from the mean plane, alternating 0.10 Å and 0.09 Å above and below, respectively.

The electronic configuration is expected to be manifested in the bond lengths of Ni-N⁴⁴. The spin state of Ni(II) change upon axial ligation. The nickel d_x^2 - y^2 orbital is empty in the tetracoordinate complex, however, the addition of two axial ligands to form hexacoordinate complexes II forces one of the d_z^2 electrons into the d_x^2 - y^2 orbital. The presence of this electron should lengthen the Ni-N bond compared to the tetracoordinate complexes. Similarly, the axial Ni-N pyridine bonds are expected to be long, because the unparied electron in the dz^2 orbital.

The diameter of the coordination core, 4.14 Å for structure II and 4.13 Å for structure III (average of the two transannular N, N distances) is distinctly larger than the core size of 3.87Å, for the structure I and 3.91 Å.for Ni(P-dione)⁴¹. The average lengths of the four equatorial Ni-N bonds

is 2.07Å for II and 2.08 Å for III. It closely matches the corresponding values (2.11Å) found in unstrained Ni(II)N₄ octahedral complexes²⁸, and 2.04 Å of bis(imidazole) NiTMPyP⁴³.

The axial nickel-nitrogen bond is free of steric constraints of the porphyrinato core, and is extented somewhat further to 2.190 Å, and 2.20 Å, respectively. These are comparable to Ni-N bonds in other hexacoordinate nickel porphyrinoid complexes, for example, the distance of Ni-N pyrrole bond in bis(imidazole)NiTMPyP⁴³ is 2.160 Å. The Ni-N bond length of the pyridine ligands also agrees well with the the bond length of 2.115 Å in trans-Ni(acac)₂(py)₂⁴⁴.

As noted in structure I, the deformation allows the ligand system to adjust its coordination sphere to the specific requirements of the Ni(II) ion, but at the same time it builds up the conformation strain. Ni(P-dione), with two reduced pyrrole ring compared with structure I, should have less conformation strain. We believed that a process leading to lengthen Ni-N bonds is due to the presence of an electron in the nickel d_x^2 - y^2 orbital, and at the same time the strain energy associated with the saddle deformation could be released upon the axial ligation. As consequence of the longer equatorial Ni-N bonds, the hexacoodinate complex III exhibits an almost flat ring geometry compared with tetracoodinate complex Ni(P-dione). However, the hexacoodinate complex II does show a residue ruffled geometry possibly due to the steric crowd at the methine bridge.

CONCLUSION

In this study, we illustrated the fact that the tendency toward axial ligation in Ni(II) tetrapyrroles does not necessarily correlate with the extent of ring ruffling. The presence of electron-withdrawing substituents is one of the major factors contributing to the increase of axial ligand affinity of nickel porphyrinoids. We also demonstrated that basicity and reduction potentials of free base porphyrinoids provide a quantitative prediction of the ligand binding equilibrium constants. In general, electron-withdrawing or positively charged Ni(II) porphyrinoids favor the formation of hexacoordinate complexes.

A novel tetracoordinate Ni(AcOOEP-trione) complex has been isolated and characterized by single crystal X-ray studies. The structural analysis reveals that Ni(AcOOEP-trione) has a characteristic saddle shaped conformation of most nickel hydroporphyrinoids. Two most significant hexacoordinate nickel(II) porphyrinoids, which were grown in neat pyridine, have been successfully isolated and chracterized. X-ray structure of Ni(AcOOEP-dione)(py)₂ and Ni(OEP-dione)(py)₂ illustrates Ni(OEP-dione)(py)₂ has an almost perfect planar structure, however, Ni(AcOOEP-trione)(py)₂ shows a residue ruffled geometry possibly due to the steric crowd at methine bridge.

EXPERIMENTAL SECTION

1. Materials

com

met

Руг

Sili

(34) ana

2.*P*

spe Inc

FA

ma

3. (

Sys

vol

but rati

4.]

All solvents and regents were of reagent grade, purchased commercially, and used without further purification except mentioned. Pyridine and pyrrolidine were distilled from barium oxide. Toluene and methylene chloride were distilled from calcium hydride shortly before use. Silica gel for column chromatography (60-200 mesh) was from J.T. Baker (3405). Preparative silica gel plates were from Analtech, Inc. For analytical TLC, Eastman 13181 chromatography sheets were used.

2.Physical Measurements

¹H NMR spectra was recorded on a Varian Germini-300 spectrometer, in "100%" chloroform-d (min. 99.96 atom% D, from Isotec Inc.) with the residual CHCl₃ as the internal standard set at 7.26 ppm. FAB mass spectra were obtained on a JEOL HX-110 HF double focusing mass spectrometer operating in the positive ion detection mode.

3. Cyclic voltammetry

All cyclic voltammograms were measured using a Bioanalytical System CV-1A unit in a specieally constructed glass cell. The cell consists of two platinum bead electrodes sealed through the cell wall and a total volume of 0.2 ml. All measurements were carried out in 0.1M tetra-n-butylammonium perchlorate-dichloromethane solution under argon, scan rate 100mVs⁻¹.

4. Preparation of Ni(II)Porphyrinoids

 H_2OEP was synthesized and oxidized with H_2O_2 in concentrated H_2SO_4 according to literature procedures⁴⁵. The crude reaction products were separated to afford H_2OEP , $H_2(OEP\text{-one})$, $H_2(OEP\text{-dione})$, and $H_2(OEP\text{-trione})$. $H_2(MeOEC)$ was prepared from $H_2(OEP\text{-one})$ by reacting with freshly prepared methyl lithium in THF and working up according to literature procedures⁴⁵. H_2TPP and $H_2T(F_5)PP$ were synthesized by the method of Alder et. al^{46} . $H_2(DFDPTMP)$ was prepared as described⁴⁷.

Nickel(II) porphyrinoids were generally prepared in the following method: The free base porphyrin (50mg) was dissolved in a saturated solution of Ni(OAc)2 in 20 ml of DMF containing 2mg NaOAc. The mixture was refluxed under nitrogen and monitored spectrophotometrically until there was no residual Soret band from the starting free base (ca. 30-60 min). The DMF solution was then poured into an ice bath to give microcrystalline precipitates. After filtration the precipitate was redissoved in dichloromethane (20ml) and washed with brine (2x50ml). The organic solution was dried over Na₂SO₄ and the solvent evaporated under reduced pressure. The collected material is allowed to crystallize by slow evaporation of the solvent or recrystallize in a minimum of CH₂Cl₂/CH₃OH to yield shining crystals of microcrystalline material. The yield were 85-95%. All the nickel porphyrinoids were further characterized by ¹H-NMR and high resolution mass spectrometry. The material is stable in the solid form and is stable in solution when protected from light and stored under inert gas.

5. Preparation of Ni(OEP-trione) (4) and Ni(AcOOEP-trione) (5)

2,2,7,7,12,12,17,18-octaethyl-3,8,13-porphinetrione (58.2mg, 0.1mmol) and Ni(OAC)₂·4H₂O (100mg, 0.4mmol) were dissolved in glacial acetic acid (30ml). A trace amount of sodium acetate (5mg) was added and the solution was refluxed for 2h. Dichloromethane (40ml) and water (80ml) were added when the reaction vessel reached room temperature. The nickel complex was extracted into dichloromethane. The mixture was further washed with water (30ml), sat'd. NaHCO₃ solution (30ml), and brine (2x30ml). The organic solution was then dried over Na₂SO₄ and the solvent removed under reduced pressure. The crude product was purified by chromatography (30% hexane/CH₂Cl₂) on a TLC plate and gave the nickel(II)-2,2,7,7,12,12,17,18-octaethyl-3,8,13-porphinetrione (21mg, 33%) followed by the nickel(II)-15-acetoxy-2,2,7,7,12,12,17,18-octaethyl-3,8,13-porphinetrione (36mg, 52%).

Ni(OEP-trione)(4): UV-visible λ_{max} (toluene): nm (ϵ_{M}), 424 (42 000), 626 (11 500), 668 (15 000), 716 (61 200). ¹H-NMR (CDCl₃), 300MHz): d 0.41 (12H, t, CH₂CH₃), 0.52 (6H, t, CH₂CH₃) 1.46, 1,56 (3H each, t, CH₂CH₃), 2.28-2.36 (12H, m, CH₂CH₃), 3.36, 3.39 (2H each, q, sat. CH₂CH₃), 7.90 (1H, s, 10-H), 7.95 (1H, s, 5-H), 7.97 (1H, s, 15-H), 8.75 (1H, s, 20-H). HRMS found: m/z 638.2763 for (M)+, ϵ_{M} C₃₆H₄₄O₃N₄Ni requires m/z 638.2767.

Ni(AcOOEP-trione)(5): UV-visible λ_{max} (toluene): nm (ϵ_{M}), 426 (38 200), 617 (9 600), 658 (11 000), 706 (41 500). ¹H-NMR (CDCl₃), 300MHz): 0.30, 0.32, 0.33, 0.43, 0.52, 0.57, 1.41, and 1.49 (3H each, t, CH₂CH₃), 2.0-2.25 (6H, m, CH₂CH₃), 2.35-2.50 (6H, m, CH₂CH₃), 2.52 (3H, s CH₃CO₂-), 2.70-2.82 (m, 1H, CH₂CH₃), 2.98-3.10 (m, 1H, CH₂CH₃), 3.20-3.42 (m, 2H, CH₂CH₃), 7.70 (1H, s, 10-H), 7.81 (1H, s, 5-H), 8.61 (1H, s, 20-H). HRMS: m/z 696.2856 for (M)+, C₃₈H₄₆O₅N₄Ni requires 696.2822.

6. Preparation of PhOEPNi+ (ClO4)(6)48

To a THF solution of H₂(OEP-one) (22mg, .04 mmol), phenyl lithium reagent (0.5ml of 1.8M in cyclohexane/diethyl ether) was added at room temperature until the solution turned green. The reaction mixture was quenched and washed with water; the organic layer was seperated and evaporated. The crude product was further purified on a silica gel column with 40% hexane/CH₂Cl₂ as eluent to afford 2-hydroxy-2-phenyloctaethylporphyrin (22mg, 81%). After nickel insertion by the methodology discussed above, the Ni complex was further washed by HClO₄ (70%) to yield Ni+(PhOEP)ClO₄- quantitatively.

Ni⁺(PhOEP)(CLO₄⁻)(7): UV-visible λ_{max} (toluene): nm (ϵ_{M}), 406 (27 000), 584 (5 400), 628 (8 600). ¹H-NMR (CDCl₃), 300MHz): d 0.22 (6H, t, CH₂CH₃), 0.85, 0.88 (3H each, t, CH₂CH₃) 1.35 (3H, t, CH₂CH₃), 1.39-1.50 (9H, m, CH₂CH₃), 2.28-2.36 (2H, m, CH₂CH₃), 2.51-2.60 (2H, m, CH₂CH₃), 2.89-3.00 (4H, m, CH₂CH₃), 3.02-3.25(8H, m, CH₂CH₃), 7.85 (1H, s, 10-H), 7.87 (1H, s, 5-H), 7.91 (1H, s, 15-H), 7.96 (1H, s, 20-H). HRMS found: m/z 667.3311 for (M)⁺, C₄₄H₄₉N₄Ni requires m/z 676.3330.

7. The basicity of Porphyrinoids

To the anionic SDS detergent solution (2.5% sodium dodecyl sulfate with fixed pH value), a small quantity of porphyrinoids in CH₂Cl₂ was added. The mixture was stirred vigorously until the colored porphyrinoids solution became homogenerous (if not soluble, the mixture was adjusted to a lower pH value to enhance solublility in micelles). pK₃ values were measured on a Cary 219 spectrophotometer by monitoring the absorbance of

pH at five different wavelengths. However, if the pK₃ was lower than 1.5 the pH value of the micelle solution was hard to control precisely. Thus, a series of organic acids were chosen as acidic benchmarks to approximate the pK₃ of the porphyrinoid. The acids used were CH₃COOH (pK_a 4.75), HCOOH (pK_a 3.75), ClCH₂COOH (pK_a 2.86), Cl₂CHCOOH (pK_a 1.26), CCl₃COOH (pK_a 0.64), and CF₃COOH (pK_a .23).

8. Spectrophotometric Titrations

Typical ligand binding titrations were performed in toluene. The concentration of Ni(II) porphyrinoids were approximately 10-5 M and ligand concentrations were varied over as a wide range as posssible. Data were collected typically at six to eight different concentrations on Cary 219 spectrophotometer. The equilibrium constants Keq for the formation of pyridine or pyrrolidine adduct(s) of Ni(II)porphyrinoids have been determined by the method of Walker and coworkers^{33f}; the data analysis was verified by the method of Bent and French⁴⁹.

9. Crystallography

Crystals of Ni(AcOOEP-trione) (I) suitable for x-ray study were grown by the slow diffusion of hexanes into a methylene chloride solution. Crystals of Ni(AcOOEP-trione)· C_6H_{14} were obtained. Ni(AcOOEP-dione)(py)₂ (II) and Ni(OEP-dione)(Py)₂ (III) were crystallized from pyridine to afford (NiC₄₆H₅₄N₆O₂)· C_5H_5 N and (NiC₄₈H₅₆N₆O₅)· C_5H_5 N, respectively. Although the crystals appears air-stable, they were covered with thin coats

of epoxy resin to prevent losing hexane or pyridine solvent molecules before mounting on a glass fiber for x-ray single-crystal structure analysis.

The X-ray structural determinations were carried out at the Department of Chemistry, National Taiwan University, in collaboration with Professor Shih-Ming Peng. The data were collected on a Nonius CAD-4 diffractometer with graphite-monochromated Mo K α radiation in the scane range. Accurate unit cell parameters for all the compounds were obtained from the least-squares refinement on the 2ϕ , ω , ψ and θ values of 25 machine-centered reflections. The stability of the experimental setup and crystal integrity were monitered by measuring three standard reflections periodically during the course of data collection. No crystal decay was detected, the raw data were reduced to net intensities. Empirical absorption convertions (π scan) were applied and the equivalent reflections were averaged. In all compounds the hydrogen atom positions were calculated and were included in the structure factor calculations but were not refined.

CHAPTER II

SYNTHETIC MODELS FOR ASSIMILATORY NITRITE RESUCTASE.

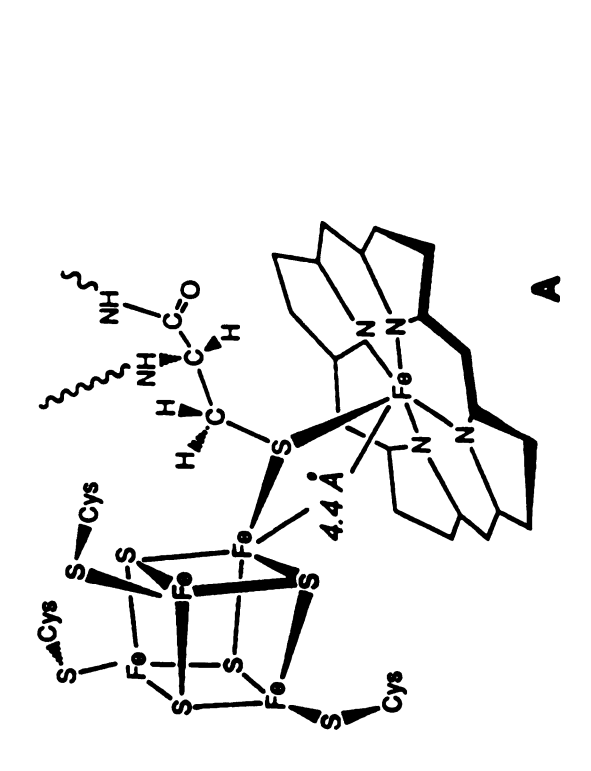
INTRODUCTION

On a global scale, it is estimated that more than 10 billion tons of nitrogen are incorporated into plants annually⁵⁰. Apart from a relatively small number of species that have a symbiotic association with nitrogen-fixing bacteria^{15,16,51}, the bulk of the plant nitrogen arises from the reduction of nitrate taken from soil. Studies have shown that assimilatory nitrite reductase has two metal cofactors, a Fe₄S₄ cluster and an iron isobacteriochlorin named siroheme (Figure 14). Siroheme is the active site where NO₂- interacts and receives electrons derived photosynthetically via an electron transport chain consisting of chlorophyll-->NADPH-->FAD-->FMN-->siroheme¹⁰⁻¹². The ability of this enzyme to mediate the 6-electron reduction of NO₂---> NH₄+ without releasing any intermediate is remarkable. Siroheme is also found in assimilatory/dissimilatory sulfite reductase⁵². That these 2 enzymes can often reduce both substrates^{10,11} suggests that they have common structural and mechanistic features.

Owing to the now classic investigations of Siegel and coworkers, E. Coli. sulfite reductase (EcSiR) (which also reduce NO_2 -) is the best understood of these enzymes. The enzyme is a complex hemoprotein (Mr = 685,000) with an $\alpha_8\beta_4$ subunit composition⁵². Spectroscopic investigations^{22,53} of the catalytically-active β subunit of this enzyme indicated that siroheme and an Fe₄S₄ cluster are exchange-coupled. This coupling is maintained at all levels of oxidation states (shown in Table 7), implicating the presence of a common bridging ligand. The active site structure from X-ray analysis⁵⁴ is depicted schematically in Figure 14, with a 4.4 Å separation between the siroheme iron atom and the nearest iron



90 HOO



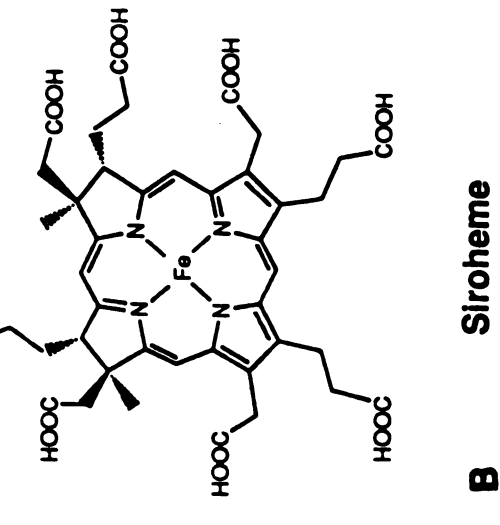


Figure 14. (a) Schematic description of the bridging cofactors, Fe₄S₄ cluster and siroheme of nitrite/sulfite reductases. (b) The structure of siroheme.

Table 7. The Various Oxidation States of E. Coli Sulfite/Nitrite Reductase

State	cluster	siroheme
oxidized (SiR ⁰)	$[Fe_4S_4]^{2+}$ $(S=0)$	Fe(III), $S = 5/2$ (as isolated) $S = 1/2 (SO_3^{2}, CN^{-})$
<pre>semireduced (SiR¹-)</pre>	$[Fe_4S_4]^{2+}$ $(S=0)$	Fe(II), $S = 1$ or 2 S = 0 (CN ⁻ , CO)
<pre> reduced (SiR²⁻) (catalytic)</pre>	$[Fe_4S_4]^{2+}$ $B = 2.53, 2.29, 2.07$	Fe(II), $S = 1$ or 2
	g = 5.1, 2.6, (4.9, 3.3, 2.1) g = 2.03, 1.93, 1.91	Fe(II), $S = 0$ (CO, CN', S^2)

atom in the cluster. The bridging ligand is most likely a cysteinyl sulfur atom; however, crystallography at 3.0 Å resolution is not sufficient to reveal the identity of the bridge. This view has recently been challenged on the basis of a study of a dissimilatory sulfite reductase from *Desulfovibrio vulgaris* $(D_v \operatorname{SiR})^{55}$. The ligand bridging the $[F_4S_4]$ -siroheme cluster is apparently exchanged by $^{35}S^{-2}$ in both oxidized and reduced enzyme. No X-ray structural data are available for these enzymes.

A simple and attractive picture of substrate reduction by Ec SiR involves (i) substrate binding at the vacant axial site of siroheme, (ii) coupled steps of electron transfer from cluster to substrate, and (iii) protonation until sulfide is formed. The electron-transfer pathway may involve the bridge, or possibly pass directly to siroheme. From electron density maps, the Fe₄S₄ cluster and periphery of the siroheme ring appear at or near van der Waals contact¹⁴.

Synthetic models of protein-active sites have provided valuable information concerning catalytic principles and structure-function relationships of many metalloproteins. As the structural features of the active site of sulfite/nitrite reductases are now available, it becomes timely to construct models for these redox centers. Only recently has an initial approach to the synthesis of biologically bridged assemblies been reported by Holm $et\ al^{56}$.

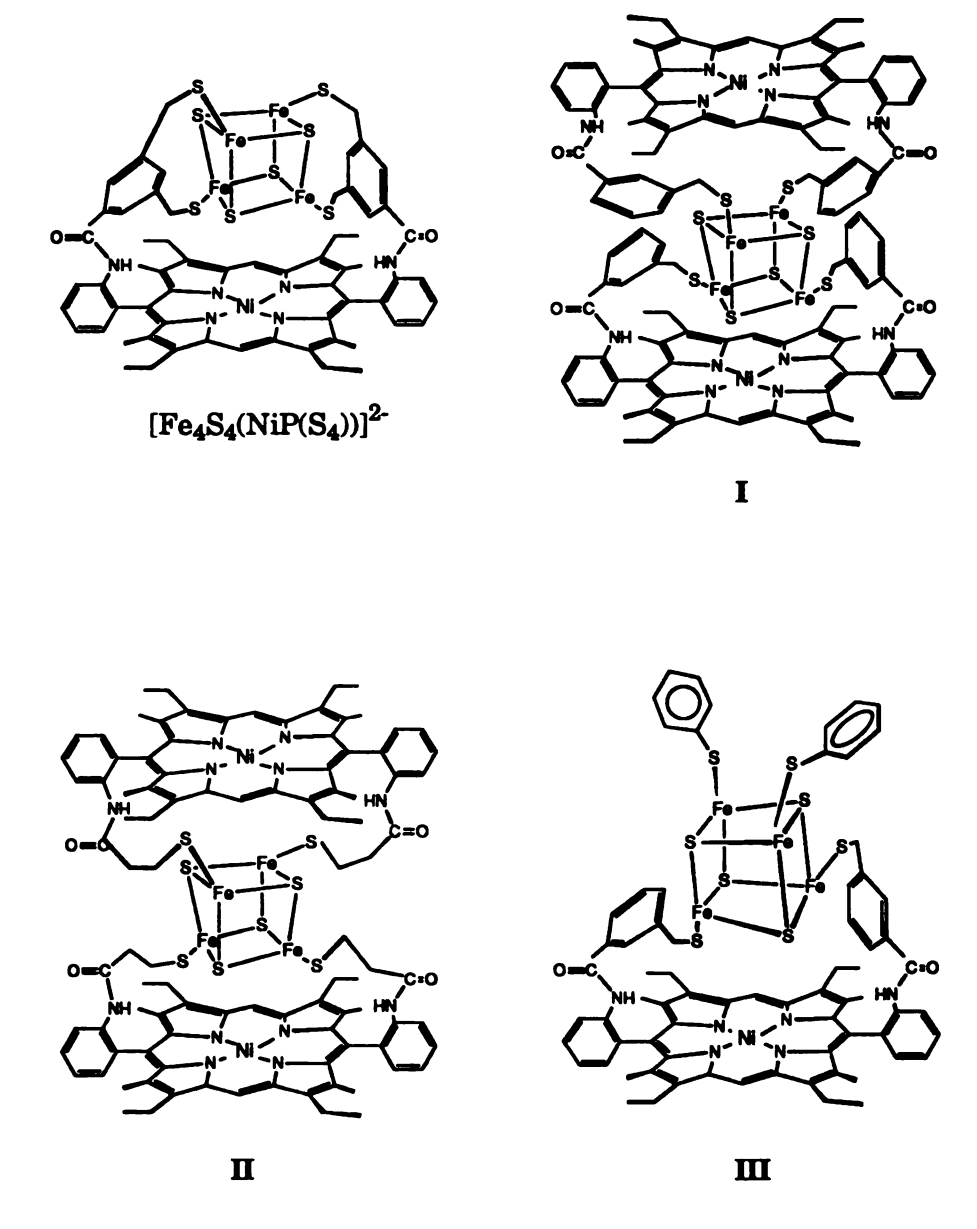
Here we describe our efforts in persuit of an active site model of the siroheme-dependent nitrite reductase. The present systems are not necessarily intended as true structural models of the native [Fe₄S₄]-

siroheme assembly. Rather, we demonstate the design to synthesize appropriately tailored porphyrin-based ligands to achieve particular Fe₄S₄-nickel porphyrin configurations.

RESULTS AND DISCUSSION

1. Ligand Design

Our aim was to synthesize appropriately tailored porphyrin macrocycles equipped with thiol ligands capable of attaching to Fe₄S₄ units. Specifically modified porphyrins with appended thiols such as NiP(S₄) are designed to achieve Fe₄S₄-heme linkages (Scheme I). Nickel porphyrin tetrathiol ligand 7a was thought to be well-suited in achieving our goal because (i) they are synthetically practical⁵⁷; (ii) the appended thiols are placed in proper arrangement to span Fe--Fe distances in the Fe₄S₄ cube and hold it in close proximity to the macrocyclic metal center; (iii) extrusion of Fe₄S₄ core with similar thiols, i.e. m-xylyl dithiol has been demonstrated by Holm et al^{58} . The model compound provides a full complement of thiolato ligands and is expected to hold the Fe₄S₄ center with maximum stability, as shown in the structure [Fe₄S₄(NiP(S₄))]²- of scheme I. In connection to this approach, we also prepared some bidentate thiol ligands. such as NiP(SAc)₂ (7b) and NiP(SAc)₂ (7c), as well as two meso-substituted porphyrin nickel complexes (21a and 21b), which provide a monodentate thiol function. These thiol ligands would be able to link themselves to the Fe₄S₄ cluster in various configurations as depicted by the structures I, II, and III in Scheme I.



Scheme I

2.

3,

Yo

is

ar de

a

tł c:

7 C

Ţ

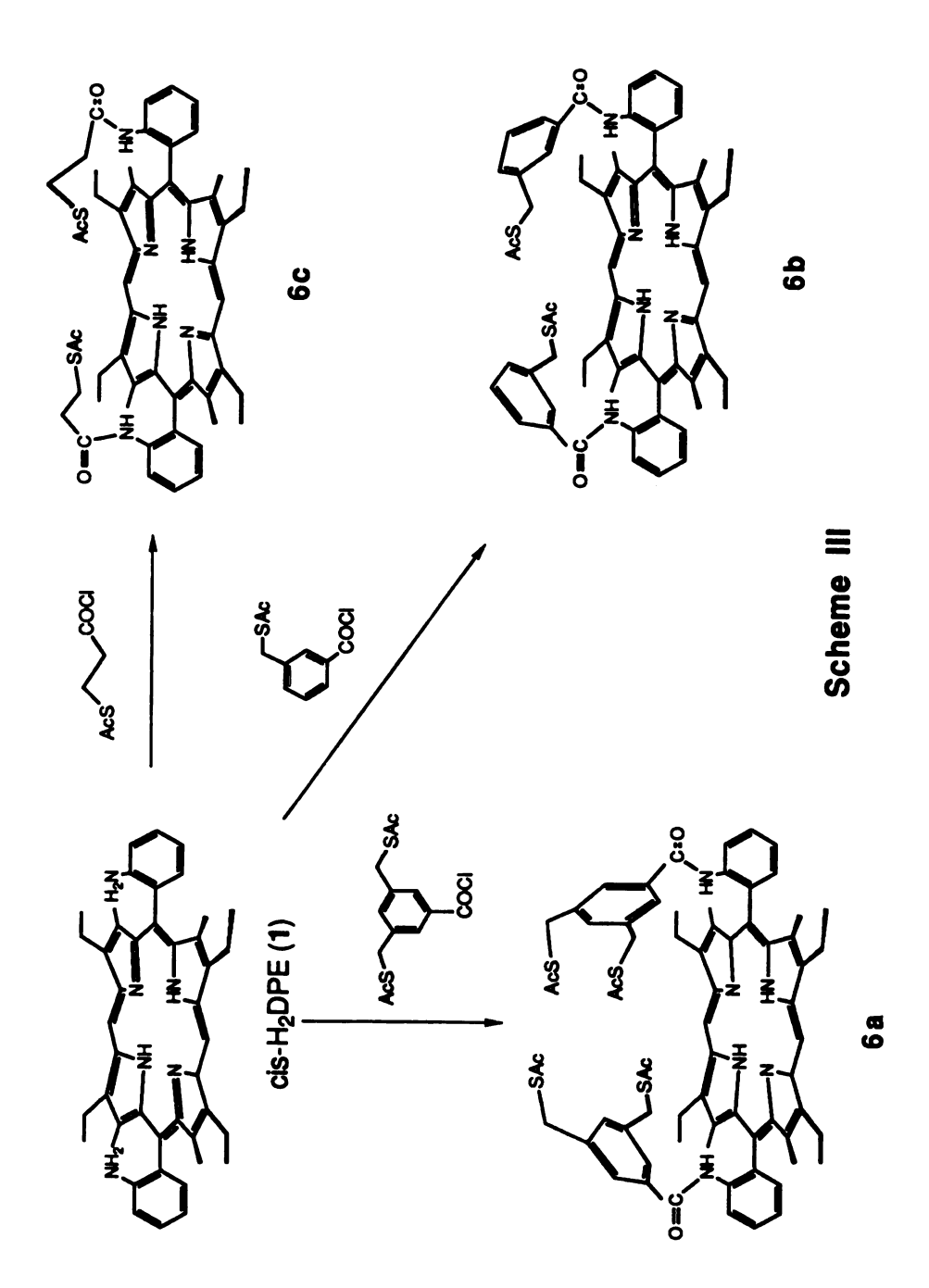
ń

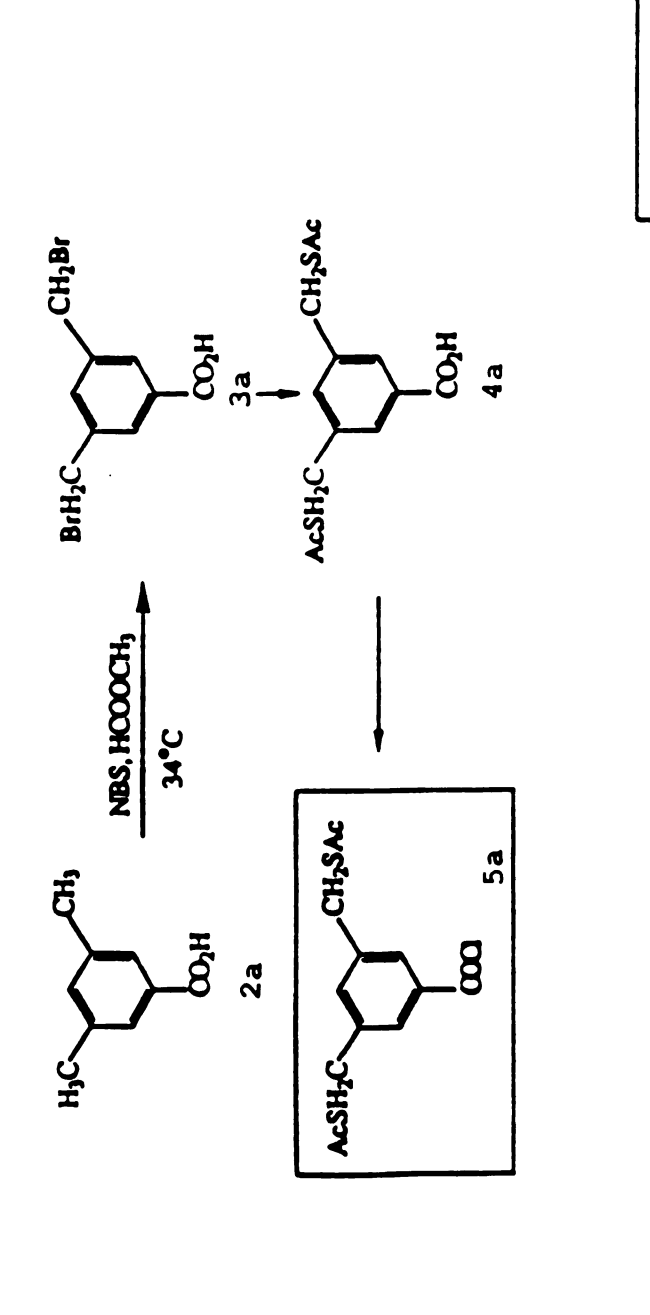
2. Synthesis of appended nickel porphyrin-thiol ligands

The key ligand precursor bis(o-aminophenyl)-2,8,12,18-tetraethyl-3,7,13,17-tetramethyl prophyrin(NH₂)₂DPE(1) was obtained as a mixture of cis and trans isomers via the procedure shown in Scheme II, published by Young and Chang⁵⁷. After seperation of the mixture of cis and trans isomers, thermal atropisomerization of the trans isomer in a manner similar to that reported by Lindsey⁵⁹ allowed isolation of more pure cis isomer (1).

The strategy for the preparation of the appended porphyrin-thiol ligands is depicted in Scheme III. Attachment of sulfur-containing appendages to the o-amino group was accomplished with acid chloride derivatives (5a-5c) bearing thiol-acetates. As shown in Scheme IV, the acid chlorides were freshly prepared by treating SOCl2 with the corresponding acid: 3,5-bis(thioacetoxymethyl)-benzoic acid (4a), 3-(thioacetoxymethyl) benzoic acid (4b), and 3-thioacetoxypropionic acid (4c), respectively. Thus, the appended porphyrin thiol derivatives 6a-6c were synthesized by treating cis-(NH₂)₂OPE(1) with the corresponding acid chloride in the presence of N(Et)₃. The desired compounds **6a-6c** can be obtained in excellent yields: 72%, 58%, and 67% respectively. The IR spectrum exhibits an amide carbonyl stretching at 1670-1680 cm⁻¹. The ¹H NMR spectra readily demonstrate the presence of ligation to the o-aminophenyl substituents. Detailed assignments of proton resonances of complexes 6a-6c are listed in Table 8. The upfield shift of the terminal CH_3COS indicated that the appended thioacetoxy functional group is within the shielding porphyrin ring current. A particularly useful information in the ¹H NMR spectra of

Scheme II





Scheme IV

Table 8. ¹H NMR (8) Assigments for Free Base Porphyrins (6a-6c) and Nickel Porphyrins (7a-7c)(300MHz, CDCl₃).

Positon		MP(SAc)4		MP(SAc) ₂		MP(SAc) ₂	
		$M= H_2$	Ni	$ m H_2$	Ni	H_2	Ni
NH		-2.30, s		-2.40, s		-2.51, 8	
COCH ₃		1.53, s	1.78, s	1.56, s	1.75, s	1.43, s	1.56, s
Ethyl	sat.	1.75, s	1.57, 8	1.80, s	1.58, s	1.76, s	1.65, s
	unsat.	4.01, q	3.67, q	4.03, q	3.67, q	4.01, q	3.73, q
Methyl		2.58, s	2.30, 8	2.61, s	2.31, 8	2.52, в	2.28, 8
CH_2S		2.70, s	3.06, s	2.86, s	3.11, s	1.58, s	1.96, 8
$-CH_2$						2.59, s	2.69, в
Ar'		6.11, d	6.10, d	6.29-6.38, m	6.45, d		
		6.46, d	6.31, d	6.43, d	6.53-6.56, m		
				6.66, d	6.84, d		
NHCO		7.77, 8	8.04, 8	7.93, в	8.14, 8	6.85, в	7.22, 8
		7.60, t	7.57, t	7.56, t	7.42, t	7.52, t	7.37, t
		7.72, t	7.82, t	7.80, t	7.49, t	7.84, t	7.44, t
		8.01, d	8.90, d	9.01, d	7.81, d	8.75, d	7.74, d
		8.91, d			8.94, d		8.68, d
meso-H		10.26	9.55	10.27	9.54	10.27	9.49

these types of compounds is the *meso*-proton of porphyrins which is typically well-seperated from other signals. The chemical shift of the meso proton can be diagnostic of the type of complex; while the number of signals in this region gives an indication of the purity of the sample. In the free-base ligand, such as **6a**, the *meso* proton appears at 10.27 ppm. The UV-visible spectrum exhibits a Soret band at 408 nm and four visible bands at 508, 542, 577, 627 nm.

To prepare nickel porphyrins, free base porphyrin (6a-6c) in CHCl₃ was treated with freshly prepared methanolic solutions of Ni(II) ions to give nickel complexes NiP(SAc)₄(7a), NiP(SAc)₂(7b), and NiP(SAc)₂(7c), respectively. After 4-6 h of heating at reflux, the UV-visible spectra of the reaction mixtures showed that the four bands of the free base collapsed to a two band pattern, which signals the completion of metal insertion. FAB mass spectra of the complexes exhibit the expected molecular ion cluster peaks for nickel complexes. Further evidence for the insertion is derived from ¹H NMR spectrum, for example, NiP(SAc)₂(7b) in Figure 15. The proton resonances of internal pyrrole NH are no longer present in the NMR spectra. Interestingly, the purity of the nickel complexes could be readily ascertained by a dramatic high-field shift of the single meso-proton resonance from 10.27 to 9.45 ppm.

3. Synthesis of mono-substituted Porphyrin Thiol Ligand

As shown in Scheme V, the key ligand precursor, biladiene-ac dihydrobromide (8) was prepared by condensation of 3,3'-diethyl-5,5'-diformyl-4,4'-dimethyldiprromethane and 3,4-diethylprrole via the



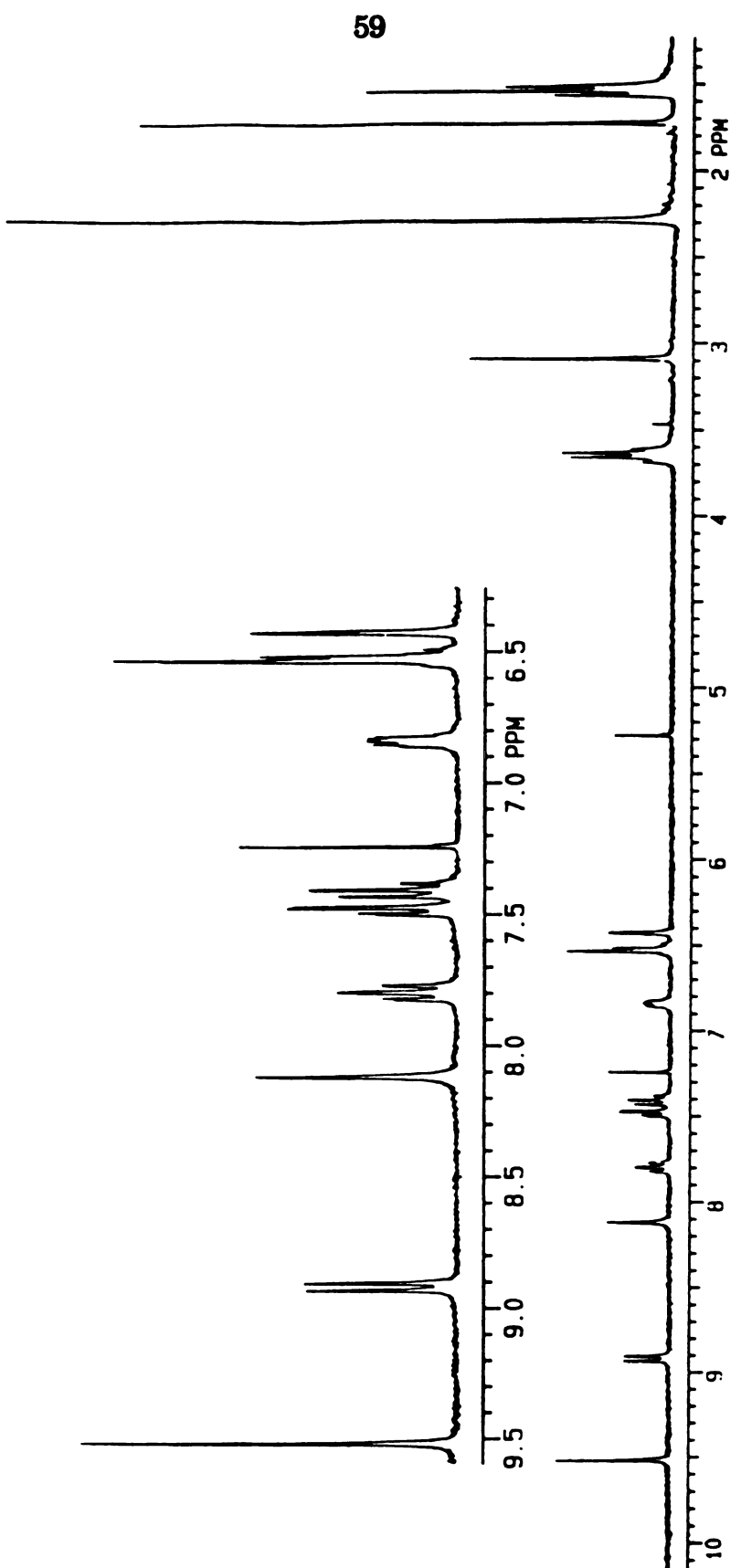
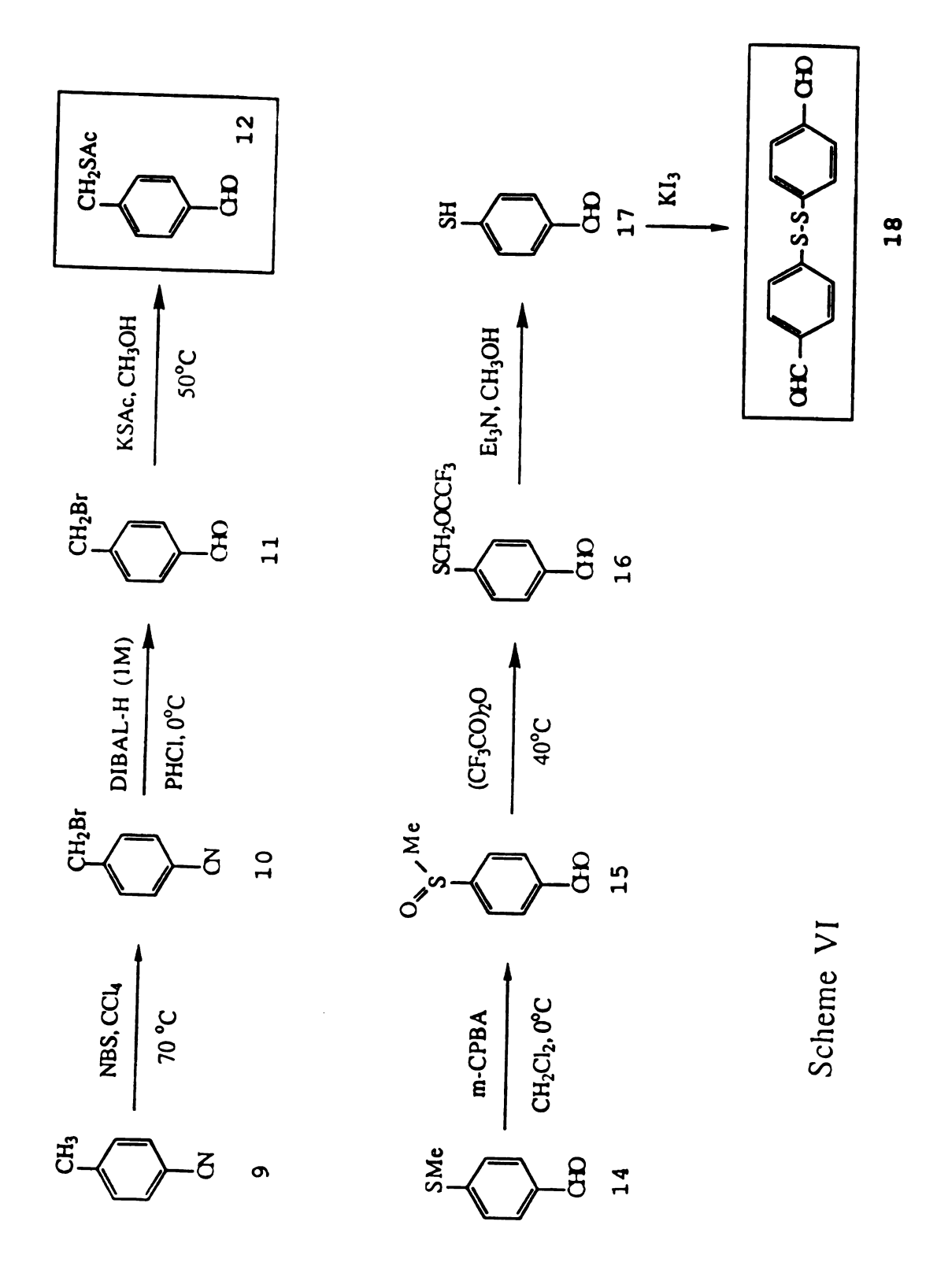


Figure 15. ¹H NMR spectrum (300 MHz, CDCl₃) of NiP(SAc)₂(7b), Me₄Si peak is not shown.



procedures developed by Johnson and Kay⁶⁰. The strategy for the preparation of mono-substituted porphyrin thiol ligand is based on the method of condensing linear tetrapyrrole and aldehydes bearing a thiol function⁶¹. p-Thioacetoxymethylbenzaldehyde(12), obtained in three steps from the a-bromo-p-tolunitrile (9) (Scheme VI)⁶², was allowed to react with ac-biladiene (8) to afford 5-(p-thioacetoxyphenyl)-etioporphyrin. Similarly, 4,4'-diformydiphenyl disulfide (17) obtained in four steps from 4-(methylthio)benzaldehyde (14)63, was reacted with ac-biladiene (8) to afford the disulfides. All of these porphyrins were converted to nickel (II) complexes to give NiPSAc (13), (NiPS)₂ (19), and NiPS₂ (20) which were formed in high yield from the corresponding free base porphyrin by the reaction of methanolic nickel acetate. The UV-visible spectra of 13, 19, and 20 exhibit a Soret band at 403 nm and two visible bands at 526, 561 nm. The ¹H NMR spectrum of nickel porphyrin(13) (Figure 16a) demonstrate the presence of the thioacetoxymethyl phenyl group. For example, proton resonance of CH_3COS centered at 2.5 ppm and CH_2SAc at 4.43 ppm. Again, the chemical shift of the meso proton can be diagnostic of these porphyrins. The chemical shift and their integration of two different meso-protons gives an indication of the purity of the compound 13., (e.g. 15-H at 9.51 ppm, and 10H, 20H at 9.58 ppm., respectively). Detailed assignments of proton resonances of nickel porphyrins 13, 19, and 20 are listed in Table 9. FAB-MS data also provided the expected molecular ion peaks for nickel complexes.

The removal of the acetyl group from Ni(PSAc)(13) was readily achieved to afford NiPSH(21a) by treating with 3N HCl in methanol/CHCl₃.

1H NMR spectroscopy (Figure 16b) demonstated the proton resonance of SH

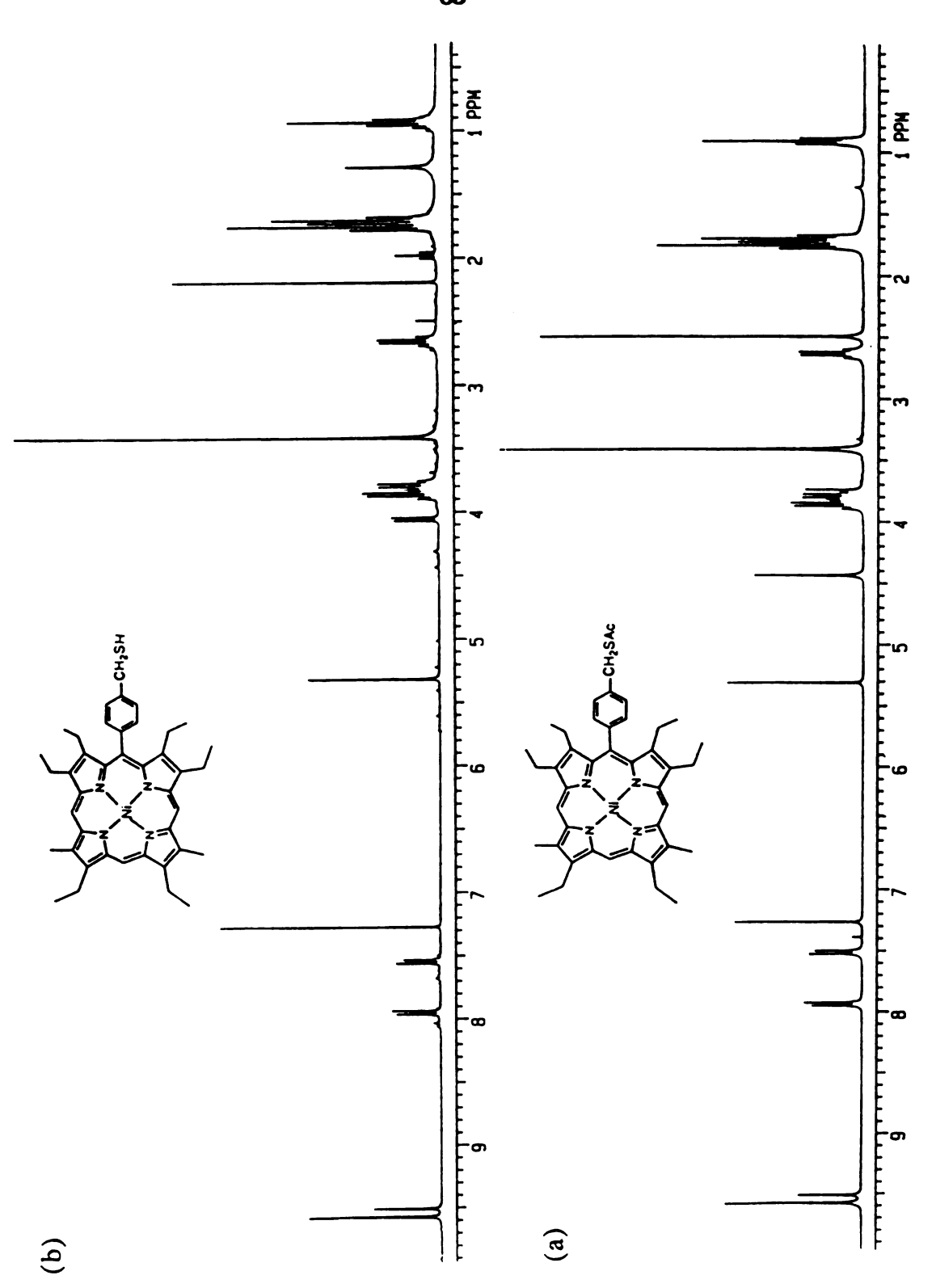


Figure 16. ¹H NMR spectrum (300 MHz, CDCl₃) of (a) NiPSAc (18). and NiPSH (21a).

Table 9. ¹H NMR (8) Assignents of NiPSAc(13), NiPS₂(19), (NiPS)₂(20) and NiPSH(21a), NiPSH(21b) (300MHz, CDCl₃).

	NiPSAc (13)	$NiPS_2(19)$	$(NiPS)_2(20)$	NiPSH (21a)	NiPSH (21b)
CH_3CH_2	0.91, t	0.97, t	0.86, t	0.92, t	0.91, t
CH_3CH_2	1.70, t; 1.76, t	1.66, t; 1.75, t	1.68, t; 1.74, t	1.70, t; 1.76, t	1.70, t; 1.76, t
CH_3 CO /or	2.49, s				
SH				1.98, t	3.50, в
CH_3CH_2	2.63, q	2.71, q	2.62, q	2.65, q	2.69, q
0 - CH_3	3.41, 8	3.40, s	3.36, в	3.40, s	3.40, в
$CH(OCH_3)_2$			3.39, в	3.80, q	3.78, q
CH_2CH_3	3.74-3.84, m	3.26, q; 3.86, q	3.77,q; 3.84, q	3.86, q	3.82, q
$CH_2 \mathrm{SAc}$ /or	4.44,8				
CH_2SH					
$CH(OMe)_2$			5.44, d	4.05, d	
Ar	7.51,d; 7.93, d	7.90, d; 8.08, d	7.49, d; 7.65, d	7.51, d; 7.93, d	7.49, d; 7.90, d
			7.76, d; 7.94, d		
meso-H(15-H)	9.51, s	9.51, s	9.49, s	9.51, s	9.50, s
10-H & 20-H	9.57, 8	9.57, 8	9.55, в	9.57, s	9.57, s

at 1.98 ppm, as well as the chemical shift of methylene at 4.05 ppm. In order to prepare NiPSH(21b) from disulfide complexes 19 and 20, reduction was performed with NaBH₄. Again, ¹H NMR spectroscopy revealed the proton resonance of SH at 3.5 ppm. FAB-MS data provided the expected molecular ion peaks for both compounds.

4. Synthesis of Iron-Sulfur Clusters

The synthesis of all iron-sulfur cluster complexes were carried out under strictly anaerobic and moisture-free conditions. The synthesis of [Fe₄S₄Cl₄]²- clusters has been reported previously by a simple spontaneous self-assembly process as shown in equation 3⁶⁴.

$$2FeCl_2 + 3KSPh + (Bu_4N)Cl \text{ or } (Ph_4P)Cl + 5S --> [Fe_4S_4Cl_4]^{2-}$$
 (3)

The synthesis of the [Fe₄S₄(SPh)₂Cl₂]²- cluster is readily accomplished by the stoichiometic reaction between [Fe₄S₄Cl₄]²- and PhS- ligands shown in equation 4⁶⁵.

$$[Fe_{4}S_{4}Cl_{4}]^{2-} + 2KSPh ---> [Fe_{4}S_{4}(SPh)_{2}Cl_{2}]^{2-} + 2KCl \qquad (4)$$

The successful isolation of these clusters from equilibrium mixtures of $[Fe_4S_4(SPh)_nCl_{4-n}]^{2-}$ is attributed mainly to the crystallization characteristics of the $(Ph_4P)^+$ salts that are relatively insoluble in the solvent used.

5. Preparation of the Ni-Porphyrinyl-Fe₄S₄ assemblies

To connect an Fe₄S₄ cluster with nickel-porphyrin thiol ligands, various types of complexes can be conceived. During the course of two years, we attempted ligand exchange reactions using the deprotected NiP(SAc)_n 7a-7c, (n=4, or 2), the monothiol NiPSH (21a-21b) and the Fe₄S₄ clusters with either halide ligands(22-24) or mixed ligand [Fe₄S₄(SPh)₂Cl₂]²-(25) as starting materials. Unfortunately, despite repeated efforts, this approach to the most desired assembly Fe₄S₄-NiP(S₄) was unsuccessful. The results described here focus on the preparation and the characterization of assembly complexes I-III (shown in Scheme I).

(i) Deprotection (Deacetylation). The removal of the acetyl group of NiP(SAc)₂(7b or 7c) was readily achieved under basic conditions. Generally, a slightly excess amount of freshly prepared NaOMe was added into a NiP(SAc)₂-DMF solution (eq 5),

$$NiP(SAc)_2 + 2 NaOMe \longrightarrow (Na^+)_2[NiP(S)_2] + 2AcOMe$$
 (5)

the mixture was kept at room temperature for ca. 3h with stirring. The resultant thiol groups are susceptible to oxidation to form disulfide, thus, all manipulations were carried out under nitrogen. The sodium salts were not isolated for characterization and used freshly for the ligand exchange reaction.

(ii) Ligand exchange reaction. In order to synthesize the $[Fe_4S_4(X)_4]_{2n}(NiP(S_2)_n]^{2-}$ clusters, the deprotected $NiP(S_2)$ was first prepared by a simple metathetical reaction which was performed in DMF (eq 6),

all ma

[

dropwi

precipi

produc Two c

Schem

Consec

succes

[(Na)₂[

[Fe₄S₄

6. Cho

major

ray di

becaus

a Infr

$$[Fe_{4}S_{4}Cl_{4}]^{2-} + n((Na)_{2}[NiP(S)_{2}] \longrightarrow$$

$$[Fe_{4}S_{4}Cl_{4-2n}(NiP(S)_{2})_{n}] + 2nNaX \qquad (6)$$

$$n = 1, 2$$

all manipulations were carried out under nitrogen. The freshly prepared DMF solution of $(Na)_2[NiP(S)_2]$ is added into a Fe₄S₄ clusters-DMF solution dropwise keeping the mixture at 50-60°C for 6h. The product was then precipitated by the addition of a THF/ diethyl ether mixture. In general, the product was further purified by re-precipitation from DMF/ether twice. Two classes of nickel-porphynyl-Fe₄S₄ clusters (I and II)(as shown in Scheme I) were obtained in relatively low yield (< 30%) as reddish powder. Consequently, an assembly complex $[Fe_4S_4(SPh)_2(NiP(S_2))]^{2-}$ (III) was successfully prepared by treating $[Fe_4S_4(SPh)_2Cl_2)]^{2-}$ with 1 eq. $[(Na)_2[NiP(S)_2]$ as shown in eq 7.

$$[Fe_4S_4(SPh)_2Cl_2)]^{2-} + [(Na)_2[NiP(S)_2] \longrightarrow$$

$$[Fe_4S_4(SPh)_2(NiP(S)_2)]^{2-} + 2NaX \qquad (7)$$

6. Characterization of the Ni-Porphyrinyl-Fe₄S₄ Assembly

In the course of our work, both IR and ¹H NMR spectra provided the major evidence of the formation of nickel-porphyrinyl-Fe₄S₄ assemblies. X-ray diffraction quality crystals of the products have not been obtained, because the possibility of polymer formation cannot be completely ruled out.

a. Infrared Spectroscopy

The most useful diagnostic features that differentiate iron sulfur clusters and the assembly complexes are found in the far-infrared spectra, exemplified in Figure 17. The skeletal vibrations of the clusters result in absorption bands with distinct energies and profiles that make it possible to distinguish III with weak vibrations at 349 and 362 cm⁻¹ from [Fe₄S₄(SPh)₂Cl₂]²- at 339, 356, 371, and 383 cm⁻¹. Especially interesting is the disappearance of 356 cm⁻¹ corresponding to an Fe-Cl vibration band. In the mid-IR region, features corresponding to (Ph₄P)+ cation ion at 529, and 534 cm⁻¹ further give evidence of the existence of complexes (III) in the solid state. The feature of NHCO at 1670 cm⁻¹ and the other vibrational modes corresponding to nickel porphyrin were not shown in Figure 17.

b. ¹H NMR spectroscopy.

Selected assignments of proton resonances of complexes I-III are listed in Table 10. The isotropic shifts of the methylene protons of S-CH₂ group centered ca. 13-15 ppm, can be diagnostic of the formation of nickel-porphriynyl-Fe₄S₄ assembly complexes. The integrations of the methylene protons, however, demonstrate that the equilibria intervene in the solution behavior; various components could present in the solution such as $[NiP(S_2)_2-Fe_4S_4]^{2-}$, and $[NiP(S_2)-Fe_4S_4Cl_2]^{2-}$ (according to reaction 6).

The ¹H NMR spectrum of complex (III), Figure 18, deserves more discussion. In general, chemical shifts corresponding to the two portions of the assembly, the cluster and nickel porphyrin, are satisfactionly identified.

(i) Clusters. The phenyl ring proton resonances of the mixed terminal ligand "cubane" clusters, [Fe₄S₄(SPh)₂NiP(S₂)]²- show isotropic shifts

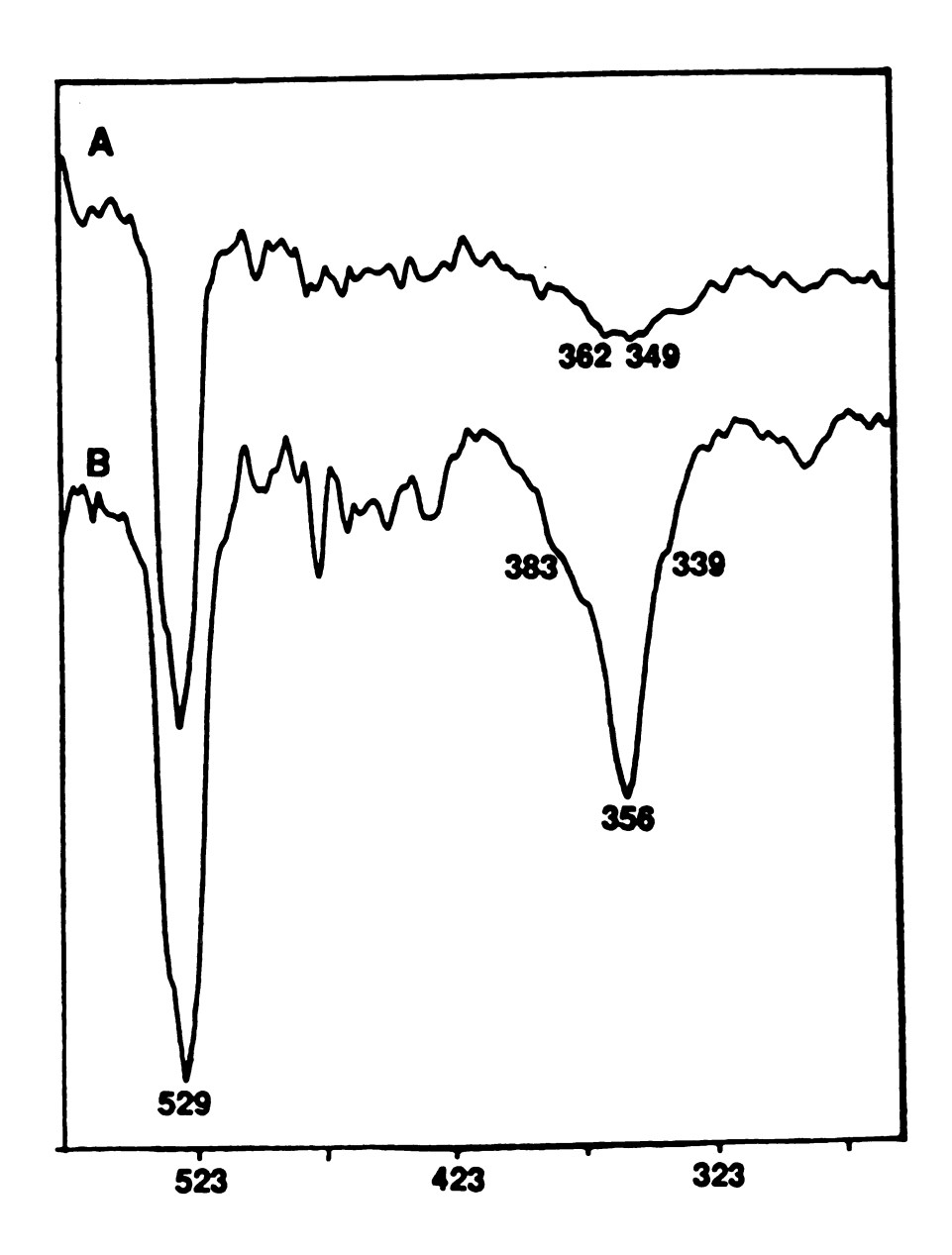


Figure 17. Far-infrared spectra of (a) $(Ph_4P)_2[Fe_4S_4(SPh)_2(NiP(S_2))]$ and (b) $(Ph_4P)_2[Fe_4S_4(SPh)_2Cl_2]$. The vibration mode at 529 cm⁻¹ corresponds to the aromatic C-H bending of Ph_4P^+ .

Table 10. Selected ¹H NMR (8) Assignents for Complexes I-III (300MHz, CDCl₃).

:	,	F	,	;		
Position	Ia	g	2	IIa	qm	111
	7b+23	7b+23	7b+23	7c+24	7c+24	7b+25
Porphyrin						
CH_2S	13.81, 15.31	13.12	13.42, 15.03	12.59	11.26, 12.00, 13.36	13.36
					12.50	
CH_2 - CH_2 S				6.10	6.21	
meso-H	9.40	9.56	9.50	9.39	9.38	9.62
NHCO	8.15	8.11	8.10	8.01	8.20	obscured
Fe4S4 -						
Cluster						
SPh						5.22 (p-H)
						5.75 (m-H)
Cation	0.92,1.60,	0.92,1.60,	7.6-8.4, m	0.92,1.60,	0.92,1.60,	7.6-8.4, m
	1.70, 2.86	1.70, 2.86		1.70, 2.86	1.70, 2.86	

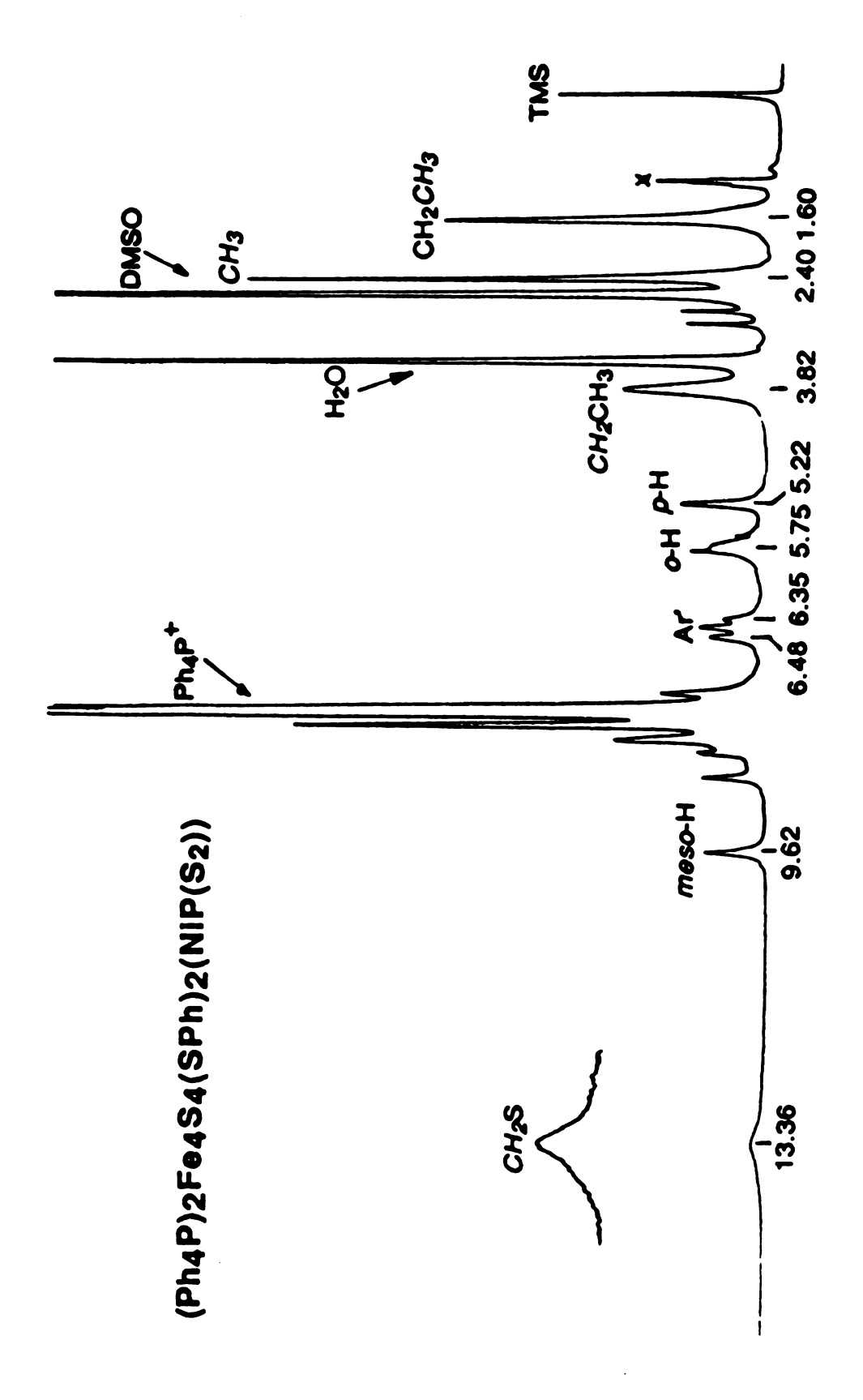


Figure 18. ¹H NMR spectrum (300 MHz, DMSO- d_6) of [Fe₄S₄(SPh)₂(NiP(S₂))]²- (III).

(Figure 18) similar to those of $[Fe_4S_4(SPh)_2Cl_2]^{2-}$ (Figure 19). The o-H and p-H signals remain essentially unchanged at 5.22 and 5.75 ppm respectively, while the m-H signal appears at 7.7-8.4 ppm overlapping with the signals corresponding to NHCO, and aromatic proton of cation (Ph_4P^+) .

(ii) Nickel porphyrin thiol ligand. Taking the spectra of NiP(SAc)₂ (7b) as references (Figure 15), the isotropic shift of methylene proton centered at 13.36 ppm, as shown in Figure 18, is characteristic of the binding of the thiol ligand to the Fe₄S₄ core. The particularly useful signal of the meso-H of nickel porphyrin remains unchanged at 9.6 ppm. Signals corresponding to ethyl and methyl functional groups of etioporphyrin are similar to the NiP(SAc)₂ (7b) in the region 1.8 (CH₃CH₂) 3.8 (CH₂CH₃) and 2.4 ppm (CH₃) respectively. Most of the phenyl protons corresponding to nickel porphyrin remain undisturbed in the region of 7.6-8.8 ppm. The only exception is the upfield shift of the o-H signal of the tailored phenyl ring centered at 5.80 ppm.

An extensive ¹H NMR investigation of the synthetic assemblies (III) convincingly demonstrates that the Fe₄S₄ cluster and the nickel porphyrin are coupled in a 1:1 fashion, rather than as an equilibrium mixture in the solution.

SUMMARY

The following are the principal findings and conclusions of this investigation.

(1) A series of nickel-porphyrin thiol ligands (7a-7c) has been successfully synthesized. Attaching of ligating appendages to the amino

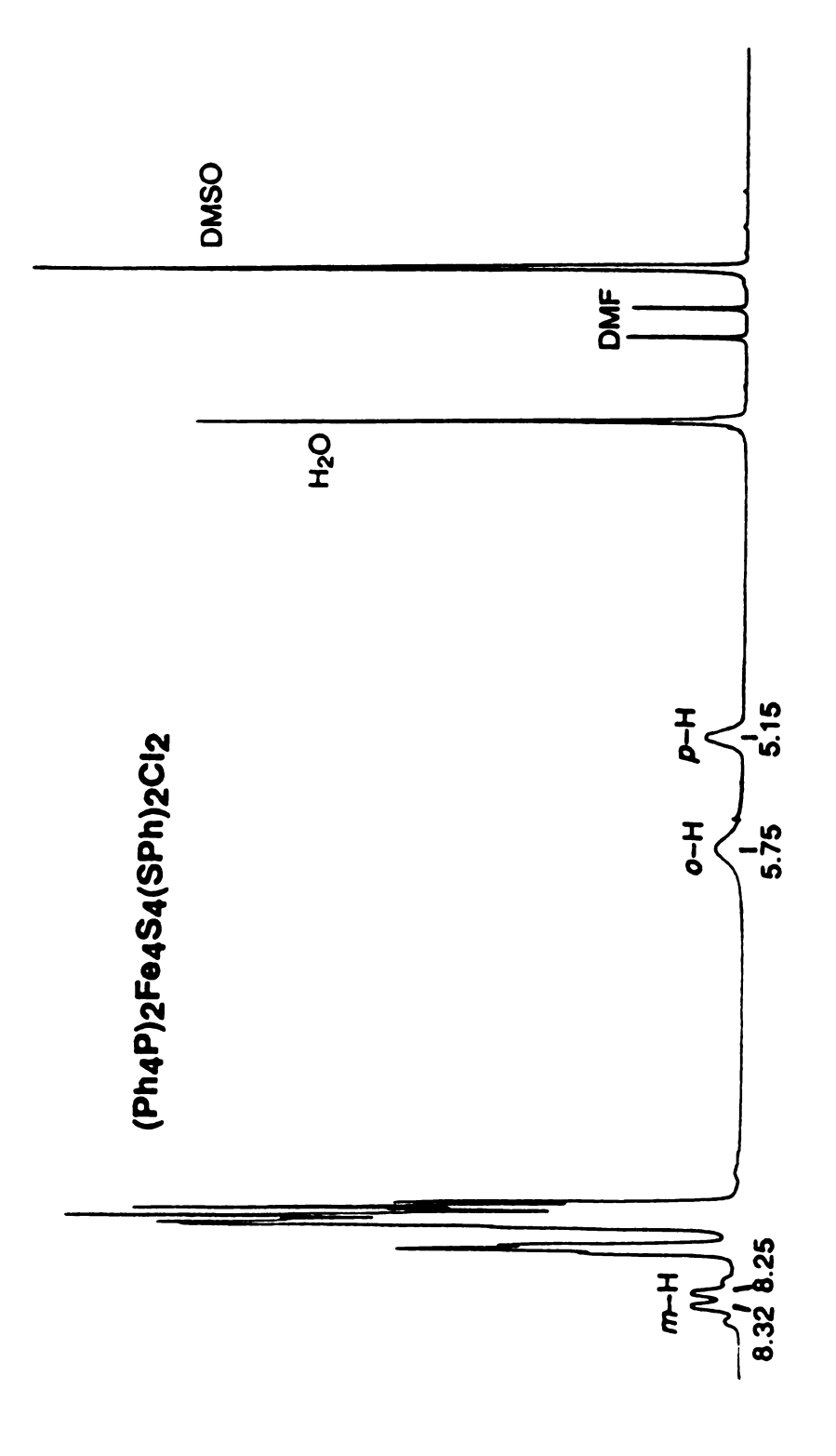


Figure 19. ¹H NMR spectrum (300 MHz, DMSO-d₆) of $[\text{Fe}_4\text{S}_4(\text{SPh})_2\text{Cl}_2]^2$ -(25).

substituents was accomplished by adding acid chlorides bearing thiol functions(5a-5c) to the key precursor cis-(NH₂)DPE(1). The purity of free base porphyrins (6a-6c) and their nickel complexes (7a-7c) has been characterized using various spectroscopic means.

- (2) Using biladiene dihydrobromide (8) condensation with aldehydes 12 and 17, which bear mono-thiol function, we could successfully synthesize two meso-substituted porphyrin thiol ligand 21a and 21b.
- (3) [Fe₄S₄] clusters 22-24 reacted with nickel porphyrins 7b and 7c to give two novel classes of nickel porphyrinyl-Fe₄S₄ assemblies I and II. However, ¹H NMR demonstrate that disproportionation components could be present in solution.
- (4) The assembly complex $[Fe_4S_4(SPh)_2(NiP(S)_2)]^2$ -(III) was prepared by treating $[Fe_4S_4(SPh)_2Cl_2]^2$ -(25) with 1 equivalent of $(Na^+)_2[NiP(S)_2]$. Both IR and ¹H NMR provided evidence to support the existence III. However, satisfactory FAB-MS and elemental analysis has not been obtained.

This work provides the initial experimental protocol for the construction of [Fe₄S₄]-siroheme assemblies. Unfortunately, a deliberate approach to synthesize the complex [Fe₄S₄(NiP(S₄)]²- was not successful. The preparation of the mixed ligand complex III appeared to be closest example of nickel-porphyrinyl-Fe₄S₄ assembly, even there the polymer formation could not be completely ruled out.

EXPERIMENTAL SECTION

1. Physical Measurements

¹H NMR spectra and ¹³C NMR spectra were recorded on a Bruker WM-250 or Varian Germini-300 spectrometer, in "100%" chloroform-d or dimethyl sulfoxide-d₆ (min. 99.96 atom% D, both from Isotec Inc.) with the residual CHCl₃ or DMSO as the internal standard set at 7.26 or 2.49 ppm, respectively. IR spectra were recorded on a Nicolet FTIR-42 spectrometer, the samples were prepared as a thin film on NaCl plates or as a KBr pellet. Melting points were obtained on an Electrothermal melting point apparatus uncorrected. Mass spectra were obtained with a Finnignan 4000 GC/MS system using the direct inlet mode at 70eV ionization energy. FAB mass spectra were obtained on a JEOL HX-110 HF double focusing mass spectrometer operating in the positive ion detection mode.

2. Materials

All solvents and reagents were of reagent grade quality, purchased commercially, and used without further purification except where mentioned. Methylene chloride, triethylamine and acetonitrile were distilled from calcium hydride; THF was distilled from LiAlH₄; methanol and ethanol were distilled from sodium. DMF was stored in 4Å molecule sieves for 24h, then distilled at ca. 30°C under reduced pressure. Thionyl chloride was distilled from triethylphosphite. Silica gel for column chromatography (60-200 mesh) was from J.T. Baker (3405). Preparative silica gel plates were from Analtech, Inc. For analytical TLC, Eastman 13181 chromatography sheets were used.

3. Syntheses of appended porphyrins

cis-Bis(o-aminophenyl)-2.8.12.18-tetraethyl-3.7.13.17-tetramethylporphyrin (1)

The cis and trans mixture of bis(o-aminophenyl)-2,8,12,18-tetraethyl-3,7,13,17-tetramethylporphyrin, (NH₂)₂DPE, was prepared by the well developed procedure⁵⁷. These isomer mixtures could be easily seperated by silica gel column chromatography using 2% CH₃OH/CH₂Cl₂ as eluents. The trans isomer could be further converted to the cis/trans isomer mixture by (atropimerization), using the following procedure.⁵⁹ A mechanically stirred mixture of toluene (1.5 1, dried over molecular sieves) and 100g of silica gel was heated at reflux for 1h. under nitrogen. Trans-(NH₂)₂OPE (3g) was added and heating at reflux was continued for 24h. After cooling to room temperature, the slurry was poured into a 15 cm diameter coarse glass frit and rinsed with toluene to remove the remaining trans isomer first, until the washings were clear. Cis-(NH₂)₂DPE was eluted from the silica gel with 2% CH₃OH/CH₂Cl₂, and isolated by removing the solvent under reduced pressure to yield 1.35 g (45%) of purple solid. The purity of the cis and trans isomers was checked by analytical TLC (SiO2, CH2Cl2-CH₃OH; 99:1) and ¹H NMR spectroscopy. The ¹H NMR spectra agree well with literature values⁵⁷.

3.5- Bis(bromomethyl) benzoic acid (3a)

A stirred mixture of 3,5-dimethylbenzoic acid(2a)(12g, 0.08mol), N-bromosuccinimide (31.33g, 176 mmol), benzoyl peroxide (200mg), and methyl formate (200 ml) was refluxed under illumination (270W Sun Lamp) for 12h. The resulting red solution was pumped to dryness in *vacuo*. After extracting with ether and washing two times with H_2O (300ml x 2), the organic fraction was dried over Na_2SO_4 and the solvent was evaporated

in vacuo. The residue was recrystallized several times from CH₂Cl₂/hexane. The white product was *intense* by *lachrymatory*, and yield 12.5g (51%). m.p.: 139-140°C. ¹H NMR (CDCl₃): δ 4.58 (s, 4H, CH_2), 7.65 (s, 1H, Ar), 8.04 (s, 2H, Ar); ¹³C NMR (CDCl₃): δ 31.52 (CH_2 Br), 130.71, 130.83, 134.83, 139.33, 170.41 (CO_2H). MS (RI): 305/307/309 (M+, 13/25/12).

3.5-Bis(thioacetoxymethyl) benzoic acid (4a)

A mixture of 3,5-bis(bromomethyl) benzoic acid(3a) (2.0g, 6.5 mmol) and potassium thioacetate (3.7g, 32.4 mmol) in methanol (50ml) was heated to 50°C for 30 min. The solution was cooled to room temperature and potassium bromide precipitates were filtered out. The solvent was removed in *vacuo* and the residue was redissolved in ether (50ml) and water (50ml). After the pH value was adjusted to 6 using conc. HCl, the aqueous phase was extracted with ether (50ml x 3). The combined organic fractions were washed with brine and dried over Na₂SO₄. The solvent was removed in *vacuo* and the residue was recrystallized from CH₂Cl₂/hexane. Yield: 1.71g (88%). mp: 147-149 °C. ¹H NMR (CDCl₃): δ 2.38 (s, 6H,CO-CH₃), 4.17 (s, 4H, Ar-CH₂), 7.49 (t, 1H, Ar), 7.9 (d, 2H, Ar); ¹³C NMR (CDCl₃): δ 30.15, 32.66, 129.62, 130.19, 134.80, 139.03, 171.20. MS (RI): 298 (M⁺, 19).

cis-5.15-Bis{o-[3.5-bis(thioacetoxymethyl)benzoylamidolphenyl)} 2.8.12.18teraethyl-3.7.13.17-tetramethylporphyrin (6a)

To a 20 ml CH₂Cl₂ solution of 3,5-bis(thioacetoxymethyl)benzoic acid(4a) (200mg, 0.66 mmol), 0.2 ml freshly distilled thionyl chloride was added dropwise. The mixture was heated to reflux for 3h and the excess SOCl₂ and CH₂Cl₂ was then removed in *vacuo*. The crude acid chloride (5a) was redissolved in dry CH₂Cl₂ (20ml) and added dropwise to a 50 ml CH₂Cl₂

solution of cis-bis(o-aminophenyl) porphyrin (150mg, 0.23 mmole) and triethylamine (1ml). The resulting mixture was refluxed under argon and the progress of the coupling reaction was monitored by TLC. After 6h, the solution was washed with 5% HCl (2 x 100ml), H₂O (100ml), NaHCO₃(sat. aq. 100ml), and H₂O (100ml), then evaporated to dryness. The reaction mixture was purified on a silica gel plate, eluting with CH₂Cl₂ containing 1% methanol. Recrystallization of the major band from CH₂Cl₂/CH₃OH produced 200mg (72%). ¹H NMR: δ -2.30 (br s, 2H, NH_{pyrrole}), 1.53 (s, 12H, COCH₃), 1.75 (t, 12H, CH₃CH₂), 2.58 (s, 12H, CH₃), 2.70 (s, 8H, CH₂S-COMe), 4.01 (m, 8H, CH₂CH₃), 6.11 (d, 4H, Ar'), 6.46 (s, 2H, Ar'), 7.60 (t, 2H, Ar), 7.77 (s, 2H, NHCO), 7.92 (t, 2H, Ar), 8.01 (d, 2H, Ar), 8.91 (d, 2H, Ar), 10.26 (s, 2H, meso-H). FAB-MS: m/z 1221 (M+H)+. UV-visible (λ_{max}): 408, 508, 542, 577, 627 nm

3-Bromomethyl benzoic acid (3b)

A stirred mixture of m-toluic acid(2b) (11.7g, 0.1mol), N-bromosuccinimide (19.58g, 0.11mol), and benzoyl peroxide (200mg) in CCl₄ (200 ml) was refluxed vigorously. The progress of the reaction was monitored by ¹H NMR. After 3h the mixture was cooled and the solid was filtered and washed with CCl₄, the filtrate was evaporated to dryness to yield a yellow solid which was recrystallized in CH₂Cl₂-hexanes to give an off white power (13.5g, 73%); mp 150-152°C; ¹H NMR (CDCl₃-acetone-d₆): δ 4.53 (s, 2H, CH₂), 7.47 (t, 1H, J=7.8Hz, Ar), 7.66 (d, 1H, J=7.8Hz, Ar), 8.06 (d, 1H, J=7.8Hz, Ar), 8.14 (s, 1H, Ar). MS(RI): 214/216 (M+, 12/11), 116 ((M-Br)+, 100).

3-Thioacetoxymethyl benzoic acid (4b)

This benzoic acid was prepared as described for the acid 4a. Yield: 90%, m.p. 90-91°C, 1 H NMR (CDCl₃): δ 2.37 (s, 3H, CO- 2 CH₃), 4.18 (s, 2H, Ar- 2 CH₂), 7.40 (t, 1H, J=7.8Hz, Ar), 7.55 (d, 1H, J=7.8Hz, Ar), 7.99 (d, 1H, J=7.8Hz, Ar), 8.01 (s, 1H, J=7.8Hz, Ar); 13 C NMR (CDCl₃): δ 30.17, 32.84, 129.07, 129.33, 130.00, 130.69, 134.52, 138.61, 172.05. MS (RI): 210 (M+, 16), 193 ((M-OH)+, 16), 150 ((M-OH-MeCO)+, 100).

cis-5.15-Bis{o-[(3-thioacetoxymethyl)benzoylamidolphenyl}- 2. 8. 12. 18-tetraethyl-3.7.13.17-tetramethylporphyrin (6b)

The appended porphyrin **6b** was prepared from the 3-thioacetoxymethyl benzoic acid (5b) as described for the appended porphyrin **6a**. Yield: 58%. IR: 1670 cm⁻¹ and 1710 cm⁻¹. ¹H NMR (CDCl₃): δ -2.40 (s, 2H, NH_{pyrrole}), 1.56 (s, 6H, CH_3CO), 1.80 (t, 12H, CH_2CH_3), 2.61 (s, 12H, CH_3), 2.86 (s, 4H, CH_2Ar'), 4.03 (q, 8H, CH_2CH_3), 6.29-6.38 (m, 4H, Ar'), 6.43 (s, 2H, Ar'), 6.66 (d, 2H, Ar'), 7.56 (t, 2H, Ar), 7.80 (m, 4H, Ar), 7.93 (s, 2H, NHCO), 9.01 (d, 2H, Ar); 10.27 (s, 2H, meso-H). FAB-MS: 1045 (M+H)+.

3-Thioacetoxypropionic acid (4c)

This benzoic acid was prepared from 3-bromopropionic acid(3c) as described for the acid 4b. Yield: 80%. m.p. 51-52°C. ¹H NMR (CDCl₃): d: 2.32 (s, 3H, CH_3 CO), 2.68. (t, 2H, CH_2 SCOMe), 3.09 (t, 2H, CH_3 CO₂H), 10.65 (s, 1H, CO_2 H). MS(RI): 148 (M+, 16), 131((M-OH)+, 14), 88 ((M-OH-MeCO)+, 100).

cis-5.15-Bis{o-[(3-thioacetoxypropionyl)amidolphenyl}- 2, 8, 12, 18-tetraethyl-3.7.13.17-tetramethylporphyrin (6c)

The appended porphyrin (6c) was made from the 3-thioacetoxypropionic acid (5c) in an analogous fashion as porphyrin 2c Yield: 67%. ¹H NMR (CDCl₃): δ : -2.51 (s, 2H, NH_{pyrrole}), 1.43 (s, 6H, CH_3CO), 1.58 (t, 4H, - CH_2SCOMe), 1.76 (t, 12H, CH_2CH_3), 2.52 (s, 12H, CH_3), 2.59 (s, 2H, - CH_2CH_2CO), 4.01 (q, 8H, CH_2CH_3), 6.85 (s, 2H, NHCO), 7.52 (t, 2H, Ar), 7.84 (m, 4H, Ar), 8.75 (d, 2H, Ar); 10.27 (s, 2H, meso-H). FAB-MS: 921(M+H)+.

Nickel Porphyrin Complexs

To prepare a nickel complex, NiP(SAc)₄(7a), for example, a stirred solution of appended porphyrin P(SAc)₄(5a) (0.20 g, 0.25mmol) in 10 ml CHCl₃/MeOH (9:1) was added a solution of nickel acetate (0.25 mmol) in 5 ml MeOH with stirring. The resulting reaction mixture was heated at reflux for 4h. After evaporating the solvent to dryness, 200 ml water and 20 ml 1N HCl were added to the flask and the suspension was stirred for 20 min before being extracted with CH₂Cl₂. The CH₂Cl₂ solution was dried over Na₂SO₄, filtered and concentrated to 2ml. After recrystallization from CH₂Cl₂/MeOH, the precipiated solid was filtered, washed with n-hexane and dried in *vacuo* at ambient temperature. Yield: 80% of red solid. UV-visible (λ_{max}): 408 (soret), 530, 566 nm. NiP(SAc)₂(7b) and NiP(SAc)₂(7c) were prepared in an analogous fashion as described above.

NiP(SAc)₄(7a): ¹H NMR (CDCl₃): δ : 1.57 (t, 12H, CH₂CH₃), 1.78 (s, 6H, CH₂CO), 2.30 (s, 12H, CH₃), 3.06 (s, 2H, ArCH₂-S), 3.67 (m, 8H, CH₂CH₃), 6.31 (d, 4H, Ar), 7.57 (d, 2H, Ar), 7.82 (t, 2H, Ar), 8.04 (s, 2H, NHCO), 8.90 (d, 2H, Ar), 9.55 (s, 2H, meso-H) FAB-MS: m/z 1276.2 (M)⁺

NiP(SAc)₂(7b): ¹H NMR (CDCl₃): δ : 1.58 (t, 12H, CH₂CH₃), 1.75 (s, 6H, CH₂-CO), 2.31 (s, 12H, CH₃), 3.11 (s, 4H, ArCH₂-S), 3.67 (q, 8H, CH₂CH₃), 6.45 (s,

2H, Ar'), 6.53-6.56 (m, 4H, Ar'), 6.84-6.88 (m, 2H, Ar'), 7.42 (t, 2H, Ar), 7.49 (d, 2H, Ar), 7.81 (t, 2H, Ar), 8.14 (s, 2H, NHCO), 8.94 (d, 2H, Ar), 9.54 (s, 2H, meso-H) FAB-MS: m/z 1100.7 (M)+

NiP(SAc)₂(7c): ¹H NMR (CDCl₃): δ : 1.56 (s, 6H, CH_3 -CO), 1.65 (t, 12H, CH_2CH_3), 1.96 (t, 4H, CH_2CH_2SCO), 2.28 (s, 12H, CH_3), 2.69 (t 4H, OC- CH_2CH_2), 3.73 (q, 8H, CH_2CH_3), 7.22 (s, 2H, NHCO), 7.37 (t, 2H, Ar), 7.44 (d, 2H, Ar), 7.74 (t, 2H, Ar), 8.68 (d, 2H, Ar), 9.49 (s, 2H, Meso-H). FAB-MS: m/z 976.3 (M)+

4. Syntheses of mono-substituted porphyrin thiol ligand(21a-21b)

1.19-Dideoxy-7.13-dimethyl-2.3.8.12.17.18-hexaethyl-biladiene-ac dihydrobromide (8) 60

3,3'-Diethyl-5,5'-diformyl-4,4'-dimethyl-2,2'-dipyrrylmethane (286 mg, 1 mmole) and 3,4-diethylpyrrole (250 mg, 2.01 mmol) in methanol (20 ml) were treated with hydrobromic acid (2 ml, 48%), the solution was heated on a steam bath for 5 min, and kept at room temperature for ca. 2 h. The product was separated, washed with methanol (containing a little hydrobromic acid), then with ether, and dried in air to give red-brown prisms with a green luster (491 mg, 81%). mp > 300 °C. 1 H NMR(CDCl₃): δ : 0.68 (t, 6H, CH₂CH₃), 1.22 (t, 12H, CH₂CH₃), 2.27 (s, 6H, CH₃), 2.50, 2.57 (q, 4H each, CH_{2} CH₃), 2.72 (q, 4H, CH_{2} CH₃), 7.23 (s, 1H x 2, 15-H and 20-H), 7.69(d, 2H, 10-H), 13.32, 13.54 (s, 2H each, NH).

α -Bromo-p-Tolunitrile(10)

A stirred mixture of p-tolunitrile(9) (11.7 g, 0.1 mmol), N-bromosuccinimde (19.58 g, 0.11mmol), and benzoyl peroxide (200mg) in 200

ml of methyl formate was refluxed under illumination (270 Watt Sun Lamp) for 2 h. The volatile component were removed by evaporation, the residue was taken into ether (100 ml) and washed with water (100 ml x 2). After drying over Na₂SO₄, the solvent was evaporated to dryness. Recrystallization twice from CH₂Cl₂-hexane afforded pure bromide 13.5 g (73%). mp 115-116 °C. 1 H NMR(CDCl₃): δ 4.45 (s, 2H, CH_{2} Br). 7.47 (d, 2H, J=8Hz, Ar), 7.62 (d, 2H, J=8Hz, Ar). 13 C NMR(CDCl₃): δ 31.43, 112.13, 118.31, 129.66, 132.52, 142.78. MS(RI): 195/197 (M+, 12/11), 116 (M-Br)+, 100.

p-Bromomethylbenzaldehyde(11)⁶²

A 1M solution of diisobutylaluminum hydride (DIBAL) in hexane (36.8 ml) was added in a dropwise manner over a period of 20 min to a solution of a-bromo-p-tolunitrile(10) (6.00 g, 30.6 mmol) in 60 ml of chlorobenzene at 0 °C. The resulting mixture was stirred at 0 °C for 1 h and then diluted with 100 ml of CHCl₃. This solution was shaken with 10% aq. HCl for ca. 10 min. The layer was seperated and the aqueous layer extracted with CHCl₃ (20 ml x 2). The organic solution were combined, dried over Na₂SO₄, evaporated to dryness in *vacuo*. The residue was recrystallized by dissolving in a minimum amount of CH₂Cl₂ (ca. 10 ml) and layering with a small amount of ice-cold hexane to yield 4.7g (77%) of aldehyde. m p 97-98 °C. ¹H NMR(CDCl₃): δ 4.49 (s, 2H, CH₂Br), 7.53 (d, 2H, J=8Hz, Ar), 7.84 (d, 2H, J=8Hz, Ar), 9.98 (s, 1H, CHO). ¹³C NMR(CDCl₃): δ 31.96, 129.64, 130.13, 136.06, 144.20, 191.49. MS(RI): m/z 198/200 (M+, 20/19), 119 [(M-Br)+, 100], 91 [(M-Br-CHO)+, 82].

p-Thioacetoxymethylbenzaldehyde(12)

A mixture of p-bromomethylbenzaldehyde(11) (3.95g, 0.02 mmol) and potassium thioacetate (3.42g, 0.03 mmol) in 50 ml CH₃OH was heated to 50 °C. Potassium bromide was gradually precipitated out after 10 min. The reaction was kept stirring for 20 min. After filtration, the filtrate was stripped to dryness. The residue was redissoved in ether, and washed with H₂O(50 ml x 2) and brine (50ml). The organic fraction was dried over Na₂SO₄, and then concentrated to give a yellow oil. The crude product was further purified on silica gel column chromatography using 30% hexane-CH₂Cl₂ for elution. The main fraction was collected and the solvent removed in vacuo to give colorless oily product 3.3g (85%). ¹H NMR(CDCl₃): δ 2.35 (s, 3H, CH₃COS), 4.14 (s, 2H, CH₂SCOMe), 7.44 (d, 2H, J=8Hz, Ar), 7.80 (d, 2H, J=8Hz, Ar), 9.99 (s, 1H CHO). ¹³C NMR(CDCl₃): δ 30.29, 33.13, 129.46, 130.05, 135.37, 144.84, 191.69. MS(RI): m/z 194(M+, 35), 152 [(M+H-CH₃CO)+, 100].

5-[p-(thioacetoxymethyl)phenyl]-etioporphyrinato Nickel (II)(13)61

The mixture of 1,19-dideoxyl-7,13,-dimethyl-2,3,8,12,17,18-hexaethyl-biladiene-ac dihydrobromide (102 mg, 0.15 mmol), p-thioacetoxymethylbenzaldehyde(12) (250 mg, 1.29 mmol), and 4 drops of acetic acid saturated with hydrobromide in methanol (25ml) was refluxed for 24 h. The resulting solution was cooled and treated with an excess of solid sodium bicarbonate. After filtration, the crude product was washed with water, dried in the air, and redissolved in chloroform-acetic acid (25:1). A saturated methanolic solution (2 ml) of nickel acetate was then added, and the mixture was heated under reflux for 3 h. The solution was cooled, and washed with water (50 ml x 2) and then sat. NaHCO₃ solution (50 ml). The solvent was removed from the dried chloroform extract, and

the residue redissolved in CH_2Cl_2 . The crude product was chromatographed on silica gel column using 50% hexane- CH_2Cl_2 for elution. The main fraction was collected and the solvent removed in *vacuo*. Recrystallization from CH_2Cl_2 -hexane give the nickel derivative(13) as purple crystals. ¹H NMR(CDCl₃): δ 0.91 (t, 6H, CH_2CH_3), 1.70, 1.76 (t, 6H each, CH_2CH_3), 2.49 (s, 3H, CH_3COS), 2.63 (d, 4H, CH_2CH_3), 3.41 (s, 6H, CH_3), 3.74-3.87 (m, 12H, CH_2CH_3), 4.44 (s, 2H, CH_2SAc), 7.51 (d, 2H, Ar), 7.93 (d, 2H, Ar), 9.51 (s, 1H, 15-H), 9.57 (s, 2H, 10-H and 20-H). FAB-MS: m/z 726 (M⁺).

4-(Methylsulfoxy)benzaldehyde(15)

To a stirred solution of 4-(methylthio)benzaldehyde(14) (0.76 g, 5 mmole) in dry dichloromethane (100 ml) at 0°C, 85% m-chloroperbenzoic acid (1.0 g, 5.9 mmole) in dichloromethane (50 ml) was added dropwise. The mixture was stirred at 0°C for 1h. and then treated with Ca(OH)₂ (0.55 g, 7.5 mmole) for 15 min. After filtration, the solvent was evaporated in *vacuo*. The crude product was recrystallized from hexane-CH₂Cl₂ to give colorless plates. mp: 85-86°C. ¹H NMR(CDCl₃): δ 2.80 (s, 3H, CH₃SO), 7.83 (d, 2H, Ar), 8.06 (d, 2H, Ar), 10.10 (s, 1H, CHO). ¹3°C NMR(CDCl₃): δ 43.54, 124.07, 130.26, 137.98, 152.15, 191.04. MS(RI): m/z 168 (M+, 100); 139 [(M-CHO)+, 91].

4.4'-Diformyldiphenyl disulfide (18)63

The mixture of the sulfoxide(15) (1.68 g, 0.01 mole) with trifluoroacetic anhydride (10ml) was heated under reflux for 1h. The volatile components were removed by evaporation and the crude trifluroacetoxymethylthiobenzaldehyde(16) was directly hydrolyzed in

methanol-triethylamine (100 ml, 1:1) without isolation. After stirring at room temperature for 30 min, the volatile components were removed in vacuo. The residue was redissolved in chloroform (50 ml), washed with 1N HCl (50 ml x 1), and then with sat. NH₄Cl (50 ml x 1). After drying over Na₂SO₄, the solvent was evaporated to dryness to provide 4-mercaptobenzaldehyde(17). The crude thiol was converted to the corresponding disulfide(18) by shaking a CHCl₃ solution with excess aquous KI₃. After washing with saturated. Na₂SO₃ solution, drying over Na₂SO₄, the solvent was evaporated to dryness. Recrystallization of the residue from EtOAc-hexane gave yellow crystals 0.97g (71%). mp: 105-106°C. ¹H NMR(CDCl₃): δ 7.61 (d, 2H, Ar), 7.80 (d, 2H, Ar), 9.94 (s, 1H, CHO). ¹³C NMR(CDCl₃): δ 126.23, 130. 31, 135.07, 143.74, 190.92. MS (RI): m/z 274 (M⁺, 46), 137 (M/2⁺, 27), 109 (M/2⁺+H-COH, 100).

Bis(nickelporphyrinyl)diphenyl disulfide (19)61

The disulfide was prepared from the diformyldiphenyl disulfide(18) and biladiene-ac dihydrobromide(8) as described for the nickel porphyrin (13). The crude compounds were separated on silica gel TLC using 70% hexane/CH₂Cl₂ for elution. The desired disulfide(19) was shown to be the minor product which eluted faster, and the major component was the dimethylacetal of the formyl compound(20). Recrystallization from methylene chloride-hexane give small red needles.

Disulfide(19). ¹H NMR(CDCl₃): δ 0.97 (t, 12 H, CH₂CH₃), 1.66, 1.75 (t, 12H each, CH₂CH₃), 2.71 (q, 8H, CH₂CH₃), 3.40 (s, 12H, CH₃), 3.76, 3.86 (q, 8H each, CH₂CH₃), 7.90 (d, 4H, Ar), 8.08 (d, 4H, Ar), 9.51(s, 2H, 15-H), 9.57 (s, 4H, 10-H and 20-H). FAB-MS: m/z 1338 (M+).

Disulfide(20). ¹H NMR(CDCl₃): δ 0.86 (t, 6 H, CH₂CH₃), 1.68, 1.74 (t, 6H each, CH₂CH₃), 2.62 (q, 4H, CH₂CH₃), 3.36 (s, 6H, CH₃), 3.39 (s, 6H, CH(OCH₃)₂), 3.77, 3.84 (q, 8H each, CH₂CH₃), 5.44 (s, 1H, CH(OMe)₂), 7.49 (d, 2H, Ar), 7.65(d, 2H, Ar), 7.76(d, 2H, Ar), 7.94 (d, 2H, Ar), 9.51(s, 1H, 15-H), 9.57 (s, 2H, 10-H and 20-H). FAB-MS: m/z 852 (M+).

$5-[p-(\alpha-Mercaptomethyl)phenyl]-etioporphyrinato Nickel (II)(21a)$

Etioporphyrinato Nickel(II) (13) (73 mg, 0.1 mmol) in CHCl₃ (25 ml) was treated with 3N HCl in methanol (5 ml) under nitrogen. The mixture was refluxed for 12 h. The resulting solution was cooled and pumped to dryness in *vacuo*. The residue was redissolved in CHCl₃ and washed with H₂O (10 ml) and brine (10 ml). After drying over Na₂SO₄, the solvent was evaporized in *vacuo*. Recrystallization from CH₂Cl₂-hexane in a glove box under nitrogen give purple crystals 70 mg (90%).

¹H NMR(CDCl₃): δ 0.92 (t, 6H, CH₂CH₃), 1.70, 1.76 (t, 6H each, CH₂CH₃), 1.98 (t, 1H, SH), 2.65 (d, 4H, CH₂CH₃), 3.40 (s, 6H, CH₃), 3.80, 3.8 (q, 6H each, CH₂CH₃), 4.05 (d, 2H, CH₂SH), 7.51 (d, 2H, Ar), 7.93 (d, 2H, Ar), 9.51 (s, 1H, 15-H), 9.57 (s, 2H, 10-H and 20-H). FABMS: m/z 684 (M⁺).

$5-[p-(\alpha-Mercaptophenyl]-etioporphyrinato Nickel (II)(21b)$

The diacetal porphyrin dissulfide(20) (170 mg, 0.2 mmol), under a stream of argon, was dissolved in 100 ml of 100% ethanol and treated with 500 mg of NaBH₄. The mixture was stirred at room temperature for 12 h. An equal volume of H₂O was then added to the reddish solution. The aquous layer was discarded, and the organic layer was further washed with brine (100 ml x 2), dried briefly over Na₂SO₄, filtered, and taken to dryness.

The residue was purified by flash chromatography under nitrogen with 30% hexane-CH₂Cl₂; the major band was separated from several trailing bands. The solution was collected, evaporated, and crystallized inside a nitrogen box from hexane/CH₂Cl₂. Yield: 33 mg (49). ¹H NMR(CDCl₃): δ 0.91 (t, 6H, CH₂CH₃), 1.70, 1.76 (t, 6H each, CH₂CH₃), 2.65 (d, 4H, CH₂CH₃), 3.40 (s, 6H, CH₃), 3.50 (s, 1H, SH), 3.80, 3.8 (q, 6H each, CH₂CH₃), 7.49 (d, 2H, Ar), 7.90 (d, 2H, Ar), 9.50 (s, 1H, 15-H), 9.57 (s, 2H, 10-H and 20-H). FABMS: m/z 670 (M+).

5. Preparation of Iron-Sulfur clusters

The iron-sulfur cluster complexes were prepared and purified by published procedures^{64,65}. Typical experimental procedures are as follows.

a.<u>Bis-(tetraphenylphosphonium)-tetrachloro-tetrakis-(µ3-sulfide)</u> tetraferrate (2II, 2III), (Ph4P)₂Fe₄S₄Cl₄ (22)

1.26 g (10 mmol) of anhydrous FeCl₂, 2.23 g (15 mmole) of KSPh, 1.87 g (5 mmole) of Ph₄PCl, and 0.4 g (12.5 mmol) of elemental sulfur were placed in a 125 ml Erlenmeyer flask. To that mixture, CH₃CN (40 ml) was added with continuous stirring. The resulting reaction mixture was stirred at room temperature for ca. 45 min. During that time, the reaction mixture became brown-green. The solution was filtered to remove KCl and unreacted elemental sulfur. To the filtrate, 100 mL of diethyl ether was added and the solution was allowed to stand for ca. 12 h at room temperature. A black crystalline solid was deposited. The product was isolated by filtration, washed twice with diethyl ether, and dried under

vacuum; yield: 2.14 g (73%). The UV-visible spectrum of the crystalline product was obtained in CH₃CN and was found identical with that of the previously reported (Ph₄P)₂Fe₄S₄Cl₄.

(Bu₄N)₂Fe₄S₄Cl₄(23) and (Bu₄N)₂Fe₄S₄Br₄(24) were prepared in an analogous fashion as described above.

b.Bis(tetraphenylphosphonium)bis(thiophenolato)dichloretrakis(µ₃-sulfide) tetraferrate (2II, 2III), (Ph₄P)₂,[Fe₄S₄(SPh)₂Cl₂](25)

To a solution of 1.00 g (0.86 mmol) of (Ph₄P)₂[Fe₄S₄Cl₄] in 50 mL of dimethylformamide (DMF) was added 0.20 g(1.72 mmol) of solid KSPh. After stirring for 20 min, the brown-green solution was filtered and to the filtrate was added 200 mL of anhydrous ether. The oil that formed was crystallized from CH₃CN following the addition of anhydrous ether. A 0.95 g sample of analytically pure crystals was obtained; yield: 86%. The X-ray powder pattern, visble spectra, and isotropically shifted NMR spectra of this compound are identical with those of an "authentic" sample⁶⁵

6. Preparation of the Ni-Porphyrinyl-Fe₄S₄ assemblies

Typical experimental procedures to prepare the nickel porphyrin-Fe₄S₄ assemblies are as follows.

Complexes (III). To a 10 ml DMF solution of NiP(SAc)₂ (7b) (66 mg, 0.06 mmol) was added one portion of freshly prepared NaOMe (11 mg, 0,20 mmol) in 5 ml DMF/CH₃OH (4:1) solution. The resulting reaction mixture was stirred at room temperature for ca. 3h. To a 10 ml DMF solution of (Ph₄P)₂Fe₄S₄(SPh)₂Cl₂(25) (66 mg, 0.05 mmol), the above freshly prepared solution was added dropwise, and the mixture was heated to 50-60 °C and

kept stirring for 6h. The resulting solution was filtered, and to the filtrate 20 ml of ether/THF (1:1) was added. After the solution was allowed to stand for ca. 12 h, the reddish precipitates were collected by filtration and washed with ether. Recrystallization from DMF/ether afforded 56 mg (25%) of reddish powder. UV-visible (λ_{max}): 408, 527, 564 nm. ¹H NMR (DMSO-d₆): δ 1.80 (br s, 12H, CH₂CH₃), 2.40 (br s, 12H, CH₃), 3.82 (br s, CH₂CH₃), 5.22 (s, 2H, p-H of SPh), 5.75 (Br s, 4H, o-H of SPh), 5.80 (s, 2H, Ar'), 6.35-6.48 (m, 4H, Ar'), 7.6-8.4 (m, 2H,40H,4H,2H, NHCO, Ar of Ph₄P, m-H of SPh, Ar), 8.65 (s, 2H, Ar), 9.62(s, 2H, meso-H), 13.36 (br s, 4H, CH₂S).

CHAPTER III

CHARACTERIZATION OF THE IRON-SULFUR CLUSTERS BY FAB MASS SPECTROMETRY

INTRODUCTION

Proteins containing iron-sulfur clusters frequently serve as redox enzymes, and participate in electron transfer reactions associated with processes such as photosynthesis, nitrite reduction and nitrogen fixation^{66,67}. At present, four distinct types of Fe-S cluster cores, in various oxidation states, have been identified in such enzymes: FeS₄, Fe₂S₂, Fe₃S₄, and Fe₄S₄. The iron centers in these clusters form bridges in proteins, usually by bonding to sulfur atoms of cysteine residues. Most of these clusters participate in one-electron redox processes⁶⁸. They frequently contain iron atoms in one or more oxidation states, usually Fe³⁺ and Fe²⁺. A variety of iron/sulfur core oxidation states have been established for the various Fe/S clusters present in proteins. Those identified to date include: [Fe₂S₂]^{1+,2+}, [Fe₃S₄]^{0,1+}, and [Fe₄S₄]^{1+,2+,3+}.

In view of the diversity of structures and biological functions, these complexes are difficult to characterize by direct studies of the proteins themselves. Fortunately, synthetic analogs of the mono-, bi- and tetra-iron centers have been developed to provide insights into their intrinsic properties in the absence of protein-imposed contraints. Of the structurally characterized synthetic models for the various [Fe_mS_n] clusters now available, the cubane-type, [Fe₄S₄], core geometry appears to be the most commonly encountered, and has been the focus of an intensive body of structural, spectroscopic and magnetic studies for the last two decades^{69,70}. A wide variety of model complexes of the type [Fe₄S₄X₄]²⁻ have been made in which the anionic components, X-, are a variety of thiolates (SR-)⁶⁴, halides

(Cl⁻, Br⁻, and I⁻)^{64,65}, and alkoxides (OR⁻)⁷¹, as well as combinations of these ligands⁶⁴. Recently, the 'subsite-differentiated' analogs of biological [Fe₄S₄]²⁺ clusters⁵⁶, as well as synthetic peptide model complexes⁷²⁻⁷⁴ have also been explored. Generally, the characterization of such compounds has always relied on UV-visible spectroscopy, elemental analysis, NMR spectroscopy (where applicable for complexes in solution), and single-crystal x-ray crystallography.

Although conventional electron impact mass spectrometry is a standard spectroscopic method for the characterization of inorganic compounds, it is not readily applicable for the analysis of ionic, nonvolatile compounds such as those that contain the [Fe₄S₄X₄]²- core. Recently, fast atom bombardment (FAB) ionization⁷⁵ has been used for the mass spectrometric analysis of a variety of inorganic compounds including classical inorganic salts, organometallic compounds, coordination complexes, and bioinorganic systems⁷⁶. The main advantage of FAB-MS⁷⁷ and the related techniques of liquid secondary ion mass spectrometry (LSIMS)⁷⁸ is the facility with which ions can be generated from nonvolatile/thermally-labile inorganic compounds. Successful completion of the experiment frequently depends on an appropriate choice of the viscous liquid matrix to assist in the desorption and ionization processes.

This is the first report documenting the utility of FAB-MS for the characterization of [Fe₄S₄X₄]²-clusters. Results of both positive and negative ion FAB-MS are presented here in the characterization of a series of salts of anionic iron-sulfur clusters which include:

(a) (A)₂Fe₄S₄Br₄, A= Bu₄N, Pr₄N, Et₄N; (b) (A)₂Fe₄S₄Cl₄, A=(Ph₃P=)₂N (PPN), Ph₄P, Bu₄N, Me₄N; (c) (A)₂Fe₄S₄(SPh)₄, A=Ph₄P, Bu₄N; (d) (A)₂Fe₄S₄(SEt)₄, A=Ph₄P, Ph₄As; and (e) (Ph₄P)₂Fe₄S₄(SPh)₂Cl₂. The results reported herein demonstrate that useful mass spectra can be obtained by choosing proper matrices. When negative ion FAB is employed, identification of the intact core, as the univalent anion, [Fe₄S₄X₄]-, is straightforward. Thus, FAB-MS analysis can be employed as a valid method for rapid molecular weight determination. A variety of fragment ions have also been observed; mechanisms for their formation are proposed.

The mass spectral results show that, in the gas phase, the ironsulfur cubane core undergoes unimolecular dissociation following desorption/ionization. The fragment ions, which contain 4, 3 and 2 iron atoms, have interesting parallels with known species that have been synthesized/identified in condensed phase studies. These parallels, and their implications, will be discussed.

EXPERIMENTAL SECTION

Mass spectrometric analyses were performed on a JEOL HX-110 HF double-focusing mass spectrometer, operated in either positive ion or negative ion mode. Ions were produced by fast atom bombardment (FAB) with a beam of 6 keV Xe atoms or by LSIMS using a 20 keV cesium ion beam. The mass spectrometer was operated using an accelerating voltage of 10 kV and a resolution of at least 3000. The instrument was scanned at a

rate of 2 minutes over the range of 1-6000 Daltons. Data reported represent mass spectra obtained in a single scan.

A variety of liquid matrices including glycerol, thioglycerol, 3-nitrobenzyl alcohol (NBA) and 2-nitrophenyl octyl ether (NPOE) were evaluated. Glycerol and thioglycerol both lead to significant complicated additions to the ionic clusters formed. The terminal ligand-matrix exchange reactions such as dehalogenation⁷⁹ or ligand substitution have been observed⁸⁰. Both NPOE and NBA were found to be most appropriate for analyzing complexes that contain halides ligands⁸¹, because reactions between analytes and matrices do not occur. Iron-sulfur clusters with thiolate ligands also show sensitivity to the matrix NBA, and only NPOE was found to be an suitable matrix in those cases. Samples to be analyzed were dissolved in DMF, and 1 ml of the solution (ca. 10 mM) was mixed with 2 ml of the matrix (NBA or NPOE) on the FAB probe tip.

The iron-sulfur cluster complexes were prepared and purified by published procedures^{64,71}. The purity of the complexes was generally established by UV-visible spectroscopy, ¹H-NMR spectroscopy, and x-ray powder pattern analysis. To avoid oxidation, all of the samples were handled under a flow of pure nitrogen during their preparation and introduction into the mass spectrometer.

RESULTS AND DISCUSSION

1. Mass Spectral Characterization of Iron-Sulfur Clusters

Presented here are experimental results and observations in the FAB-MS analysis of various salts containing the iron-sulfur cubane core. As will be shown, positive FAB-MS gives molecular weight and structural information for the analytes (A)₂Fe₄S₄Br₄ and (A)₂Fe₄S₄Cl₄. However, the positive ion FAB-MS studies of complexes containing thiolate ligands, (A)₂Fe₄S₄(SPh)₄, and (A)₂Fe₄S₄(SEt)₄, as well as the mixed-ligand complex, (Ph₄P)₂Fe₄S₄(SPh)₂Cl₂, gave limited information related to the molecular formula. In contrast, negative-ion mass spectra of all iron-sulfur cubane clusters display peaks representing the unique features of the intact [Fe₄S₄X₄] core, as well as a variety of fragment ions.

Since most of the ions observed contain atoms which have a number of isotopic forms, isotopic clusters of peaks are observed to represent a single elemental formula. In the following discussion, the nominal m/z value is used to represent an ion of a given composition, calculated by using the lowest mass isotope of each element present (i.e., 56 u for Fe, 35 u for Cl, 79 u for Br and 32 u for S). In the data presented, reported relative intensities represent the most abundant isotopic peak of an isotopic cluster.

(A). Positive- and negative-ion FAB mass spectra of halogenated clusters, $(A)_2Fe_4S_4Br_4$, and $(A)_2Fe_4S_4Cl_4$:

Both NBA and NPOE are suitable matrices for positive- and negativeion FAB-MS studies of (A)₂Fe₄S₄X₄ compounds, where X= Br, and Cl. In general, when FAB is used in the analysis of ionic analytes of the form [A+][B-], the intact cation [A]+, and possibly its fragment ions, will dominate the positive ion mass spectrum, while, [B]- and charged fragments thereof will be present in the negative ion spectrum. In the FAB-MS analysis of these ionic complexes, which can be written as $(A^+)_2[Fe_4S_4]^{2+}(X^-)_4$, the cation $(A)^+$ is seen as the base peak in the positiveion spectra. However, the positive-ion FAB spectra are disappointing in that they give limited structural information in the mass range below m/z 800. Most of the peaks in this range are due to the ions formed from interactions between the intact cation, A+, and matrix molecules, to yield clusters of the type [NBA_n+A]+, or molecular fragments that do not contain either iron or sulfur, such as [2(A)+X]+. However, the most significant spectral features in the positive ion spectra are three clusters of peaks in the higher mass range. In the positive-ion spectrum of (Et₄N)₂Fe₄S₄Br₄ as shown in Figure. 20, the significant high mass ions represent the ionic species $[(Et_4N)_2Fe_4S_4Br_3]^+$ (m/z 849); $[(Et_4N)_2Fe_4S_4Br_4]^+$ (m/z 928); and [(Et₄N)₃Fe₄S₄Br₄]+ (m/z 1058), respectively. These can also be written as variants of the neutral salt molecule, M, as [M-Br]+, [M]+, and [M+A]+ respectively. The gas phase [M+A]+ adduct represents the peak at the highest m/z value in the spectrum, and is presumably formed by complexation of the (Et₄N)+ cation with the desorbed neutral (Et₄N)₂Fe₄S₄Br₄ molecule. The molecular ion peak, [(Et₄N)₂Fe₄S₄Br₄]+, which provides direct molecular weight information, is also observed.

In contrast, the negative-ion FAB mass spectrum of $(Et_4N)_2Fe_4S_4Br_4$ (Figure 21), obtained using the matrix NPOE, is much richer than the cation spectrum. Dominant high mass ions include the [M-A]- complex, formed by loss of a tetraethylammonium cation, at m/z 798. The intact ironsulfur cubane cluster, as a -1 ion, $[Fe_4S_4Br_4]$ - (m/z 668) is also observed. The molecular anion $[(Et_4N)_2Fe_4S_4Br_4]$ - (m/z 928) is present in the negative

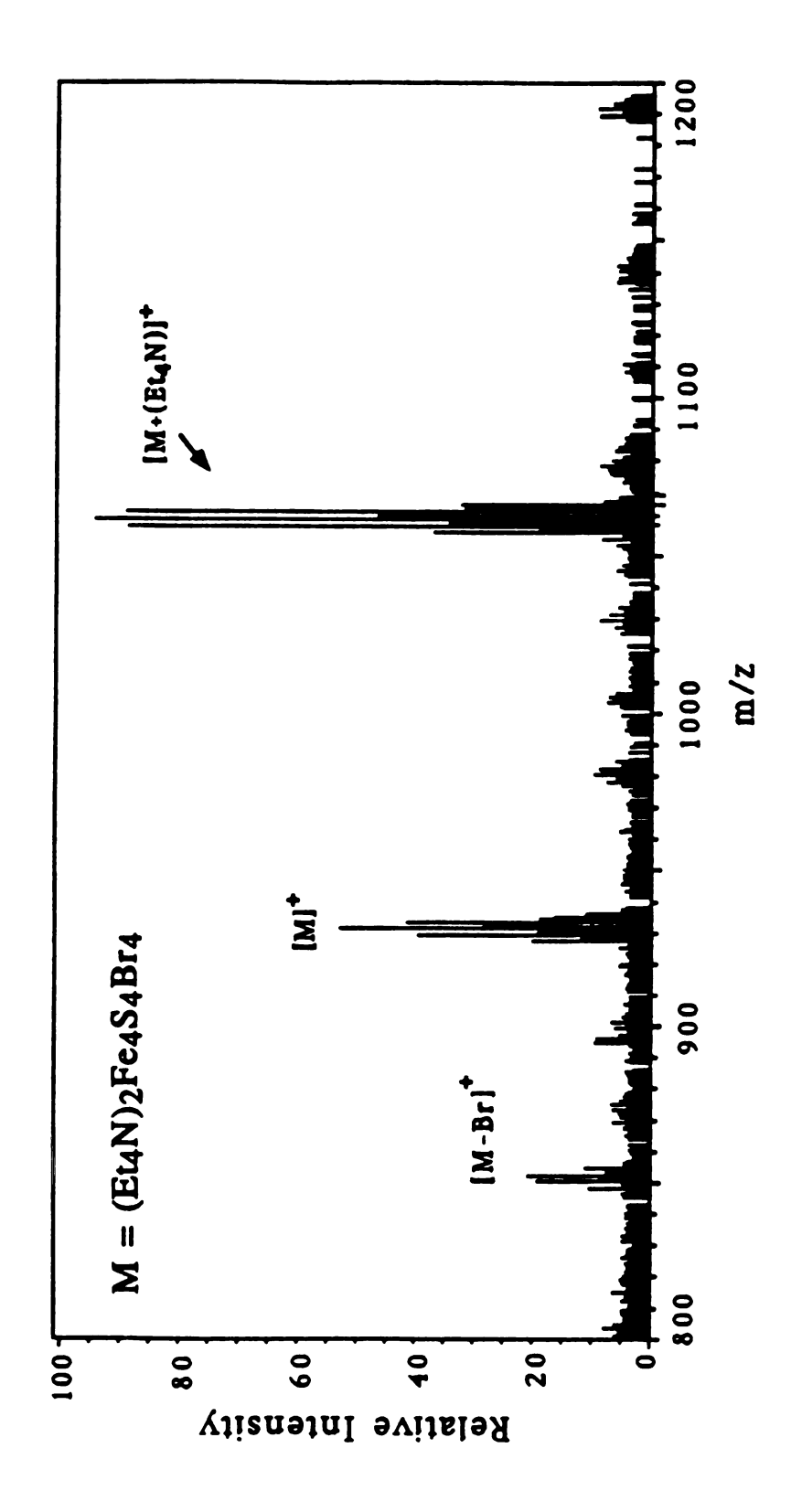


Figure 20. A portion of the Positive-ion FAB mass spectrum of [(Et4N)₂Fe₄S₄Br₄] (M), using the matrix NBA.

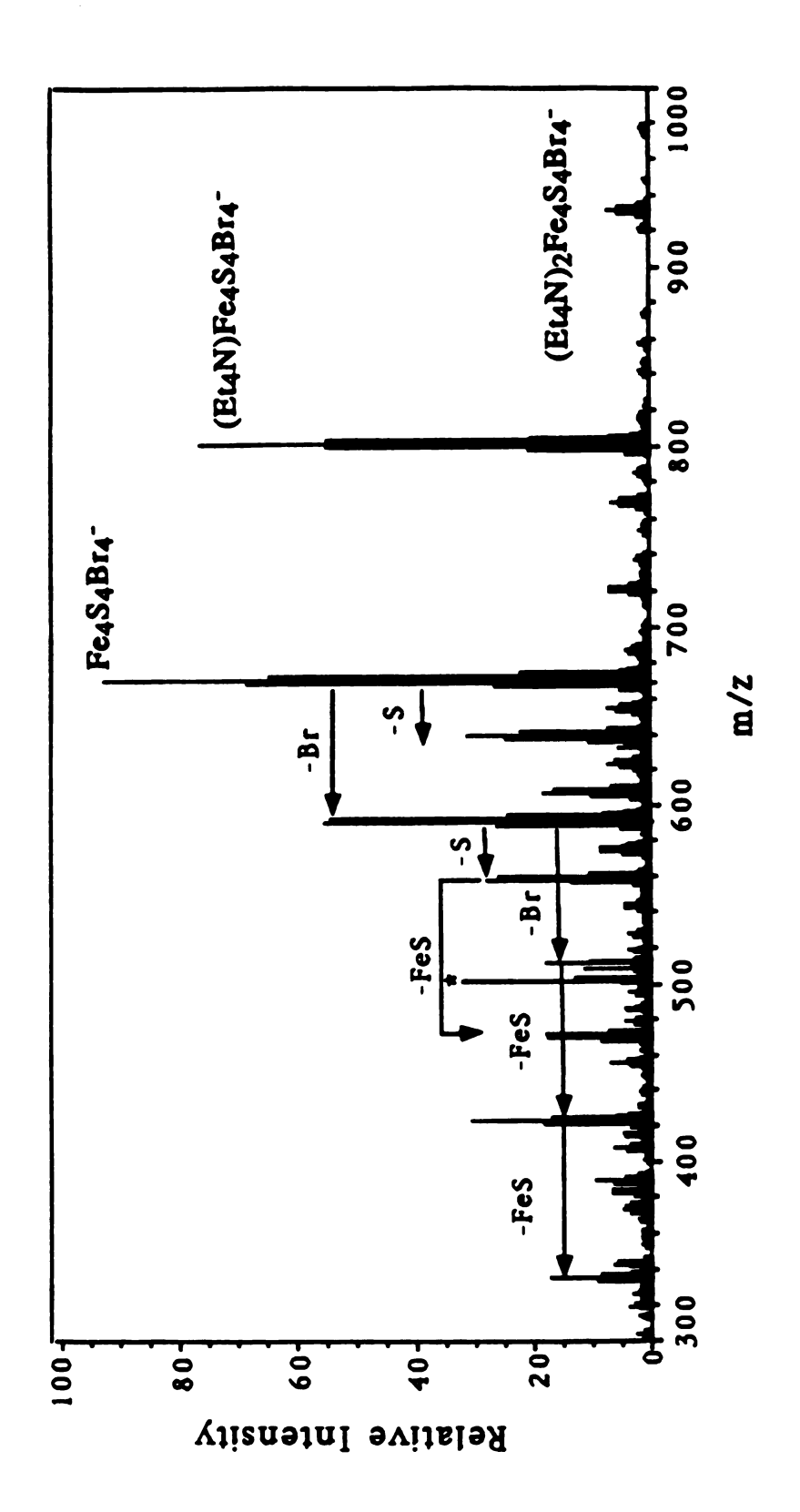


Figure 21. Negative-ion FAB mass spectrum of [(Et4N)₂Fe₄S₄Br₄] using the matrix NPOE. Matrix ions are designated by an (*).

ion spectrum, but the peak is of very low intensity. The positive and negative ion FAB mass spectra of the halogenated complexes such as (A)₂Fe₄S₄Br₄ and (A)₂Fe₄S₄Cl₄ give similar spectra to that shown for (Et₄N)₂Fe₄S₄Br₄, and these spectra are tabulated in Tables 11 and 12. All of the elemental formulae listed for the ions observed were confirmed based on the close agreement of observed/calculated isotopic distributions for the molecular formulae listed. Thus, the formula weight of the complex could be deduced from these clusters of mass spectral peaks without ambiguity. As an example, Figures 22a and 22b show the comparison between calculated and observed isotopic abundances of [(Et₄N)₃Fe₄S₄Br₄]+ and [Fe₄S₄Br₄]-, respectively. Combining the spectra from both positive- and negative-ion FAB-MS studies, a rapid molecular weight determination of iron-sulfur cluster complexes has been successfully achieved.

In addition to peaks that provide molecular weight information, Figure 21 exhibits several other peaks formed by fragmentation of the iron-sulfur cubane core. Fragment ions represented by the quartet at m/z 589, 591, 593, 595 and the triplet peak cluster at m/z 510, 512, 514 correspond to the anionic species [Fe₄S₄Br₃] and [Fe₄S₄Br₂] respectively. The relatively low intensity quartet at m/z 719, 721, 723, 725 corresponds to the cluster [(Et₄N)Fe₄S₄Br₃]. Surprisingly, we observed a number of abundant anionic fragments of the [Fe₄S₄Br₄] core structure. For example, the fragment [Fe₄S₃Br₄], appears at m/z 636-644; [Fe₄S₃Br₃] is formed, and is seen at m/z 557-563; [Fe₃S₂Br₃], is present at m/z 469-475; [Fe₃S₃Br₂], is seen at m/z 422-426; and [Fe₂S₂Br₂] is seen at m/z 334-338. In each of these cluster peaks, the bromine content dominates the isotopic "fingerprint" pattern, which allows a facile identification of these various fragment ions. The

Table 11. Cations in the FAB Mass Spectra of Complexes, (A)₂Fe₄S₄X₄ (designated as M), X = Br and Cl, using the matrix NBAa.

	(A) ₂ Fe	(A) ₂ Fe ₄ S ₄ Br ₄			(A) ₂ Fe ₄ S ₄ Cl ₄	4Cl4	
A=	Et4N	Pr_4N	Bu4N	Me4N	Bu4N	Ph4P	PPNb
$[M+A]^+$	1058	1226	1394	714	1218	1509	2106
	(100)	(100)	(100)	(100)	(100)	(100)	(100)
[M]+	928	1040	1152	040	916	1170	1568
	(52)	(45)	(10)	(32)	(32)	(16)	(41)
[M -X]+	849	3 81	1117	902	931	1135	1533
	(23)	(32)	(11)	(19)	(6)	(12)	(10)

a. Numbers in the table refer to the nominal m/z value and the relative intensities of the identified ions. Intensities, listed in paratheses, are relative to 100 for the most abundant analyte ion listed. b. PPN= $(Ph_3P)_2N$. c. $[M+A]^+ = [(A)_3Fe_4S_4X_4]^+$, $[\mathbf{M}]^+ = [(A)_2 \mathrm{Fe}_4 \mathrm{S}_4 \mathrm{X}_4]^+, \text{ and } [\mathbf{M} \cdot \mathrm{X}]^+ = [(A)_2 \mathrm{Fe}_4 \mathrm{S}_4 \mathrm{X}_3]^+.$

Table 12. Relative Intensities of Anions in the Negative Ion FAB Mass Spectra of Complexes, (A)2Fe4S4X4, X = Br and Cl, using the matrix NPOE.

				Relativ	Relative Intensities ^a	g,		
		2	(A)2Fe4S4Br4	Šr4		(A)	(A)2Fe4S4Cl4	
Ions Observed	A =	EtyN	Pr	Βυ ₄ Ν	Me4N	Bu4N	Me4N Bu4N Ph4P	(Ph ₃ P=) ₂ N
[(A) ₂ Fe ₄ S ₄ X ₄]-		=======================================	7		 -			
[(A)Fe ₄ S ₄ X ₄]-		82	78	83	83	52	53	42
[(A)Fe4S4X3]-		11	11	14	•	•	•	•
[Fe4S4X4]-	1	8	100	100	100	100	100	100
[Fe4S3X4]-		83	39	42	4	35	82	32
[Fe4S4X3]-		89	78	87	78	20	47	8
[Fe4S3X3]-		30	37	55	4	5	12	15
$[Fe_4S_4X_2]$ -		19	88	43	35	37	18	27
[Fe4S3X2]-		•	•	•	6	6	æ	7
$[Fe_4S_4X_1]$ -			•	•	10	15	12	6
[Fe ₃ S ₂ X ₃]-		20	30	39	\$	53	∞	83
[Fe ₃ S ₃ X ₂]-		33	83	09	65	8	15	39
[Fe ₂ S ₂ X ₂]-		18	33	12	40	55	47	33

a. Internsities are relative to 100 for the most abundant analyte ions.

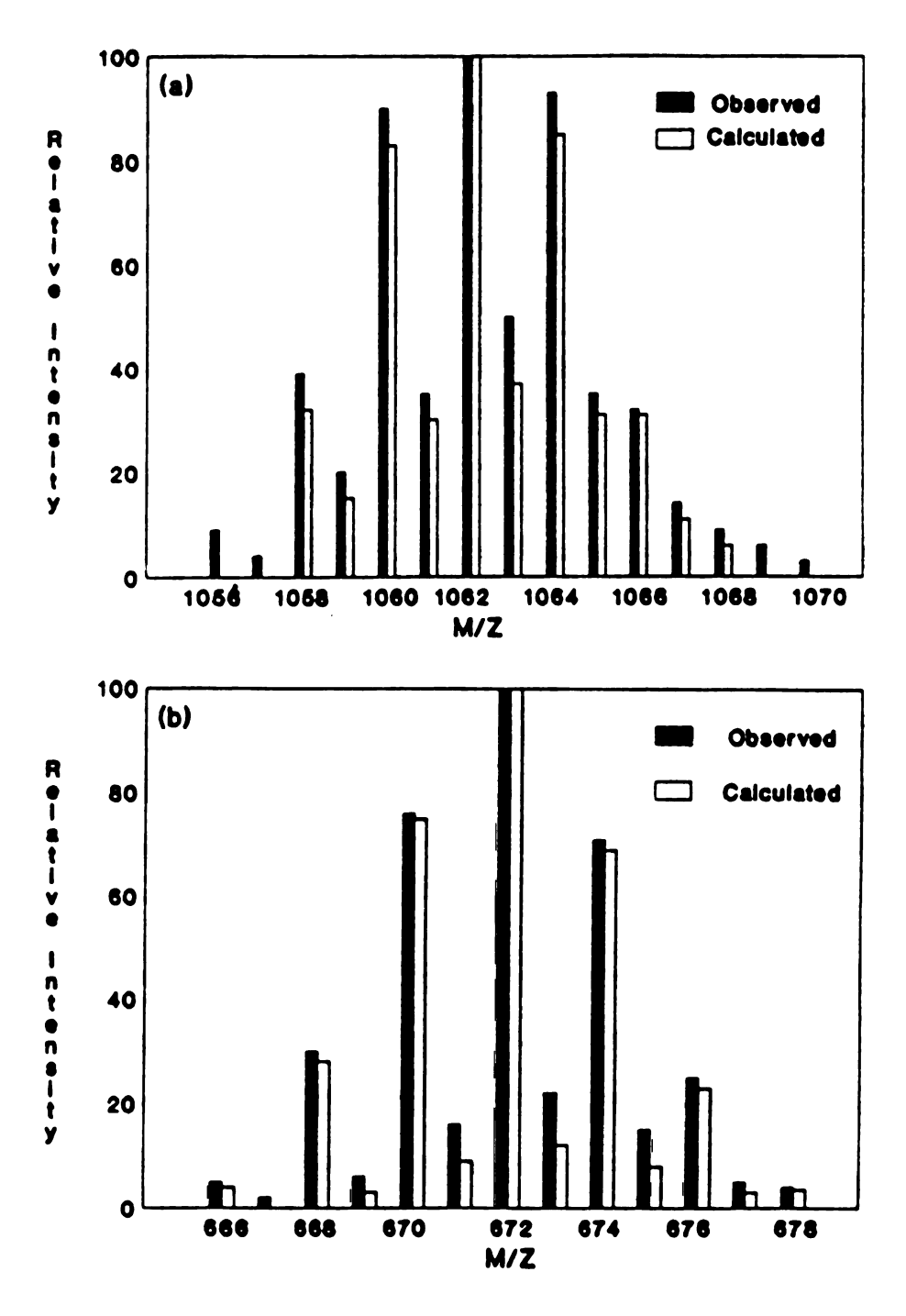


Figure 22. Comparison of isotope abundance for an experimentally observed (scribed bar) and theoretically calculated (blank bar) clusters (a) [(Et₄N)₃Fe₄S₄Br₄]+ and (b) [Fe₄S₄Br₄]-.

rich fragmentation observed in negative ion FAB-MS is also important in establishing the presence of the intact [Fe₄S₄] cluster core. Additional features of the negative ion spectrum that should be noted are the low-intensity signals appearing 16u and/or 32u above each of the major fragment peaks. These are most likely due to oxygen atom transfer reactions involving matrix molecules such as NBA or NPOE. Oxygen additions have been observed before in the FAB-MS of organometallic compounds⁸². The chemistry may well take place in the gas phase, between iron-sulfur-containing anions and individual matrix molecules. In support of this possibility, we note that McElvany and Allison⁸³ have reported the gas phase, bimolecular chemistry of transition-metal containing anions such as Fe(CO)₃- with n-nitroalkanes, using ion cyclotron resonance (ICR) mass spectrometry. In these systems, products such as [Fe(CO)₃O]- are formed due to oxo-transfer from the NO₂ group of the organic molecule.

The negative ion FAB mass spectra of these iron-sulfur cubanes are dominated by ions with a net charge of -1. Of particular interest in these experiments would be the detection of the doubly-charged core, [Fe₄S₄Br₄]². This ion has the same nominal mass as the singly-charged fragment [Fe₂S₂Br₂]. The two species can be easily distinghuished, since the -1 ion will exhibit isotopic peaks due to the presence of Br, which will be separated by 2 m/z units. If the doubly-charged anion peak is present, it will have the same nominal mass, but a much richer isotopic pattern, since it contains four bromine atoms. In addition, for the -2 ion, the major isotopic peaks will be separated by 1 m/z unit. Doubly-charged ions have been previously reported in the FAB analysis of transition metal-containing compounds.

For example, abundant doubly-charged cations, such as [Ru(bpy)₃]²⁺, from ruthenium(II) complexes, have been generated in FAB mass spectrometry⁸⁴. The spectrum of (Et₄N)₂Fe₄S₄Br₄ (Figure 12), reveals an isotopic cluster of peaks with a nominal m/z value of 334, however careful analysis of the isotopic pattern indicates that no peak due to [Fe₄S₄Br₄]²-species is present; the m/z 334 cluster only represents the anion [Fe₂S₂Br₂]. In this case, the doubly-charged anion may not be a stable species in the gas phase. While the dianion certainly exists in solution, there are a number of reasons why it may not be observed in the FAB experiment. In the desorption process, it may transfer an electron to the nitroaromatic matrix, following a lower energy pathway. Even if the dianion is desorbed intact, it may either eject an electron spontaneously, or lose an electron in a subsequent collision with a desorbed matrix molecule.

(B). Negative-ion FAB mass spectra of thiolated iron-sulfur cubane clusters, $(A)_2Fe_4S_4(SR)_4$, R=Ph and Et.

Our experience with the halide-containing Fe/S compounds demonstrated that negative ion FAB mass spectrometry is superior for the analysis of such compounds. Therefore only negative ion spectral results will be presented for the complexes that contain sulfur-based terminal ligands. The features of the negative-ion FAB mass spectrum of $(A)_2Fe_4S_4(SPh)_4$, Figure 23, obtained using the matrix NPOE, are analogous to those presented for $(A)_2Fe_4S_4Br_4$ and $(A)_2Fe_4S_4Cl_4$. For example, the negative-ion spectrum of the molecule $(Ph_4P)_2Fe_4S_4(SPh)_4$ displays clusters of peaks representing the [M-A]- fragment, $[(Ph_4P)Fe_4S_4(SPh)_4]$ -, at m/z = 1127, and the intact $[Fe_4S_4(SPh)_4]$ core, as the -1 ion at m/z 788. Dominant

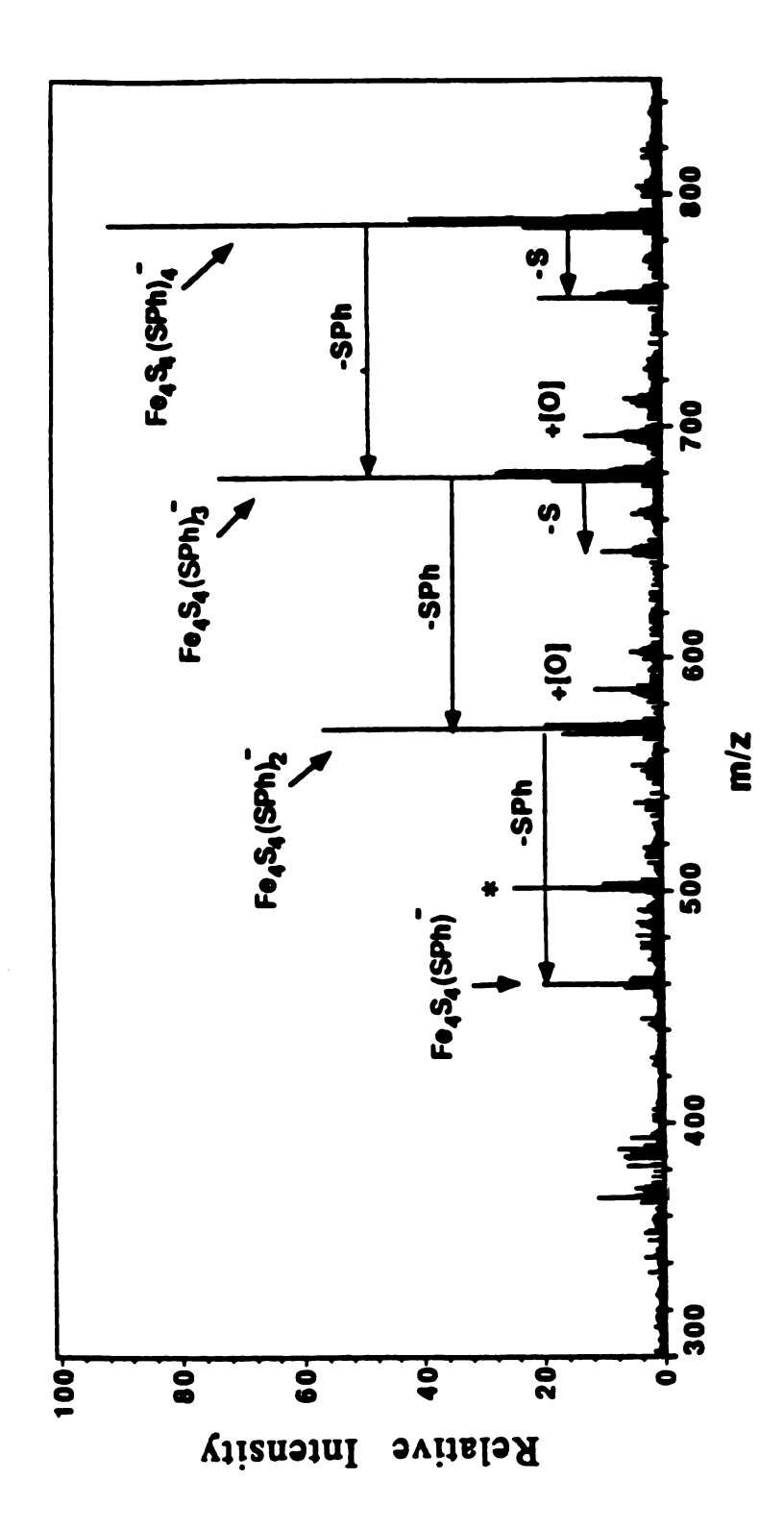


Figure 23. Negative-ion FAB mass spectrum of (Ph4P)2Fe4S4(SPh)4, using the matrix NPOE. Matrix ions are designated by an (*).

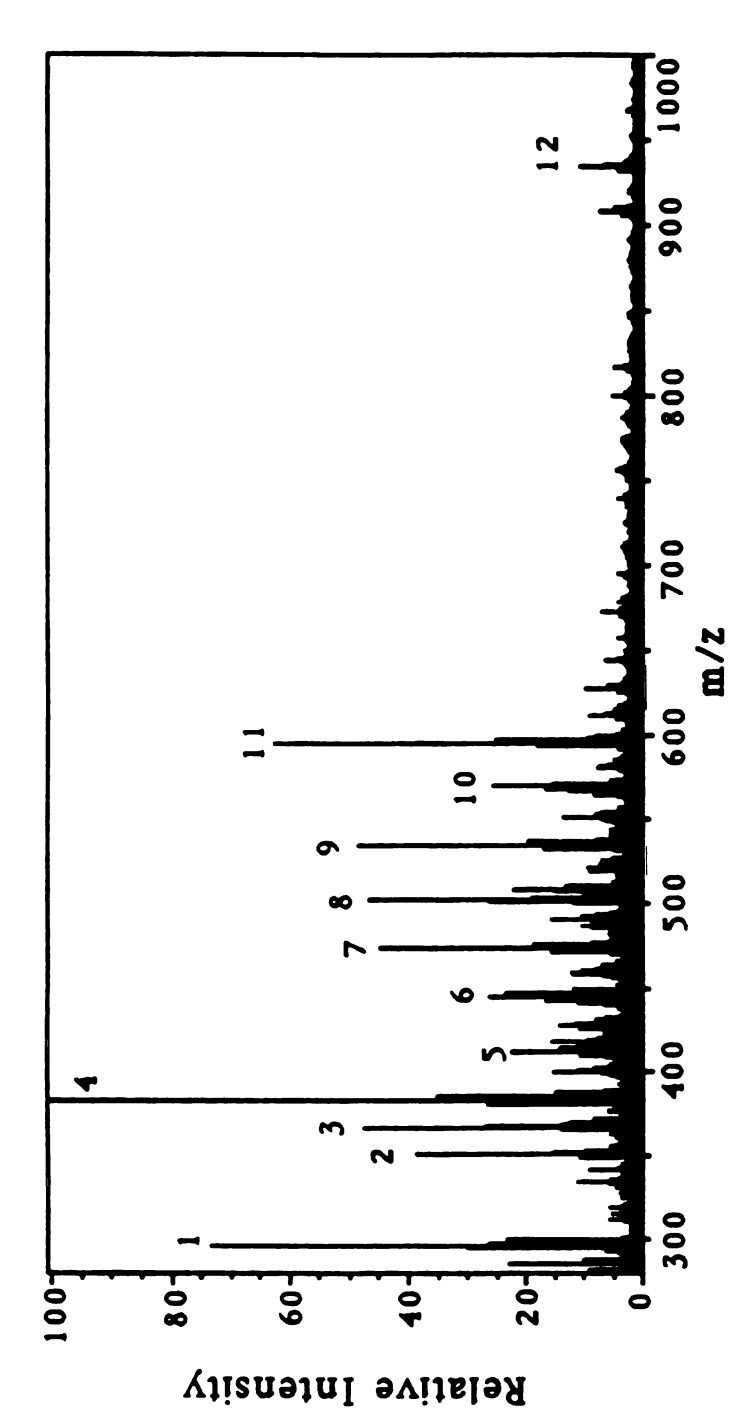
fragment ions include $[Fe_4S_3(SPh)_4]^-$ (m/z 756), $[Fe_4S_4(SPh)_3]^-$ (m/z 679), $[Fe_4S_3(SPh)_3]^-$ (m/z = 647), $[Fe_4S_4(SPh)_2]^-$ (m/z 570), and $[Fe_4S_4(SPh)]^-$ (m/z 460) (Figure 5). The negative ion spectra, for two different counter cations (A+), are summarized in Table 13.

In the negative ion FAB analysis of the A₂Fe₄S₄X₄ compounds, certain ions are always seen, and can be thought of as important indicators These include: $[AFe_4S_4X_4]$ -, $[Fe_4S_4X_4]$ -, for cubane-based analytes. $[Fe_4S_4X_3]$ -, $[Fe_4S_4X_2]$ -, $[Fe_4S_4X]$ -, and $[Fe_2S_2X_2]$ -. These are observed when X = SPh and SEt as well as when X = Br and Cl. However, the two thiolato clusters also reveal important differences in their mass spectra. More extensive fragmentation is observed when X = SEt, than when X = SPh. This can be seen in the negative ion spectrum of (Ph₄P)₂Fe₄S₄(SEt)₄, shown in Figure 24. A series of unusual fragment ions deriving from C-S cleavage processes and not found in the spectrum of the SPh analog, are $[Fe_4S_5(SEt)_3]$ - (m/z 567), $[Fe_4S_5(SEt)_2]$ - (m/z 506), $[Fe_4S_5(SEt)]$ - (m/z 445), and $[Fe_4S_5]$ -, (m/z 384). These observations are consistent with the fact that the SEt ligand contains a relatively weak bond. For RS radicals, the C-S bond of CH₃S is almost 20 kcal/mol weaker than the C-S bond in the PhS radical⁸⁵. Thus, alkyl C-S bond cleavage is certainly not surprising in the -SEt containing complexes. Also notable in this spectrum are the peaks representing [Fe₄S₄], m/z 352. This is the only example of an iron/sulfur cubane compound that exhibits an anion which represents the [Fe₄S₄] core. The extremely active species $[Fe_4S_4]$ - can further react with desorbed matrix molecules, as described earlier, to produce the $[Fe_4S_4(O)]$ - ion (m/z =368). We note that this is analogous to the $[Fe_4S_5]$ - ion that is observed as a

Table 13. Relative Intensities of Peaks in the Negative Ion FAB Mass Spectra of Complexes, (A)₂Fe₄S₄(SR)₄, R=Et and Ph, using the matrix NPOEa.

		Relative	Intensities	
	(A) ₂ Fe ₄ S ₄ (SEt) ₄	4(SEt)4	(A) ₂ Fe ₄ S ₄ (SPh) ₄	SPh)4
Ions Observed	Ph	PhyAs	Ph4P	Bu ₄ N
(A)Po.Q.(QP)	1.9	10	41	14
(x)/F.e4D4(D10)4	1 8	3 5		1 6
Fe454(SR)4-	3	19	001	F3
$\text{Fe}_{4}\text{S}_{5}(\text{SR})_{3}$ -	22	25	•	•
$Fe_4S_3(SR)_4$ -	•	•	8	•
$\text{Fe}_{4}\text{S}_{4}(\text{SR})_{3}$	48	43	74	83
Fe4S5(SR)2-	22	30	•	•
$Fe_4S_3(SR)_3$	•	•	13	•
$\text{Fe}_4\text{S}_4(\text{SR})_2$ -	45	. 25	22	40
$\mathrm{Fe_4S_5(SR)_1}$ -	5 2	15	•	•
$\text{Fe}_{4}\text{S}_{4}(\text{SR})_{1}$	83	12	07	19
Fe4S5-	100	100	•	•
Fe4S4-	38	32	•	•
Fe ₂ S ₂ (SR) ₂ -	74	65	ro	100

a. Intensities are relative to 100 for the most abundant ions.



the matrix NPOE. Matrix ions are designated by an (*). Assignment of Figure 24. Negative-ion FAB mass spectrum of (Ph4P)2Fe4S4(SEt)4, using cluster peaks: 1. [Fe₂S₂(SEt)₂]-, 2. [Fe₄S₄]-, 3. [Fe₄S₄(O)]-, 4. [Fe₄S₅]-, 5. $[Fe_4S_4(SEt)]^2$, 6. $[Fe_4S_5(SEt)]^2$, 7. $[Fe_4S_4(SEt)_2]^2$, 8. $[Fe_4S_5(SEt)_2]^2$, 9. $[\text{Fe}_4S_4(\text{SE}t)_3]$, 10. $[\text{Fe}_4S_6(\text{SE}t)_3]$, 11. $[\text{Fe}_4S_4(\text{SE}t)_4]$, 12. $[\text{Ph}_4P)[\text{Fe}_4S_4(\text{SE}t)_4]$.

fragment ion. The complete data representing the negative ion FAB analyses of the cubanes containing -SR ligands are listed in Table 13.

The data presented above for clusters with sulfur-containing ligands were obtained using NPOE as a matrix. When the matrix is nitrobenzyl alcohol (NBA), the complicated but interesting spectrum shown in Figure 25 is obtained. A rich chemistry occurs between NBA and compounds such as $(Ph_4P)_2Fe_4S_4(SEt)_4$ (M). In the mass range 900-1400, a group of cluster peaks have been assigned as [M-(Ph₄P)]- (m/z 935), [M-(Ph₄P)+NBA-HSEt]- $(m/z 1026), [M-(Ph_4P)+2(NBA-HSEt)]^- (m/z 1117), [M-(Ph_4P)+3(NBA-HSEt)]^-$ (m/z 1208), and $[M-(Ph_AP)+4(NBA-HSEt)]$ - (m/z 1299). The second group of cluster peaks in the mass range from 590 to 970 correspond to [M-2(Ph₄P)] $(m/z 596), [M-2(Ph_4P)+NBA-HSEt]^- (m/z 687), [M-2(Ph_4P)+2(NBA-HSEt)]^-$ (m/z 778), $[M-2(Ph_4P)+3(NBA-HSEt)]^-$ (m/z 869), and $[M-2(Ph_4P)+4(NBA-HSEt)]^-$ HSEt)] (m/z 960). Relative abundances of ion species are listed in Table 14. The results reveal the occurance of stepwise ligand substitution reactions. The acid-base reaction (Eq 1) proceeds to the right when R'SH is a stronger acid than RSH, the conjugate acid of the coordinatated thiolate, and this methodology has been well exploited to synthesize [Fe₄S₄] complexes with virtually any desired ligands or combination of ligands⁶⁴,⁶⁵. Averill and coworkers⁷¹ have also applied this method to synthesize phenoxide complexes such as $[Fe_4S_4(OAr)_4]^{2-}$ (Eq. 2),

$$[Fe_4S_4(SR)_4]^{2-} + nR'SH \longrightarrow [Fe_4S_4(SR)_{4-n}(SR')_n]^{2-} + nRSH$$
 (1)

$$[Fe_4S_4(SR)_4]^{2-} + nArH \longrightarrow [Fe_4S_4(SR)_{4-n}(OAr)_n]^{2-} + nRSH \qquad (2)$$

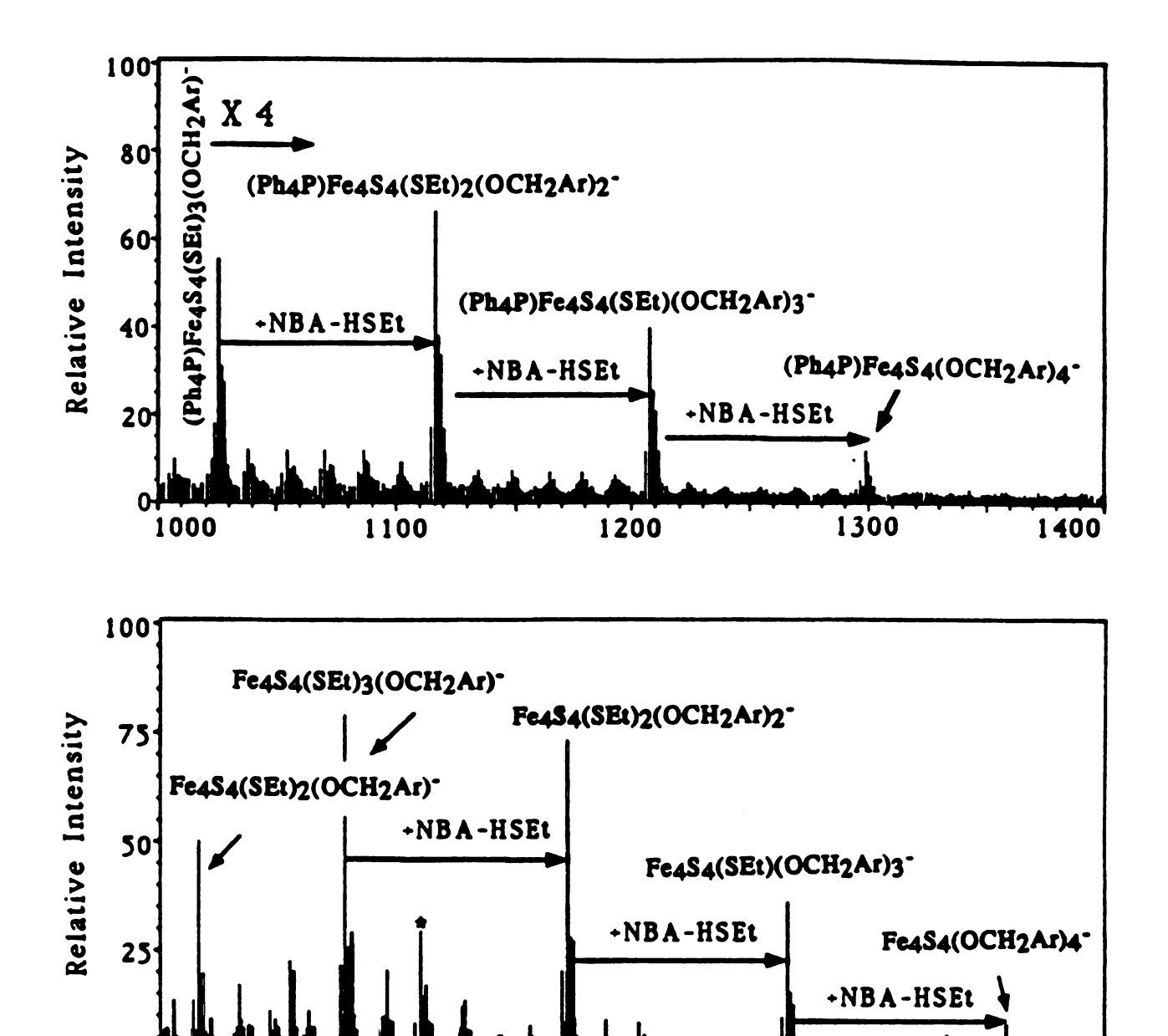


Figure 25. Negative-Ion FAB mass spectrum of (Ph₄P)₂Fe₄S₄(SEt)₄, using the matrix NBA. Matrix ions are designated by an (*).

m/z

Table 14. Relative Intensities of Peaks in the Negative FAB Mass Spectrum of (Ph₄P)₂Fe₄S₄(SEt)₄, (designed as M), using the matrix NBA.

Ions Observed	m/z	Relative Intensities ^a
[M-(Ph ₄ P)+4(NBA-HSEt)]-	1299	2
[M-(Ph ₄ P)+3(NBA-HSEt)]-	1208	6
[M-(Ph ₄ P)+2(NBA-HSEt)]-	1117	11
$[M-(Ph_4P)+(NBA-HSEt)]$	1026	8
$[M-(Ph_4P)]^-$	935	4
$[M-2(Ph_4P)+4(NBA-HSEt)]$	960	5
$[M-2(Ph_4P)+3(NBA-HSEt)]^{-}$	869	44
$[M-2(Ph_4P)+2(NBA-HSEt)]$	778	88
[M-2(Ph ₄ P)+(NBA-HSEt)]-	687	100
[M-2(Ph ₄ P)+NBA-2HSEt]-	626	47
[M-2(Ph ₄ P)]-	596	63

a.Intensities are relative to 100 for the most abundant analyte ions. Nominal mass is used for m/z value.

Although such ligand substitution reactions with thiols and phenols have been studied in solution by ${}^{1}H$ -NMR 64e,71 , similar studies involving alcohols were not reported. However, it is intuitively expected that alcohols with acidic -OH groups will behave similarly, perhaps with smaller equilibrium Obviously in this work, ligand substitution reactions are constants. occuring, involving the -SR ligand on the iron-sulfur complex, and the matrix molecules (alcohols). There are three possible explanations for this occurance. First, it could be a simple analyte/matrix reaction that occurs when the two are mixed. Second, it could be chemistry induced by the fast atom beam (again, condensed phase chemsitry). Third, it could occur for the gas phase ions, with desorbed matrix molecules, and not be representative of solution chemistry at all. Since these peaks are so dominant, such extensive conversion of reactants to products would be unlikely if the chemistry occurred in the gas phase. On the other hand, we have used ${}^{1}H$ -NMR to study the reaction between $[Fe_{4}S_{4}(SEt)_{4}]^{2}$ - and NBA in d⁶-DMSO. Ligand substitution chemistry does occur, to form [Fe₄S₄(SEt)₄. $_{n}(OCH_{2}Ar)_{n}]^{2}$, although the reaction is exceedingly slow, showing approximately 15% of the reactant being converted into products after 72 h. Thus, this may well be an example of fast atom bombardment-induced chemistry, in which the particle bombardment of the matrix facilitates the rate of the ligand exchange reactions.

(C). The FAB-MS analysis of mixed-ligand cubane clusters.

The utility of FAB-MS to analyze the mixed ligand cluster, $(Ph_4P)_2Fe_4S_4(SPh)_2Cl_2$, was evaluated. A simple spectrum representative of this analyte was not expected, since NMR studies⁶⁵ have shown that, in

solution, this complex disproportionates, and exists in equilibrium with other mixed ligand clusters represented by equations 3-5

$$2[Fe_4S_4(SPh)_2Cl_2]^{2-} \longrightarrow [Fe_4S_4(SPh)Cl_3]^{2-} + [Fe_4S_4(SPh)_3Cl]^{2-} \qquad (3)$$

$$[Fe_4S_4(SPh)Cl_3]^{2-} + [Fe_4S_4(SPh)_3Cl]^{2-} \longrightarrow [Fe_4S_4(SPh)_2Cl_2]^{2-} + [Fe_4S_4(SPh)_4]^{2-} \qquad (5)$$

The negative ion FAB-MS analysis, using the matrix NPOE, confirms the existence of these disproportionation species in solution. The ions observed are listed in Table 15. In the high mass range between 800-1100, there are four major clusters of peaks corresponding to [(Ph₄P)Fe₄S₄Cl₄] (m/z 831), $[(Ph_4P)Fe_4S_4(SPh)Cl_3]^-$ (m/z 905), $[(Ph_4P)Fe_4S_4(SPh)_2Cl_2]^-$, (m/z 979), and [(Ph₄P)Fe₄S₄(SPh)₃Cl]⁻ (m/z 1053). A second group of peaks in the middlemass range are assigned as [Fe₄S₄Cl₄]-/[Fe₄S₄(SPh)Cl]-/[Fe₄S₃(SPh)Cl₂]-(overlapping cluster peaks with nominal m/z values of 492, 496 and 499, respectively), [Fe₄S₄(SPh)Cl₂]-/[(Fe₄S₃(SPh)Cl₃]- (overlapping cluster peaks with nominal m/z values of 531 and 534, respectively), [Fe₄S₄(SPh)Cl₃] (m/z 566), [Fe₄S₄(SPh)₂Cl]-/[Fe₄S₃(SPh)₂Cl₂]-(overlapping cluster peaks with nominal m/z values of 605 and 608, respectively), $[Fe_4S_4(SPh)_2Cl_2]$ -, (m/z)640), and $[Fe_4S_4(SPh)_3Cl]^-$ (m/z 714). The group of peaks in the low mass region show fragment ions related to the ligand dissociation or core decomposition of $[Fe_4S_4Cl_4]$ - as described above. A series of oxidized fragment ions, appearing 16u and/or 32u above the major fragments, were also observed as described above.

Depending on the extent of disproportionation shown in equations 3-5, we might expect to see mass spectral features indicative of

Table 15. Relative Intensities of Peaks in the Negative Ion FAB Mass Spectrum of the complex, (Ph₄P)₂Fe₄S₄(SPh)₂Cl₂, in DMF/NPOE^a.

Fragment Ions	m/z	Relative Intesity
[(Ph ₄ P)Fe ₄ S ₄ (SPh) ₃ Cl]-	1053	7
$[(Ph_4P)Fe_4S_4(SPh)_2Cl_2]^-$	979	15
$[(Ph_4P)Fe_4S_4(SPh)Cl_3]$	905	22
$[(Ph_4P)Fe_4S_4Cl_4]^-$	831	17
$[Fe_4S_4(SPh)_3Cl]^-$	714	20
$[Fe_4S_4(SPh)_2Cl_2]$	640	52
$[Fe_4S_3(SPh)_2Cl_2]$	608	18
$[Fe_4S_4(SPh)_2Cl]^-$	605	22
$[Fe_4S_4(SPh)Cl_3]$	566	63
$[Fe_4S_3(SPh)Cl_3]^-$	534	30
$[Fe_4S_4(SPh)Cl_2]^-$	531	62
$[Fe_4S_3(SPh)Cl_2]^-$	499	25
[Fe ₄ S ₄ (SPh)Cl]-	496	45
[Fe ₄ S ₄ Cl ₄]-	492	47
$[Fe_4S_3Cl_4]^-$	460	35
[Fe ₄ S ₄ Cl ₃]-	457	85
$[Fe_4S_3Cl_3]$	425	56
$[Fe_4S_4Cl_2]$	422	100
$[Fe_4S_3Cl_2]$	390	33
[Fe ₄ S ₄ Cl]-	387	68
$[Fe_3S_2Cl_3]$	337	30
[Fe ₃ S ₃ Cl ₂]-	334	72

a. Intensities are relative to 100 for the most abundant analyte ions. Nominal mass is used for m/z value. b. Peaks with m/z values less than 300 are not listed in this table.

(Ph₄P)Fe₄S₄(SPh)₄. Representative ions of this species are not seen in the spectrum of (Ph₄P)₂Fe₄S₄(SPh)₂Cl₂. Most of the fragments can be explained by the loss and addition of SPh or Cl ligands from the mixed ligand complex. At present, three clusters of peaks representing [Fe₄S₄(SPh)Cl₃]-, [Fe₄S₄(SPh)₂Cl₂]-, and [Fe₄S₄(SPh)₃Cl]- have been identified, but no evidence was obtained for the existence of [(Ph₄P)Fe₄S₄(SPh)₄]- and/or [Fe₄S₄(SPh)₄]-. This maybe due to further equilibria established between [Fe₄S₄(SPh)₄]²- and [Fe₄S₄(SPh)_{4-n}Cl_n]²- species. This is may be expected in view of the known lability of the [Fe₄S₄X₄]²- complexes^{64e}. Our FAB mass spectral results are in excellent agreement with the aforementioned solution equilibria.

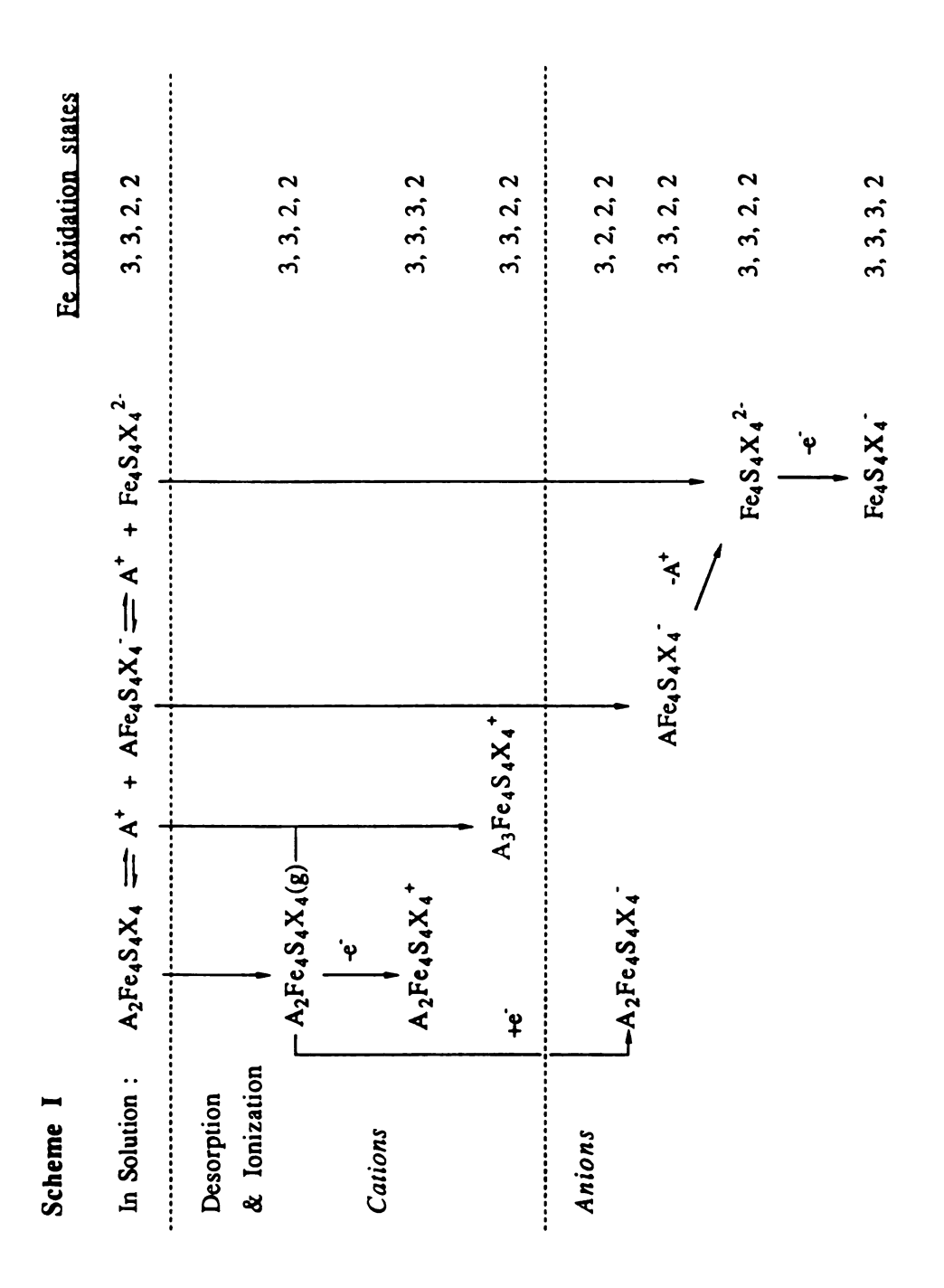
2. Proposed Fragmentation Mechanisms: Correlations between Negative Ion FAB-MS Data and Known Iron-Sulfur Cluster Chemistry in Condensed Phases

Before evaluating the types of ions observed in these experiments, first, a comment should be made on what might be expected in a mass spectral study of ions derived from salts containing the Fe₄S₄ core in which the iron atoms are in +2 and +3 formal oxidation states, as (Fe²⁺)₂(Fe³⁺)₂(S²⁻)₄. When electron impact ionization is used to ionize a compound such as Fe(CO)₅, a dominant ion in the resulting mass spectrum is Fe⁺, which represents an oxidation state not typically considered in condensed phases. Thus, one might expect to generate fragments of the Fe₄S₄ core in which unusual oxidation states of the metal are present. On the other hand, it is a general "rule of thumb" in the mass spectrometry of inorganic and

organometallic compounds⁸⁶, that the dominant ions are formed with a minimal perturbation to the formal oxidation state of the metal in the compound undergoing ionization. In the iron pentacarbonyl case, the iron atom is formally taken from an oxidation state of 0 in the neutral compound to +1 as the univalent cation (and in all fragment ions such as Fe(CO)₃+). In contrast, the Ti+ peak in the mass spectrum of TiCl₄ is a very minor peak, because its formation would require the conversion of Ti⁴⁺ to Ti+. In this case, ions such as TiCl₃+ dominate, in which no net change in the oxidation state of the metal occurs. Thus, we might expect, based on the oxidation states of iron atoms in the Fe₄S₄ core, that fragment ions will be formed in which the metal atoms are in their readily accessible +2 and +3 oxidation states.

Ionic complexes such as the (A)₂Fe₄S₄X₄ salts that are the subject of this study, once dissolved in solution, produce a variety of ionic species such as (A)+, (A)+[Fe₄S₄X₄]²-, and [Fe₄S₄X₄]²-, as suggested in Scheme I. When the solution is subjected to fast atom bombardment, desorption of neutral species and ionic complexes from the analyte/matrix target leads to a variety of gas phase species. Presumably, the neutral, intact molecule desorbs to some extent. Also, the ionic components desorb as ions ("preionized species", as they are commonly called in FAB), and from these, the ions observed in the FAB spectra are derived.

Following desorption, the intact neutral molecule $(A)_2Fe_4S_4X_4$ may be converted into the molecular ion, $[(A)_2Fe_4S_4X_4]^+$, either via a gas phase charge transfer reaction, or by a subsequent interaction of the desorbed molecule with a fast atom. The countercation, A^+ , apparently forms



adducts with gas phase species formed in the FAB process, yielding both A+-matrix complexes, as well as adducts with the desorbed neutral analyte, [(A)₃Fe₄S₄X₄]+. These are the two possible "primary" cations formed, from which fragment ions may be generated. The major fragment ion is [(A)₂Fe₄S₄X₃]+, which we propose is formed by the loss of an X radical from the molecular cation. Consider the reaction of the loss of an X ligand, not as an anion, but as a radical. When X is lost, the formal oxidation state of one of the iron atoms must change (reduction). We propose two ways to consider this simple process (which will become very powerful when anionic fragments are considered). For the unimolecular dissociation reaction (eq. 6),

$$A_{2}Fe_{4}S_{4}X_{4}^{+} \longrightarrow A_{2}Fe_{4}S_{4}X_{3}^{+} + X \tag{6}$$

One can keep track of the oxidation states of the iron atoms, or of the $[Fe_4S_4]$ core. The formal charges on the four metal atoms change in this dissociation reaction from $\{+3, +3, +3, +2\}$ to $\{+3, +3, +2, +2\}$. If the $[Fe_4S_4]$ core is considered, it changes from $[Fe_4S_4]^{+3}$ to $[Fe_4S_4]^{+2}$ (i.e., a net reduction of the core) when a ligand is lost as a radical. Apparently no fragments evolve from the adduct ion $[(A)_3Fe_4S_4X_4]^+$, in which the iron atoms are also in the oxidation states $\{+3, +3, +2, +2\}$.

Returning to Scheme I, the early steps in the chemistry that leads to the desorption/ionization of anionic species can be described, by considering the species that can be desorbed from the analyte/matrix solution. Once desorbed, the intact neutral molecule can capture an electron to form the molecular anion, $[(A)_2Fe_4S_4X_4]$. The "preformed ion", $[(A)Fe_4S_4X_4]$, can be

desorbed directly from the matrix. Presumably, the $[Fe_4S_4X_4]^{2-}$ dianion can be desorbed directly, to some extent, although the spectra suggest that, if this occurs, it is completely converted into the univalent anion, $[Fe_4S_4X_4]^{-}$. Note that, these "primary" cations and anions shown in Scheme I, from which all fragment ions will be formed, <u>all</u> contain iron atoms that only involve combinations of the +2 and +3 formal oxidation states. Thus, while it is certainly possible to generate complexes of iron in mass spectrometry that contain Fe^{+1} , none are present in these ions listed in Scheme I.

Scheme II presents proposed unimolecular fragmentation pathways to explain the evolution of the rich collection of fragment anions formed by fast atom bombardment. The pathways proposed here are based on a few simple assumptions. First, for an ion with a charge of -1 to form a fragment ion with a charge of -1, either a radical or an uncharged even-electron fragment must be lost. Obvious candidates for neutral species lost include fragments such as X and FeS. One may consider loss of the neutral [FeSX], but not [Fe] alone, because of the bonding environment in the starting material. That is, we would not expect a fragment ion with 2 or 3 iron atoms, but all four X ligands still present. Next, the loss of neutral "A" was not considered - that is, while one may expect to lose a chlorine radical, one would not lose a tetra-alkyl ammonium radical. Third, the loss of "AX" was considered as an allowable fragmentation. An example of "AX" elimination is shown in equation 7. If, for example, A+ is Et₄N+, and the cluster contains X=Br, "AX" loss is equivalent to the loss of {Et₃N and EtBr}.

$$[(Et_4N)_2Fe_4S_4Br_4]^{----}[(Et_4N)Fe_4S_4Br_3]^{-}+Et_3N+EtBr$$
(7)

Scheme II		
	Oxidation Fe Atom	States Fe-S core
	re Atom	re-s cole
$Fe_4S_4X_4$	3, 3, 3, 2	+3
AFe ₄ S ₄ X ₄	3, 3, 2, 2	+2
$A_2 Fe_4 S_4 X_4 - X$	3, 2, 2, 2	+1
-'AX' \ -S \		
AFe ₄ S ₄ X ₃	3, 2, 2, 2	+1
Fe ₄ S ₄ X ₃ -2FeSX	3, 3, 2, 2	+2
$-X$ $-Fe_4S_3X_4$	3, 2, 2, 2	+3
Fe ₄ S ₄ X ₂	3, 2, 2, 2	+1
-X' -FeSX Fe ₄ S ₃ X ₃	2, 2, 2, 2	+2
Fe ₄ S ₄ X -FeS -FeS	2, 2, 2, 2	0
-FeS Fe ₃ S ₂ X ₃	2, 2, 2	+2
Fe ₃ S ₃ X ₂	3, 2, 2	+1
-X· -FeS		
Fe ₃ S ₃ X	2, 2, 2	0
Fe ₂ S ₂ X ₂	3, 2	+1

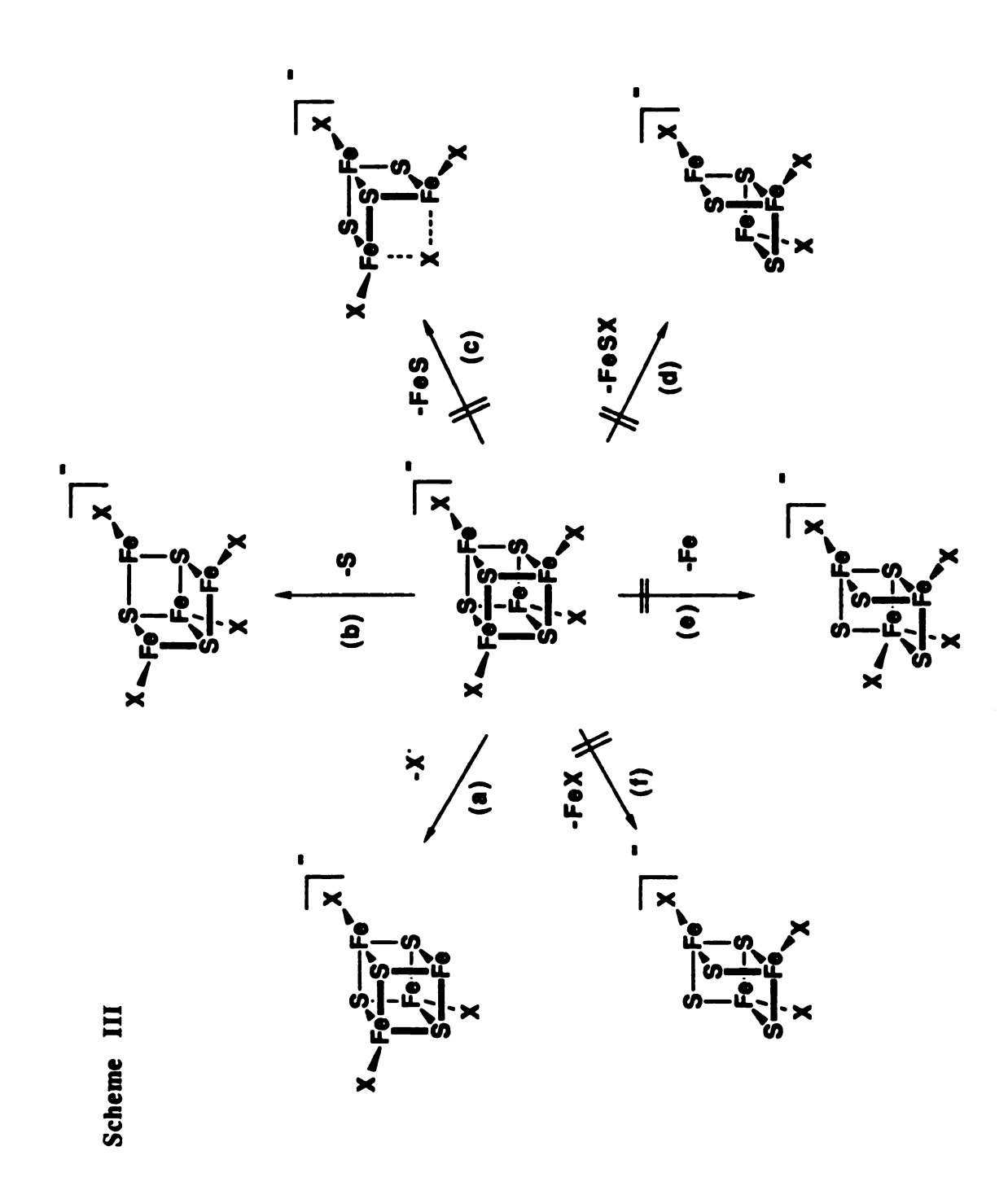
Scheme II lists the 4, 3 and 2-Fe-containing fragment ions that are observed, with various numbers of sulfur atoms and X ligands incorporated. The column on the right side of Scheme II lists the formal oxidation states of the iron atoms associated with each chemical species. It clearly shows that all of the unimolecular dissociation chemistry occurs without having to invoke the formation of exotic valence states of any of the iron atoms within the remaining core. This becomes very important in understanding and interpreting the mass spectra of such compounds. It suggests that, in the negative ion spectra of iron sulfur clusters, an anion representative of the cubane core [Fe₄S₄]- would not be expected, since this would force one of the iron atoms to be reduced from +2 to +1. In fact, the fragment ion, [Fe₄S₄]-, is only detected from ionization of [Fe₄S₄(SEt)₄]²-. Essentially, all of the ions observed are those that can exist in the context of the one restriction - maintaining the iron atoms as either +2 or +3 metals.

The observation of $[Fe_4S_4]^-$, in one case only, deserves comment. Whatever its structure, the four iron atoms must be in the oxidation states $\{+2, +2, +2, +1\}$. As seen in Table III, this anion is only formed from compounds that also form the $[Fe_4S_5]^-$ anion. The two may be chemically linked, with $[Fe_4S_4]^-$ being a fragment of the more abundant $[Fe_4S_5]^-$ species. We note that this one violation of the oxidation state restriction, that seems to hold for all other fragment ions, involves a complete cubanecore, as opposed to some cubane-fragment. Of all of the $[Fe_mS_n]$ species encountered in this work, it would surely be the intact cubane that could most effectively delocalize an extra electron. Thus it is not surprising that the only exception to the rule occurs not for a small fragment ion but for a

larger species containing four iron atoms, in which the cubic geometry is presumably intact.

Further insights into the fragmentation mechanisms, which provide a very interesting link between the ions listed in Scheme II, can be seen by considering the overall oxidation state of the [Fe_mS_n] cores of the various ions. For all of the fragmentations suggested, if the oxidation state of the iron/sulfur core is considered, only reductive eliminations, or fragmentations in which there is no change in the oxidation state, are observed. The extent to which a "primary ion" leads to fragment ions is clearly linked to its [Fe_mS_n] core oxidation state. The ion that leads to most of the fragment anions observed is $[Fe_4S_4X_4]$ -, which contains a $[Fe_4S_4]^3$ + core. Clearly, it leads to fragment ions with [Fe_mS_n] core oxidation states of +3, +2, and +1. When it fragments to form an ion with an Fe_mS_n core that is in a +3 or +2 state, that fragment dissociates further. The most dramatic example is shown in the pathway in Scheme II that leads from $[Fe_4S_4X_4]$ - to [Fe₃S₃X]-, in which the [Fe_mS_n] cores of the species involved smoothly change their oxidation state from +3 to +2 to +1 to 0! Thus, we propose here that, in the FAB analyses of iron-sulfur cluster compounds, the primary ions formed by FAB fragment through reductive chemistry in which all of the metal atoms retain +2 and +3 oxidation states, and the $[Fe_mS_n]$ core oxidation states do not increase as the unimolecular dissociations occur. Both one and two electron reductions are proposed in Scheme II.

These insights make it straightforward to interpret these mass spectra and will be important guidelines with which spectra of related compounds can be correlated with structure. For each ion that is a primary ion of FAB, we can predict which fragment ions can be formed and which can not. An example is shown in Scheme III, beginning with the ionic species, [Fe₄S₄X₄], as an example. One might expect that the ion could lose as possible neutral fragments X, S, FeS, FeX, FeSX, or Fe. We consider each of these possibilities in Scheme III: pathway a: the conversion of [Fe₄S₄X₄]- to [Fe₄S₄X₃]- suggests the dissociation of a labile ligand X as a radical. It forms a fragment ion which only incorporates Fe(II) and Fe(III)'s, thus should be expected and is observed; pathway b: the same is true for the degradation to [Fe₄S₃X₄] by the loss of S, which produces a {+3, +2, +2, +2} iron core by a two electron reduction; pathway c: the destruction of the cubane core by the loss of FeS also leads to a fragment ion in which no Fe atoms need to be in states other than +2 or +3, however, it is not observed. Presumably, the halogens are bonded to the iron atoms, and an iron cannot be lost with the ionic fragment retaining four halogens; pathway d: the fragment from the loss of a relatively large FeSX fragment is reasonable, yet is not observed (i.e. no $[Fe_3S_3X_3]$ is detected). stepwise loss of X, and then FeS is a more favorable pathway as shown in Scheme II for other ions; pathway e: Fe atom ejection from the cubane core would be unexpected for two reasons. As mentionned above, an ion cannot retain four halogens with only three Fe atoms in the core. Also, if Fe(0) were lost, the oxidation state of the remaining metals must change to {+4, +4, +3), which clearly does not occur in these systems, consistent with the fact that the product [Fe₃S₄X₄] is never observed; pathway f: the loss of the neutral FeX would also be unexpected, since the oxidation state of one of the remaining Fe atom must be changed to Fe⁴⁺.



The correlation of gas phase [Fe_mS_n] anionic species, generated from the cubane cluster by FAB, with known chemistry of iron-sulfur complexes is intriguing. In the condense phase (i.e. solution), complexes have been made in which the [Fe₄S₄] core is in an oxidation state of +1, +2, or +36,27. All three oxidation states are observed in the negative ion spectra, Scheme II. However, in the gas phase, the unusual 0 oxidation state of [Fe₄S₄] core also exists. The [Fe₂S₂] core is known in solution with +2 and +1 oxidation states in solution; the +1 state is observed in the gas phase. Thus, the oxidation states observed in solution to date provide some useful limits as what to expect in the gas phase. The gas phase data may also suggest species that <u>could</u> exist in condensed phases, and could be pursued synthetically.

With the insights gained from analysis of the negative ion FAB spectra, correlating possible fragment ions with limitations in available oxidation states, it becomes obvious why negative ion FAB is the mass spectral technique of choice, when both molecular weight and structural information is desired. This also explain why the positive ion spectra are so simple. In Scheme III, most of the fragment ions trace their origin to [Fe₄S₄X₄]-, where the four iron atoms are in the states {+3, +3, +3, +2}. Why does the corresponding cation not lead to a variety of fragment cations? In fact, the corresponding cation is not formed by FAB. To convert this anion to a cation would require the removal of two electrons, which would result in the four iron atoms having oxidation states of {+4, +3, +3, +3}. Thus, the limitations on oxidation states of the iron atoms gives fewer choices for cationic species. Obviously, there are "oxidation state bottlenecks" that would be expected for the unimolecular chemistry of cations formed by

FAB; a rich cation chemistry is not expected, that would parallel the unimolecular fragmentation anion chemistry.

CONCLUSIONS

We have reported herein the utility of FAB-MS for the characterization of iron/sulfur cubane-containing compounds, and have discussed aspects of the fragmentation mechanisms that will assist in the mass spectral interpretation of related compounds. Both 3-nitrobenzyl alcohol (NBA) and 2-nitrophenyl octyl ether (NPOE) are suitable matrices for the FAB-MS studies of these series of complexes. It should be emphasized that, when such compounds are being characterized, it is vital that the experimentally observed and theoretically calculated isotopic patterns be compared, to assist in the correct identification of the ions formed.

Fast atom bombardment of a matrix containing iron/sulfur cubane clusters has been evaluated here, as a chemical system which generates a variety of smaller clusters in a variety of oxidation states, through unimolecular fragmentation processes. The restrictions on oxidation states that seem to dominate the fragmentation pathways yields interesting parallels with known clusters in the condensed phase.

In addition, we have successfully introduced FAB-MS analysis as a new methodology to characterize intermediates of ligand substitution reaction between analyte and matrix such as [Fe₄S₄(SEt)₄]²- and 3-

nitrobenzyl alchohol, as well as to confirm the existence of disproportionation species in solution, (i.e., (Ph₄P)₂Fe₄S₄(SPh)₂Cl₂ in DMF). Furthermore, both NBA and NPOE participates in an unusual gas phase oxygen atom transfer reactions with the iron-sulfur complexes.

It will be interesting to compare the results presented here with FAB-based analysis of small redox enzymes that contain an iron/sulfur cubane linkage. It will be intriguing to see how the cubane core fragments when attached to a peptide relative to thiolate, since this may give insight on how peptides regulate the redox properties of Fe/S clusters. Furthermore, it should be noted that, using mass spectrometry, ion-molecule reactions of any of the anions discussed in this work could be studied and used to determine properties of anions in the gas phase such as electron affinities and reactivity. Thus, FAB-MS offers not only a facile method for analysis, but an opportunity for the generation of unusual chemical species, and the characterization of very rich gas phase chemistry.



REFERENCES AND NOTES

- Eschenmoser, A. Angew. Chem. 1988, 100, 5; Angew. chem. Int. Ed.
 Engl. 1988, 27, 5.
- 2. Dolphin, D., Ed., The Porphyrins, Vol. 1-7, Academic Press, New York, 1978.
- (a) Scheer, H. In The Porphyrins, Vol. II, Part B, Dolphin, D., Ed., Academic Press, New York, 1978. Chapter 1. (b) Clayton, R. K., Sistrom, W.R. The Photosynthetic Bacteria, Plenum Press, New York, 1978.
- 4. Dolphin, D. Ed., B_{12} , Vol. 1-2, Wiley-interscience, New York, 1982.
- 5. Eschenmoser, A. Ann. N. Y. Acad. Sci. 1986, 471, 108.
- 6. Timkovich, R.; Cork, M. S.; Taylor, P. V. J. Biol. Chem. 1984, 259, 1577.
- 7. (a) Chang, C. K. J. Biol. Chem. 1985, 260, 9520. (b) Chang, C. K.; Timkovich, R.; Wu, W. Biochemistry 1986, 25, 8447.
- 8. Losada, M. J. Mol. Catal. 1976, 1, 245.
- 9. Forget, P.; DerVartanian, D. V. Biochim. Biophys. Acta. 1972, 256, 600.
- Murphy, M. J.; Siegel, L. M.; Tove, S. R.; Kamin, H. Proc. Natl. Acad.
 Sci. USA 1974, 71, 612.
- 11. Vega, J. M.; Garret, R. H.; Siegel, L. M. J. Biol. Chem. 1975, 250, 7980.
- 12. Vega, J. M.; Kamin, H. J. Biol. Chem. 1977, 252, 896.
- Scott, A. I.; Irwin, A. J.; Siegel, L. M.; Schoolery, J. N. J. Am. Chem. Soc. 1978, 100, 7987.
- 14. Battersby, A. B.; McDonald, E. Bioorganic Chem. 1978, 7, 161.
- 15. Payne, W. J. Denitrification 1981, Wiley, New York.
- 16. Knowles, R. Microbiol. Rev. 1982, 46, 43.
- 17. Iwasaki, H.; Saigo, T.; Matsubara, T. Plant Cell Physiol. 1980, 21; 1573.

- 18. Matsubara, T.; Frunzke, K.; Zumft, W. G. J. Bacteriol. 1982, 149, 816.
- 19. Chang, C. K.; Wu, W. J. Biol. Chem. 1986, 261, 8593.
- Chang, C. K.; Barkigia, K. M.; Hanson, L. K.; Fajer, J. J. Am. Chem. Soc. 1986, 108,1352.
- 21. Wu, W.; Chang, C. K. J. Am. Chem. Soc. 1987, 109, 3149.
- (a) Janick, P. A.; Siegel, L. M. Biochemistry 1982, 21, 3538; 1983, 22, 504.
 (b) Christner, J. A.; Munck, E.; Janick, P. A.; Siegel, L. M. J. Biol. Chem. 1983, 256, 11147.
 (c) Christner, J. A.; Janick, P. A.; Siegel, L. M.; Munck, E.; J. Biol. Chem. 1983, 256, 11157.
 (d) Christner, J. A.; Munck, E.; Kent, T. A.; Janick, P. A.; Salerno, J. C.; Siegel, L. M. J. Am. Chem. Soc. 1984, 106, 6786.
 (e) Cline, J. F.; Janick, P. A.; Siegel, L. M.; Hoffman, B. M. Biochemistry 1986, 25, 4647.
- (a) Young, L. J.; Siegel, L. M. Biochemistry 1988, 27, 2790, 5984. (b)
 Wilkerson, J.O.; Janick, P. A.; Siegel, L. M. Biochemistry 1983, 22, 5048.
- (a) Ellefson, W. L.; Whitman, W. B.; Wolfe, R. S. Proc. Natl. Acad. Sci. U.S.A. 1982, 79, 3707. (b) Ellefson, W. L.; Wolfe, R. S. J. Biol. Chem. 1980, 255, 8388. (c) Nagle, D. P.; Wolfe, R. S. Proc. Natl. Acad. Sci. U.S.A. 1983, 80, 2151.
- 25. Pfaltz, A. In *The Bioinorganic Chemistry of Nickel*; Lancaster, J. R., Ed.; VCH Publishers: New York, Chapter 12
- (a) Pfalz, A.; Jaun, B.; Fassler, A.; Eschenmoser, A.; Jaenchen, R.; Gilles, H. H.; Diekert, G.; Thauer, R. K. Helv. Chim. Acta 1982, 65, 828.
 (b) Livingston, D. A.; Pfalz, A.; Schreiber, J.; Eschenmoser, A.; Ankel-Fuchs, D.; Moll, J.; Jaenchen, R.; Thauer, R. K. Helv. Chim. Acta 1984, 67, 334.
 (c) Pfalz, A.; Livingston, D. A.; Jaun, B.; Diekert, G.; Thauer, R. K. Eschenmoser, A.; Helv. Chim. Acta 1985, 68, 1338.

- (d)Fassler, A.; Kobelt, A.; Pfalz, A.; Eschenmoser, A.; Bladon, C.; Battersby, A. R.; Thauer, R. K. Helv. Chim. Acta 1985, 68, 2287.
- 27. Kratky, C.; Waditshatka, R.; Angst, C.; Johnasen, J. E.; Plaquevent, J.
 C.; Schreiber, J.; Eschenmoser, A.; Helv. Chim. Acta 1985, 68, 1312.
- 28. Kratky, C.; Fassler, A; Pfaltz, A.; Krautler, B.; Jaun, B.; Eschenmoser, A. J. Chem. Soc., Chem. Commun. 1984, 1368.
- 29. Waditshatka, R. Kratky, C.; Jaun, B.; Heinzer, J.; Eschenmoser, A.; J. Chem. Soc., Chem. Commun. 1985, 1604.
- Kratky, C.; Angst, C.; Johnasen, J. E.; Angew. Chem., Int. Ed. Engl. 1981, 20, 211.
- 31. Fabrizzi, L. J. Chem. Soc. Dalton. Trans. 1979,1857.
- 32. Kaplan, W. A.; Scott, R. A.; Suslick, K. S. J. Am. Chem. Soc., 1990, 112, 1283.
- (a) Baker, E. W.; Brookhart, M. S.; Corwin, A. H. J. Am. Chem. Soc. 1964, 86, 4587.
 (b) Mclees, B. D.; Caughey, W. S. Biochemistry 1968, 7, 642.
 (c) Abraham, R. J.; Swinton, P. F. J. Chem. Soc. B 1969, 903.
 (d) Curthoys, G. C.; Magnusson, E. A.; Phillips, J. N. Inorg. Chem. 1972, 11, 1024.
 (e) Pasternack, R. F.; Spiro, E. G.; Teach, M. J. Inorg. Nucl. Chem. 1974, 36, 599.
 (f) Walker, F. A.; Hui, E.; Walker, J. M. J. Am. Chem. soc. 1975, 97, 2390.
- 34. Bottomly, L. A.; Olson, L.; Kadish, K. M. Inorg. Chem. 1982, 21, 1024
- 35. Fassler, A. Dissertation, RTH, Zurich Nr. 7799, 1985.
- 36. Davis, D. G. In *The Porphyrins*; Dolphin, D. Ed., Academic: New York, 1978; Vol. V, Chapter 4.
- (a) Stolzenberg, A. M.; Stershic, M. T.; J. Am. Chem. Soc. 1988, 110,
 5397. (b) Stolzenberg, A. M.; Stershic, M. T.; Inorg. Chem. 1987, 26,

- 3082.(c) Stolzenberg, A. M.; Stershic, M. T.; *Inorg. Chem.* 1988, 27, 1614.
- Chang, C. K.; Hanson, L. K.; Rickardson, P. F.; Young, R.; Fajer, J. Proc. Natl. Acad. Sci. U.S.A. 1981, 78, 2652.
- 39. Connick, P.; Macor, K. Inorg. Chem. 1991, 30, 4654
- Bottomly, L. A.; Olson, L.; Kadish, K. M. In Electrochemical and Spectrochemical Studies of Biological Redox Components; Kadish, K. M. Ed.; ACS Sym. Ser. 1982, 201, 279
- 41. Montforts, F.-P.; Romanowski, F.; Bates, J. W. Angew. Chem. Int. Ed. Engl. 1989, 28, 480.
- 42. Scheidt. W. R.; Lee, Y. J. Struct. Bonding 1987, 64, 1.
- 43. Kirner, J. F.; Garofalo, J.; Scheidt, W. R. *Inorg. Nucl. Chem. Lett.*1975, 107.
- Lynch, M. W.; Buchanan, R. M.; Pierpont, C. G.; Hendrickson, D. N.
 Inorg. Chem. 1981, 20, 1038
- 45. Chang, C. K. Biochemistry 1980, 19, 1971.
- Alder, A. D.; Longo, F. R.; Finarelli, J. O.; Goldmacher, J.; Assour,
 J.; Korsakoff, L. J. Org. Chem., 1967, 32, 476.
- 47. Chang, C. K.; Hataela, M. H.; Tuliusky, A. J. Chem. Soc. Perkin Trans. II 1983, 371.
- (a) Inhoffen, H. H.; Jager, P. Tetrahedron Lett. 1964, 1317. (b)
 Inhoffen, H. H.; Jager, P.; Mahlhop, R.; Mengler, C. D. J. Liebigs
 Ann. Chem. 1967, 704, 188.
- 49. Bent, H. E.; French, C. L. J. Am. Chem. Soc. 1941, 63, 568.
- 50. Beevers, L.; Hageman, R. H. Annuv. Rev. Plant Physiol., 1969, 20, 495.

- Ingraham, J. L. In Denitrification, Nitrification and Atmospheric Nitrous Oxide, Delwiche, C. C. Ed.; John Wiley & Sons, New York, 1981, 45.
- Murphy, M. J.; Siegel, L. M.; Kamin, H.; Rosenthal, D. J. Bio. Chem.,
 1973, 248, 2801.
- Madden, J. F.; Han, S.; Siegel, L. M.; Spiro, T. G. Biochemistry, 1989,
 28, 5471.
- McRee, E. D.; Richardson, J. S.; Siegel, L. M. J. Biol. Chem. 1986, 261, 10277.
- 55. Cowan, J. A.; Sola, M. Inorg. Chem. 1990, 29, 2176.
- (a)Holm, R. H.; Ciurli, S; Weigel, J. A. Prog. Inorg. Chem. 1990, 38, 1.
 (b) Stack, T. D. P; Weigel, J. A.; Holm, R. H. Inorg. Chem. 1990, 29, 3745.
 (c) Ciurli, S.; Carrie~, M.; Weigel, J. A.; Carney, M. J.; Stack, T. D. P.; Papaefthymiou, G. C.; Holm, R. H. J. Am. Chem. Soc. 1990, 112, 2654.
 (d) Weigel, J. A.; Holm, R. H.; Srivastava, K. K. P.; Munck, E. J. Am Chem. Chem. 1990, 112, 8015.
 (e) Whitener, M. A., Peng, G.; Holm, R. H. Inorg. Chem. 1991, 30, 2411.
 (f) Weigel, J. A.; Holm, R. H. J. Am. Chem. Soc. 1991, 113, 4184.
 (g) Liu, H. Y.; Scharbert, B.; Holm, R. H. J. Am Chem. Soc., 1991, 113, 9529.
- 57. Young, R.; Chang, C. K. J. Am Chem. Soc. 1985, 107, 898.
- Holm, R. H.; Philips, N. D.; Averill, B. A.; Mayerle, J. J.; Herskovitz,
 T. J. Am. Chem. Soc., 1974, 96, 2109.
- 59. Lindsey, J. J. Org. Chem. 1980, 45, 5215.
- 60. Johnson, A. W.; Kay, I. T. J. Chem. Soc., 1965, 1620.
- 61. Harris, D.; Johnson, A. W.; Gaete-Holmes, R. Bioorganic Chem. 1980, 9, 63.

- 62. Sun, Y.; Martell, A. E.; Chen, D.; Macfarlane, R. D.; McNeal, C. J. J. Heterocycl. Chem. 1986, 23, 1565.
- 63. Young, R. N.; Ganthier, J. Y.; Coombs, W. Tetrahedron Lett, 1984, 25, 1753.
- (a) Wong, G. B.; Bobrik, M. A.; Holm, R. H. Inorg. Chem. 1978, 17, 578.
 (b) Coucouvanis, D.; Kanatzidis, M. Simhon, E.; Baenziger, D. C. J. Am Chem. Soc. 1982, 104, 1874. (c) Kanatzidid, M. G.; Hagen, W. R.; Lester, R. K.; Coucouvanis, D. J. Am. Chem. Soc. 1985, 107, 953. (d) Kanatzidis, M. G.; Salifoglou, A.; Coucouvanis, D. Inorg. Chem. 1986, 25, 2460. (e) Coucouvanis, D.; Salifoglou, A.; Kanatzidis, Dunham, W. R.; Simopoulos, A.; Kostikas, A. Inorg. Chem. 1988, 27, 4066.
- (a) Kanatzidis, M. G.; Ryan, M.; Coucouvanis, D.; Simopoulos, A. Kostikas, A. Inorg. Chem. 1983, 22, 179.
 (b) Johnson, R. E.; Papaefthymiou, G. C.; Franke, R. B.; Holm, R. H. J. Am. Chem. Soc. 1983, 105, 7280.
 (c) Kanatzidis, M. G.; Baenziger, N. C.; Coucouvanis, D.; Simopoulos, A.; Kostikas, A. J. Am. Chem. Soc. 1984, 106, 4500.
 (d) Kanatzidis, M. G.; Coucouvanis, D.; Simopoulos, A.; Kostikas, A.; Papaefthymiou, V. J. Am. Chem. Soc. 1985, 107, 4925.
- 66. Thauer, R. K.; Schoenheit, P. In *Iron-Sulfur Proteins*; Sprio, T. G., Ed.; Wiley Interscience: New York, 1982; 329.
- 67. Thompson, A. J. In *Metalloproteins*; Harrison, P., Ed.; Verlag Chemie: Weinheim, FRG, 1985; Part I, 79.
- (a) Carter, C. W.; Kraut, J. Freer, S. T.; Alden, R. A.; Sieker, L. C.; Adman, E.; Jensen, L. H. Proc. Natl. Acad. Sci. U. S. A. 1972, 68, 3526.
 (b) Herskovitz, T.; Averill, B. A.; Holm, R. H.; Ibers, J. A.; Philips, W. D.; Weiher, J. F. Proc. Natl. Acad. Sci. U. S. A. 1972, 69, 2437.

- 69. (a) Holm, R. H. Acc. Chem. Res. 1977, 10, 427. (b) Berg, J. M.; Holm, R. H. In Iron-Sulfur Proteins; Spiro, T. G., Ed.; Wiley-Interscience: New York, 1982; 1.
- Averill, B. A. In Metal Clusters in Proteins; Que, L., Jr., Ed.; ACS Sym.Ser. 1988, 372, 258.
- Cleland, W. E. Jr.; Holtman, D. A.; Sabat, M., Ibers, J. A. Defotis, G.
 C.; Averill, B. A. J. Am. Chem. Soc. 1983, 105, 6021. (b) Cleland, W. E.,
 Jr.; Averill, B. A. Inorg. Chim. Acta 1985, 106, L17.
- 72. Nakamura, A.; Ueyama, N. in Metal Clusters in Proteins; Que, L., Jr., Ed.; ACS Sym. Ser., 1988, 372, 292.
- 73. Nakamura, A.; Ueyama, N. Advances in Inorganic Chemistry 1989, 33, 39.
- (a) Ohno, R.; Ueyama, N.; Nakamura, A. Chem. Lett. 1989, 399. (b)
 Ohno, R.; Ueyama, N.; Nakamura, A. Inorg. Chim. Acta, 1990, 253.
- 75. Barber, M; Bordoli, R. S.; Sedgwick, R. D.; Tyler, A. N. J. Chem. Soc. Chem. Commun. 1981, 325.
- 76. Miller, J. M. Mass Spectrom. Rev. 1989, 9, 319 and references therein.
- 77. Fenselau, C; Cotter, R. J. Chem. Rev. 1987, 87, 501.
- 78. Pachuta, S. J.; Cooks, R. G. Chem. Rev. 1987, 87, 647.
- 79. Sethi, S. K.; Nelson, C. C.; McClosky, J. A.; Anal. Chem. 1984, 56, 1977.
- 80. Divisia-Blohorn, B.; Kyriakakov, G.; Ulrich, J. Org. Mass. Spectrom. 1985, 22, 463.
- 81. Hegetscheveiler, K.; Keller, T.; Amrein, W.; Schneider, W. Inorg. Chem. 1991, 30, 873.
- (a) Knowalski, M. H.; Sharp, T. R. Stang, P. I. Org. Mass. Spectrom.
 1987, 22, 642. (b) Boyle, P. D.; Johnson, B. J.; Alexander, B. D.;

- Casalnuovo, J. A.; Gannon, P. R.; Johnson, S. M.; Larka, E. A.; Mueting, A. M.; Pignolet, L. H. *Inorg. Chem.* 1987, 26, 1346.
- 83. McElvany, S. W.; Allison, J. Organometallics 1986, 5, 1219.
- (a) Bojesen, G. Org. Mass Spectrom. 1985, 20, 415. (b) Miller, J. M. Balasumugan, K.; Nye, J.; Deacon, G. B.; Thomas, N. C. Inorg. Chem. 1987, 26, 560. (c) Liang, X.; Suwanrumpha, S.; Freas, R. B. Inorg. Chem. 1991, 30, 652.
- 85. Unfortunately, thermochemical information on the C₂H₅S radical is not available. Heats of formation of gas phase CH₃S, CH₃ and S suggest a C-S bond strength of 72.4 kcal/mol, which should be typical of alkyl-S bond strengths. In contrast, available data suggests a C-S bond strength of 90.2 kcal/mol in PhS. If the C-S bondstrengths in C₂H₅SH and C₆H₅SH are compared, the alkyl thiol has a bond strength 13 kcal/mol less than the aromatic compound. Complete thermochemical information on the anions are not available, however if one considers the species that are isoelectronic with C2H5S and C₆H₅S⁻, which are C₂H₅Cl and C₆H₅Cl, again the C-X bond is lower by greater than 10 kcal/mol for the alkyl group. Thus, it is safe to assume that alkyl-S bonds are weaker than phenyl-S bonds. All thermochemical data taken from S.G. Lias, J.E. Bartmess, J.F. Liebman, J.L. Holmes, R.D. Levin, W.G. Mallard, J. Phys. Chem. Ref. Data, 1988, 17, Suppl. no. 1.
- 86. Charalambous, J. Mass Spectrometry of Metal Compounds,
 Butterworth's, Boston, 1975.
- 87. O'Sullivan, T.; Millar, M. M. J. Am. Chem. Soc. 1985, 107, 4096.

MICHIGAN STATE UNIV. LIBRARIES
31293008773479